Order-Disorder Transitions and Spatio-temporal Pattern Formation in Complex Systems

By

Rajeev Singh

PHYS10200605009

The Institute of Mathematical Sciences, Chennai

A thesis submitted to the

Board of Studies in Physical Sciences

In partial fulfillment of requirements

For the Degree of

DOCTOR OF PHILOSOPHY

of

HOMI BHABHA NATIONAL INSTITUTE

July, 2013

Homi Bhabha National Institute

Recommendations of the Viva Voce Board

As members of the Viva Voce Board, we certify that we have read the dissertation prepared by **Rajeev Singh** entitled "Order-Disorder Transitions and Spatio-temporal Pattern Formation in Complex Systems" and recommend that it maybe accepted as fulfilling the dissertation requirement for the Degree of Doctor of Philosophy.

_____ Date:

Chair - M. V. N. Murthy

_____ Date:

Supervisor/Convener - Sitabhra Sinha

_____ Date:

Member 1 - Sudeshna Sinha

_____ Date:

Member 2 - Ronojoy Adhikari

Final approval and acceptance of this dissertation is contingent upon the candidate's submission of the final copies of the dissertation to HBNI.

I hereby certify that I have read this dissertation prepared under my direction and recommend that it may be accepted as fulfilling the dissertation requirement.

Date:

Place: Supervisor

STATEMENT BY AUTHOR

This dissertation has been submitted in partial fulfillment of requirements for an advanced degree at Homi Bhabha National Institute (HBNI) and is deposited in the Library to be made available to borrowers under rules of the HBNI.

Brief quotations from this dissertation are allowable without special permission, provided that accurate acknowledgement of the source is made. Requests for permission for extended quotation from or reproduction of this manuscript in whole or in part may be granted by the Competent Authority of HBNI when in his or her judgement the proposed use of the material is in the interests of scholarship. In all other instances, however, permission must be obtained from the author.

Rajeev Singh

DECLARATION

I, hereby declare that the investigation presented in the thesis has been carried out by me. The work is original and has not been submitted earlier in whole or in part for a degree / diploma at this or any other Institution / University.

Rajeev Singh

ACKNOWLEDGEMENTS

I would like to thank my supervisor Prof Sitabhra Sinha for his continuous encouragement and guidance throughout my research work. His diverse research interests have provided me an unique opportunity to work on seemingly very different problems under the umbrella of complex systems and I have learnt a lot from him during countless discussions. I would also like to thank my co-authors in the papers reporting the work described in the different chapters of my thesis, namely, Prof Subinay Dasgupta, Dr Nicolas Garnier, Dr Shakti N. Menon, Prof Alain Pumir and Dr Jinshan Xu.

I benefited from discussing with several people different aspects of the problems that have been investigated in this thesis. In particular, I would like to thank Prof Indrani Bose, Prof Bulbul Chakraborty, Prof Chandan Dasgupta, Prof Deepak Dhar, Prof S S Manna, Prof Gautam Menon, Prof Purusattam Ray, Dr Raghavendra Singh and Prof Sudeshna Sinha. Apart from the work reported in this thesis I am lucky to have the opportunity to work on other problems and I would like to thank Prof Ronojoy Adhikari, Prof S R Hassan, Prof R Rajesh and Prof R Simon for introducing me to these interesting issues and for various discussions.

Much of my research work has required intensive computation and I would like to thank the High-Performance Computing (HPC) facility at IMSc for providing computational resources, in particular, access to the “Annapurna” supercomputer. Some of the research work described here were performed as part of projects funded by different agencies, including the Indo-French Centre for the Promotion of Advanced Research (IFCPAR Project 3404-4) and the Department of Atomic Energy, Government of India (IMSc Complex Systems Project, XI and XII Plan).

Life at the institute has been very pleasant thanks to all my friends here, in particular Sandeep Goyal, Somdeb Ghose, P V Sriluckshmy, Abhrajit Laskar, Rohan Poojary, Prem Prakash Pandey, Anoop Varghese, Krishnakumar Sabapathy, Ravi Kunjwal, Rajarshi Pal, Soumyajit Pramanick, A B Belliappa, Saket Saurabh, Karteek Sreenivasaiah, Yadu Vasudev, Madhushree Basu and Neeldhara Misra. I also take this opportunity to thank my family for their love and support.

PUBLICATIONS

a. Published:

1. **Singh, R.**, Dasgupta, S. and Sinha, S. (2011). *Chimera order in spin systems*. EPL (Europhysics Letters), **95**, 10004. Arxiv Preprint, 1011.5032.

2. **Singh, R.**, Xu, J., Garnier, N., Pumir, A. and Sinha, S. (2012). *Self-Organized Transition to Coherent Activity in Disordered Media*. Physical Review Letters, **108**, 068102. Arxiv Preprint, 1201.1116.

   Highlighted in APS Physics Synopsis.

3. **Singh, R.** and Sinha, S. (2013). *Spatiotemporal order, disorder, and propagating defects in homogeneous system of relaxation oscillators*. Physical Review E, **87**, 012907. Arxiv Preprint, 1206.2896.

4. Xu, J., **Singh, R.**, Garnier, N., Pumir, A. and Sinha, S. (2013). *Large variability in dynamical transitions in biological systems with quenched disorder*. New Journal of Physics, **15**, 093046. Arxiv Preprint, 1212.3466.

b. Accepted:

c. Communicated:

1. **Singh, R.**, Menon, S. N. and Sinha, S. (2013). *Complex patterns arise through spontaneous symmetry breaking in dense homogeneous networks of neural oscillators*. Arxiv Preprint, 1305.7093.

2. **Singh, R.**, Dasgupta, S. and Sinha, S. (2013). *Extreme variability in convergence to structural balance in frustrated dynamical systems*. Arxiv Preprint, 1307.8018.

Contents

List of Figures

List of Tables

Synopsis

The appearance of simple or complex ordered patterns is a phenomenon of central importance in dynamical systems as well as in statistical physics of far-from-equilibrium systems. Several examples of the emergence of simple, regular patterns in physical systems that occur through collective order-disorder transitions, e.g., the aligned orientation of spins in Ising-like systems, are well known. In the context of nonlinear dynamics, similar simple ordering behavior can be observed in the synchronization of coupled oscillators. However, more complex patterns have recently been seen to occur in various systems under different conditions, especially in heterogeneous media. In this thesis, we have investigated how such patterns can arise by considering several models of complex systems comprising large number of components interacting with each other via non-trivial connection topologies. Such complexity is ubiquitous in the natural world (especially in living systems) and their spatio-temporal dynamics can often have functionally critical consequences for biological organisms. Our work is aimed at contributing towards building a general theory for describing pattern formation and ordering in "complex" systems.

The models we consider are capable of exhibiting a variety of novel complex patterns and collective order, some of which may in fact have manifestations in real systems, such as the mammalian uterus. We present systematic investigations of the mechanisms resulting in the generation of such patterns, which is a challenging exercise because of the large number of interacting components involved and the complicated nature of the coupling. The emergence of various dynamical regimes have been characterized in terms of distinct non-equilibrium steady state properties for systems that span a range of different types of components (in terms of their intrinsic behavior) and their interactions. At the level of component dynamics, the temporal behavior ranges from threshold-activated dynamics with either discrete-state transitions (as in "Ising"-like spins) or continuous-state behavior (as in excitable elements described by FitzHugh-Nagumo like equations) to those which display relaxation oscillations or even passive response (with any perturbation to the state decaying exponentially to the resting value). On the other hand, the nature of the interactions in the systems we have investigated range from exchange interactions (as in a system of spins) to diffusive coupling (e.g., in a system of cells coupled by electrical gap junctions describing a piece of biological tissue) to effective synapse-like connections (as between different brain areas in the cortex). In the following paragraphs we briefly describe the work reported in the thesis.

In **Chapter 1** we begin with a short overview of the physics of pattern formation and complex ordering. We present a brief review of key results from earlier studies that have used reaction-diffusion models and oscillator arrays to study such phenomena. We conclude

this chapter with a discussion of the main themes considered in the thesis.

In **Chapter 2** we show using a simple model the emergence of collective rhythms in chemical and biological systems as a result of interaction between a heterogeneous population of elements or cell types. The results of this chapter underlines one of the key lessons of complex systems theory that components whose intrinsic behavior is relatively simple often exhibit unexpectedly rich properties when coupled together. In particular, we show that the interaction of an excitable and a passive cell, both of which are quiescent in isolation, can result in (under appropriate conditions) spontaneously generated sustained oscillations. As the detailed nature of the coupling can produce a variety of different frequencies, when studying this problem for an entire system of coupled excitable and passive cells it is a challenge to understand what will be the possible types of dynamics that such a system is capable of supporting. This is not a question of theoretical interest only but rather has important biological consequences; indeed, we have used this model system to understand how the pregnant uterus, which is quiescent for most of the time, suddenly starts oscillating close to term generating the coherent contractions needed for birth of a child. For this we have considered a two-dimensional lattice of excitable cells, each coupled to its nearest neighbors and also to a varying number of passive cells. We show that increasing the coupling between the cells allow the system to show a number of transitions between very different spatiotemporal dynamical regimes: from quiescence to a state marked by clusters of cells oscillating at different frequencies to finally, global synchronization of periodic activity and coherence. Our results provide a causal connection between two previously reported experimental observations which were not known to be related, viz., that there is remarkable increase in intercellular coupling close to onset of labor and that activity is initially weak and transient, gradually increasing in intensity and duration at the late stage of pregnancy. We also discuss in the context of our modeling studies the important role played by multistability of different types of attractors in such biological phenomena.

In the work described above, the diffusive coupling between elements promotes homogeneity which results in coherent collective dynamics. While such coherent activity is indeed functionally important in systems where synchronization between different elements is necessary, e.g., in the brain for information processing and for insulin secretion in pancreatic beta-cell assemblies, it is only one of several possible spatiotemporal patterns that can emerge via different types of interactions. To explore the range of possible patterns that can be generated in complex systems, in **Chapter 3** we have investigated the collective dynamics of a system of relaxation oscillators that are effectively coupled through mutual inhibition. Our study has important applications in the real world, in particular, for understanding how biochemical oscillators coupled through reaction-diffusion mechanisms yield a large variety of spatial patterns and temporal rhythms. Furthermore, there have been recent experiments in microfluidic devices where oscillatory chemical reactions occur on beads suspended in oil where the interaction between the beads is thought to result from diffusion of an inactivator chemical constituent, thereby implementing a lateral inhibition-like mechanism. The results of these experiments have revealed a rich variety of collective phenomena including (i) anti-phase synchronization and (ii) oscillator death regimes with spatial patterns resembling Turing structures seen in various reaction-diffusion systems. We have explained the formation of these patterns by using a simple

model of coupled relaxation oscillators that allows us to analytically explain the emergence of anti-phase oscillations and the spatially patterned oscillator death (Turing-like) regime. In addition our model also exhibits a novel "chimera-like" dynamical state in which part of the system is oscillating whereas other regions show negligible temporal activity. An even more fascinating pattern consists of traveling waves of phase defect-like structures. These defects behave like particles and have non-trivial interactions with each other. For example, they can either reflect off each other or, one or both of them can annihilate upon collision. The manifestation of this phenomena in two dimensions is even more interesting. For oscillators arranged on a square lattice we have found a fundamental defect structure which is self propelling and moves around indefinitely in a medium with periodic boundaries. These patterns are reminiscent of the "gliders" observed in the well-known two-dimensional cellular automata "Game of Life". In the asymptotic state, we observe situations where gliders interact with each other continually producing complex spatio-temporal patterns. We conclude the chapter with a brief discussion of a conjecture about whether such structures can be used to construct logic gates in the manner similar to what has been done in the "Game of Life" cellular automata, which will make possible the building of chemical computers.

Although diffusive coupling between elements are capable of generating a fascinating variety of spatiotemporal patterns, as has been shown by us in the above chapters, many complex systems exhibit interactions having a very different nature. For example, neurons in the brain, apart from coupling with each other through electrical gap junctions that can be effectively modeled as a diffusive coupling, also communicate by chemical means through synapses. Synaptic coupling is fundamentally nonlinear and can give rise to phenomena distinct from those observed in diffusively coupled systems. We investigate the role of such nonlinear interactions in giving rise to a variety of different types of synchronization dynamics in **Chapter 4** where we analyze a system of globally coupled Wilson-Cowan oscillators that functions as a mesoscopic model for brain activity. One of the principal difficulties in making sense of the complex dynamical phenomena underlying cognition is associated with the wide range of scales over which the relevant processes operate. While molecular approaches to neuroscience can explicate the operation of a single synapse or neuron, it is unclear how to relate such results with cognitive science that considers the entire human brain (comprising $\sim 10^{11}$ neurons) as an unit. However, with the increasing use of brain activity mapping techniques such as fMRI, MEG, multi-electrode EEG and fluorescence imaging using voltage-sensitive dyes, it is important to come up with descriptions of phenomena at scales that span the range between the two extremes mentioned above. Such a mesoscopic-level model of the brain should ideally comprise variables that describe the activity of brain areas having thousands of neurons. Instead of building the model of a brain by the complicated process of joining together an extremely large number of detailed models of single neurons, it may be preferable to use phenomenological models that are based on experimental observations of intermediate-scale dynamical phenomena in the brain. The Wilson-Cowan (WC) model, that describes the time-evolution of the mean level of activity for a population of interacting excitatory and inhibitory neurons, provides us with a method of simulating the dynamics of large assemblies of neurons by using it as the basic unit for a network model of brain areas. We investigate the dynamical properties of coupled Wilson-Cowan oscillators and find that the system is capable of showing a range of different types of collective

behavior as the coupling strength between the oscillators is varied. While the observed patterns include those seen in many other systems such as exact synchronization, anti-phase synchronization and amplitude death, we also find states marked by the occurrence of phase and frequency clusters, as well as, homogeneous oscillator death. The occurrence of clustered synchronization states marked by the existence of multiple groups of elements having a common frequency or phase, in the absence of any heterogeneity in the connection topology (such as modularity) is a surprising result and suggests an exciting interplay between structural and dynamical organizational principles in the brain.

The models discussed above belong to the same general class of continuous-state dynamical systems. However, in order to develop a general theory of spatial patterns arising through interactions between a large number of dynamical elements, we need to ask how universal are the features that we observe and whether similarly rich variety of phenomena can be seen in dynamical systems having discrete states. With this aim, in **Chapter 5** we have investigated ordering behavior in systems of Ising spins having modular organization in their connection topology of ferromagnetic and antiferromagnetic interactions. The equilibrium properties of such a system in absence of external magnetic field are relatively easy to understand with the spins getting divided into two oppositely aligned clusters with members of each cluster oriented in the same direction. However, we have shown that at finite temperatures and in the presence of an external field this system can exhibit extremely nontrivial equilibrium behavior with one cluster being ordered while the other is disordered. This state can be called a chimera state in analogy with similar phenomena recently seen in systems of coupled oscillators. While traditionally the focus of research in oscillator systems had centered on globally synchronized states and traveling waves, the discovery of complex ordering behavior designated as chimera has generated interest in states characterized by broken symmetries of the underlying homogeneous system exhibiting stable coexistence of coherent and incoherent regions. Generalizing the concept of such "chimera" states to systems at thermal equilibrium undergoing order-disorder transition, we have shown analytically that similar complex ordering can appear in a system of discrete-state dynamical elements such as Ising spins. Using mean-field theory we show that under certain conditions a chimera-like ordering is the equilibrium state for a system of Ising spins. The identity of the cluster that is ordered and the one which is disordered can switch with a time scale that is related to the system size. This result is connected to the Kramer's exit problem from a potential well and we have investigated this using Monte Carlo simulations. We have also numerically established the existence of chimera ordering in 3-dimensional spin systems resembling layered magnetic materials, suggesting possible experimental observation of such states. The results of our study can also have significant implications for models of social dynamics. While it is expected that two polarized groups in society respond oppositely to a common stimuli, a chimera state corresponds to the same external event causing one group to become completely unanimous in their choice while the other group splits into complete confusion. It is not difficult to identify historical instances of similar phenomena, and it is interesting to speculate whether similar causal mechanisms are at play.

An important aspect of many complex systems in nature is that the interactions between the constituent elements do not remain constant but rather evolve in response to the dynamics of the system. For instance, learning in the context of neuronal networks in the

brain is considered to arise from changes in the strength of connections between neurons over time, resulting from relative timing of activation of the corresponding neurons. This suggests a fascinating interplay between dynamics at very different time-scales in complex systems: while the relatively fast dynamics of the elements cause the nature of interactions to change, the slowly evolving coupling in turn affects the global dynamics of the system. This is the subject of **Chapter 6** where we seek to understand the coevolution of nodal dynamics and the interactions strengths in networks. In other words, we observe how the structure of the network topology evolves as a result of the dynamics in the nodes, which in turn influences the collective behavior of the nodes. In particular, we focus on the emergence of structural balance in networks with adaptive dynamics, where a node can be in one of two possible states (i.e., we consider Ising-like nodal dynamics). To understand structural balance we first note that many networks in nature have signed weights associated with their links or edges, where the sign represents the nature of the interaction. For example, in a social network, “positive” links indicating affiliative relations connect friends while “negative” links implying conflict connect enemies. If signs are assigned at random to the links of a network, it is possible to arrive at a situation characterized by conflicting constraints (referred to as “frustration" in the context of spin models in statistical physics) where the dynamical states adopted by the nodes of the network cannot all be made compatible with the nature of the links connecting them. As an example, three nodes connected to each other by negative links (antagonistic relations) cannot have any assignment of binary states that simultaneously satisfy all mutual relations. Such situations are considered to be unstable and the nature of the interactions can gradually change in order to resolve the conflict. Thus, in the above example, any pair of nodes may change the sign of their interaction to form an alliance against the third, their common enemy. This allows the system to achieve “structural balance”, characterized by all cycles in the network having an even number of negative links, a classical result of graph theory due to Harary and Cartwright. Note that, a structurally balanced society will have all agents segregated into two opposing groups. Connected agents belonging to the same camp will be mutual friends and those belonging to different camps will have antagonistic relations. However, in reality, the friend of a friend may initially be an enemy, a “frustration" inducing situation implying the lack of structural balance. However, adaptation of the interactions over time may resolve all such conflicts eventually yielding a balanced structure. How frustrated systems can evolve with time under such link adaptation dynamics is an important question and has recently been the focus of activity for many physicists working on the theory of complex networks. In most of these studies, the dynamics of the nodes are not considered when the evolution of the network is investigated. In contrast, we propose a simple model for studying the transition of a frustrated network to structural balance where the nodal dynamics directly governs the evolution of interactions. The process of link adaptation we consider is inspired by the classical theory of learning in nervous systems due to Hebb, where the link strength between two nodes having the same dynamical state at a given time is positively incremented, while that between nodes having opposite states is negatively incremented. While limiting cases of this model are easy to understand, the overall properties of this apparently simple model are quite complex. For suitable parameter values, the system manages to approach balance, but the time required for this exhibits non-trivial behavior. We observe that over a range of adaptation rates and temperatures (which control the degree of noise or stochastic

fluctuations in the update dynamics of the node states) the time required to reach structural balance can become extremely long. The divergence of the time required to achieve balance poses interesting questions in the context of several real-world networks where similar adaptation may be going on (e.g., food webs or neuronal networks).

In **Chapter 7** we conclude with a discussion of how our results may contribute towards a general theory of pattern formation in complex systems and indicate possible future directions of research.

1

Introduction

> *Then the Ethiopian put his five fingers close together . . . and pressed them all over the Leopard, and wherever the five fingers touched they left five little black marks, all close together. You can see them on any Leopard's skin you like . . . Sometimes the fingers slipped and the marks got a little blurred; but if you look closely at any Leopard now you will see that there are always five spots . . .*
>
> – Rudyard Kipling, "How the Leopard got his spots" in *Just So Stories* (1902)

Spatio-temporal patterns are ubiquitous in nature. They are not only seen in the context of biological development, e.g., in the segmentation of the *Drosophila* embryo [1] and in the characteristic markings on animal skins [2], but also appear as a result of dynamical processes, such as the appearance of spiral waves of electrical excitation in the heart during episodes of abnormally rapid cardiac activity [3] and aggregation of slime-mold through chemotaxis [4]. Many of the patterns seen in nature, including some of the ones mentioned above, also have functional significance. To understand how such patterns arise, experimental systems have been developed that help us in analyzing the genesis of these structures under a controlled environment.

A class of experimental systems which has been studied in detail comprise nonlinear

chemical reactions that are capable of excitatory activity or oscillations [5]. One of the reasons why the study of these reactions have been of great interest is because they can be considered as simple models for understanding the dynamics of more complex systems, such as, electrical activity in biological tissue, including the heart. The phenomenon of chemical oscillation was discovered in the 1950s by Boris Belousov [6] but initially was disbelieved, as it was erroneously thought that this observation violated the second law of thermodynamics. It was only in the sixties, following the subsequent experiments of A. M. Zhabotinksy and others that the phenomenon of chemical oscillations was accepted to be real and at present the system is known as the Belousov-Zhabotinsky (BZ) reaction [3]. The original dramatic periodic changes in color that indicated the occurrence of chemical oscillations were observed in "well-mixed" chemical systems. In the original experimental set-up the periodic oscillation was transient and the reaction stopped once the reactants were exhausted. Later experiments were conducted in continuously stirred tank reactors where reactants were constantly fed in and the products were taken out. Here, the oscillations would continue indefinitely as long as the supply of reactants was maintained. In the last few decades, apart from minor variants of the BZ reaction, several other oscillating chemical systems have been discovered which exhibit a rich variety of dynamical behavior [5].

Another important development was the investigation of coupled chemical oscillators to understand how diffusive interaction between these would affect the collective behavior. Experiments were done to study different kinds of synchronization phenomena such as synchronized oscillations, anti-phase synchronization and oscillator death [7]. The BZ and other nonlinear reactions have also been carried out in a spatially extended framework, viz., in gels spread in thin layers on a petri dish. The departure from the well-mixed situation means that heterogeneities in the reactant/product concentrations will appear as spatial patterns. Depending on various experimental parameters, these systems manifest either excitable or oscillatory properties. A wide variety of spatio-temporal patterns, including target waves and spirals, have been observed in these experiments. The use of

photo-sensitive chemicals has allowed a high degree of control on the patterns that can be produced by suitably manipulating the light incident on the medium. Recently, chemical experiments have been designed on microfluidic devices that allow experimental realization of a large array of coupled nonlinear oscillators. Although there have been theoretical studies on such spatially extended systems, these developments allow controlled experimental realizations of tens to hundreds of coupled oscillators.

Although we have only mentioned chemical systems above, there have in fact been many experiments carried out on a range of nonlinear devices aimed at understanding pattern formation and other collective phenomena resulting from the spatio-temporal dynamics of such systems. The results of these experiments have been used to guide theoretical efforts at uncovering the mechanisms underlying pattern formation [8–15]. This had led to several models for spatio-temporal dynamics which can be classified into categories depending on whether space, time and the dynamical state in a model adopts discrete or continuous values. One of the most widely used of these are partial differential equations (PDEs) where space, time and state-space are continuous. They have been used for understanding patterns in physical systems (such as, in fluids) as well as in biological systems (e.g., the propagation of reentrant waves in excitable tissue). A widely used type of PDE for explaining pattern formation in many different situations is the system of reaction-diffusion equations that we describe in the next section. Another class of models closely related to PDEs are lattices of continuous dynamical elements, where space is discrete but time and state-space are continuous. Of particular interest within this class are the models where the dynamical elements are autonomous oscillators (limit cycles). The concept of the spatial lattice can be generalized to a network where the spatial neighborhood is replaced by an arbitrary connection topology. The study of dynamical elements coupled in a general network has gained attention in recent times because of the wide variety of natural systems it can be used to model. As many networks that exist in the real world are also seen to evolve both in terms of the nature and strength of their interactions, several models have been proposed recently to understand how the connections between elements

can coevolve with the dynamics on the nodes of a network. Another important class of models is one where the space, time and state-space are discrete, the paradigmatic example being the well-known Ising model. We briefly discuss these different categories of models for understanding spatio-temporal pattern formation in the following sections.

1.1 Reaction Diffusion Systems

As suggested by the name, reaction-diffusion models provide a natural description for the dynamics of a chemical system: the reagents are *reacting* with each other and the reactants as well as the products being transported through *diffusion*. Over time, these models have been used to analyze a wide class of spatially extended systems in chemistry, physics, biology and ecology [10, 11, 14]. Under coarse-graining, these systems are modeled using PDEs having the form:

$$\frac{\partial \mathbf{q}(\mathbf{x}, t)}{\partial t} = \mathbf{D}\nabla^2 \mathbf{q}(\mathbf{x}, t) + \mathbf{R}(\mathbf{q}),$$

where each component of $\mathbf{q}(\mathbf{x}, t)$ represents one of the several variables describing the state of a system (e.g., concentration of a chemical species in case of chemical reactions), $\mathbf{D}$ is the diffusion matrix and $\mathbf{R}(\mathbf{q})$ represents the different (nonlinear) reaction terms. Thus, the first term in the equation represents transport of the different components while the second term contains details of all the local dynamical processes operating on each of the components including production, decay, etc.

A commonly used analytical tool for understanding the dynamics of nonlinear PDEs is to perform linear stability analysis for various solutions. An important example of such analysis carried out for reaction diffusion systems is that of Alan Turing [16]. While trying to understand the mechanisms responsible for morphogenesis, Turing discovered a striking, counter-intuitive effect of diffusion, namely, a homogeneous solution of a reaction-diffusion system can be destabilized by diffusion under certain circumstances. This is surprising as diffusion usually smooths out any spatial fluctuation in a system. This cru-

cial insight of Turing has provided one of the most well-known mechanisms of pattern formation in reaction-diffusion systems and the resulting patterns are named after Turing. Several models have successfully used this mechanism to describe the generation of a wide variety of patterns, e.g., stripes and spots that occur in animal coat patterns [14].

Apart from *Turing patterns*, reaction-diffusion systems can exhibit a wide range of other spatio-temporal dynamical behavior such as travelling waves, dissipative solitons, spatiotemporal chaos, etc. While some of these can be explained through an analytical treatment, to study the rest one has to resort to numerical simulations. The first step is the discretization of the Laplacian or diffusion operator for a finite system which turns the space continuum into a discrete lattice. Thus, this process converts a system of PDEs into a large number of coupled ordinary differential equations (ODEs). Diffusion is now represented by the coupling of suitable variables at a given lattice point with those on its nearest neighbors.

Traditionally, the space continuum (and hence the system of PDEs) is assumed to represent reality, while the lattice (correspondingly, the system of coupled ODEs) is considered to be an approximation. However, with modern technology it is possible to investigate systems where the spatially discrete lattice is the more accurate description and the corresponding PDE is an approximation. Examples include recent experiments involving beads containing chemical reactants suspended in a medium within a microfluidic channel or simulations of a system of cells interacting with each other in biological tissue. In these situations it is natural to model the individual beads or cells as a single unit, so that the system is represented as a lattice of dynamical elements. It is important to make this distinction as these recent experiments report observations of phenomena that are natural for a lattice but are difficult to understand in terms of a spatial continuum, e.g., anti-phase oscillations and heterogeneous oscillator death, which are described in detail later in this thesis.

1.2 Coupled Oscillators

Oscillators (to be precise, self-sustained or limit cycle oscillators) are dynamical systems having periodic solutions which have been used to model a wide variety of physical and biological systems. Although the physical systems represented by these models have been known for a long time, their distinction with respect to other types of oscillatory dynamics was first pointed out by Lord Rayleigh when he distinguished between self-sustained oscillations and driven oscillations. The concept of a limit cycle itself is due to H. Poincaré. A systematic study of these self-sustained oscillators was performed by A. Andronov and collaborators [17] and they discovered a commonly occurring mechanism that gives rise to these oscillations, namely the *Andronov-Hopf bifurcation* (also known as Hopf bifurcation).

In this thesis, one of the systems we have focused on is an array or network of coupled oscillators. One of the most well-known collective phenomena associated with such systems is *synchronization* [18]. Possibly the first person to report it was the Dutch scientist Christiaan Huygens [19] who observed that a pair of pendulum clocks would start oscillating with same frequency if they are hung from a common support. In this state, the two pendula always move opposite to one another and if they are disturbed from this motion they return to it after some time. The phenomenon that Huygens had observed is now known as *anti-phase synchronization*. Other historically important observations of synchronization phenomenon in various systems include that in acoustical systems by Lord Rayleigh [20], in triode generators by W. H. Eccles and J. H. Vincent [21] and in large population of fireflies by the Dutch physician Engelbert Kaempfer in 1680 [22]. After replicating and extending the experimental work of W. H. Eccles and J. H. Vincent, Edward Appleton [23] and Balthasar van der Pol [24] made the first theoretical study aimed at understanding synchronization. An outcome of this work is one of the most well-known nonlinear oscillator models in the dynamical systems literature, viz., the *van der Pol oscillator* model. The relaxation oscillator model based on the FitzHugh-Nagumo systems

of equations that we use in this thesis is closely related to this model.

Apart from synchronization, coupled oscillator models are also known to exhibit other types of collective behavior such as oscillator death, amplitude death, chimera states, etc. that are described in detail later in the thesis.

1.3 Spin Models

Spin models, or rather systems of interacting elements which can be in any one of a finite number of states, are examples of discrete dynamical systems. The paradigmatic spin model is the one proposed by Ising [25] to understand spontaneous magnetization early in the last century. These models have been used extensively in statistical mechanics and condensed matter physics to understand phase transitions and other cooperative phenomena. Their simplicity has also led to the adoption of spin models to understand ordering phenomena in domains outside physics, such as, in the context of opinion formation in social systems and associative recall of patterns in neural networks.

Traditionally, in the context of condensed matter physics, spins have been arranged in regular d-dimensional lattices. However, in recent applications to problems of social or biological importance, spin-spin interactions over networks having arbitrary connection topology have been considered [26]. This has resulted in the discovery of novel collective phenomena, e.g., the occurrence of “modular order” in networks having community organization [27].

1.4 Overview of the thesis

The aim of the present thesis is to contribute towards understanding the general principles underlying the dynamics of pattern formation in complex systems. For this we have

considered different types of (a) local dynamics for the system components, (b) types of interaction between these components and (c) connection topology in which these interactions are arranged. A common property of many of the systems we investigate here is the existence of both cooperative (promoting order) and antagonistic (disrupting homogeneity) interactions between the constituent elements. The resulting *competition* leads to different types of non-trivial collective behavior as the relative strengths of the interactions are varied. These are manifested as spatio-temporal patterns, including several types of ordering and coherence, which have been described in the thesis and the processes giving rise to them analyzed in detail.

A general theme underlying the phenomena described in several of the chapters is the occurrence of *spontaneous symmetry breaking* leading to pattern formation. In other words, under these conditions, the solution of the set of equations describing the model dynamics does not possess its full symmetry. Another feature exhibited by many of the systems under consideration here is the phenomenon of *multistability*, i.e., the existence of many stable solutions for a given set of system parameters. Different patterns are seen depending on the initial condition chosen and the fraction of randomly chosen initial states that give rise to a specific pattern can be taken as a measure of the size of its basin of attraction. Further, the patterns can appear, disappear or lose stability as the system parameters are gradually changed via different kinds of *bifurcations*. We now provide an overview of the work described in each chapter of the thesis.

In **Chapter 2**, we consider a heterogeneous system whose individual components are continuous dynamical systems, in particular, excitable and passive elements. Local coupling between these different types of elements can result in oscillations and we have investigated the emergence of collective rhythmic activity in such systems. This is motivated by a puzzling observation in uterine physiology, viz., synchronized oscillations that give rise to labor during childbirth occur in the uterus even though it has been shown that none of the cells in the uterine tissue can oscillate spontaneously in isolation. Thus, the periodic

activity of the uterus is distinct from several other types of biological oscillations, such as the rhythmic pumping action of the heart, which are coordinated by specialized elements known as “pacemakers” (e.g., cells in the sino-atrial node of the heart). Although in the uterus we observe a transition from disordered activity during gestation to synchronized electrical activity giving rise to coherent contraction that ultimately leads to birth, there is no experimental evidence for the presence of such specialized coordinating elements in this organ. We have proposed a novel explanation for the emergence of coherent activity in this system through increased coupling among heterogeneous dynamical elements. For this purpose, we use a lattice model of disordered excitable system (disorder being in the form of a variable number of passive cells connected to each excitable cell). On increasing the strength of coupling between the elements comprising the system, we observe a transition from a quiescent state to coherent activity via several non-trivial collective dynamical states. Our results help in causally connecting two apparently unrelated experimental observations: (i) coupling between uterine cells increases remarkably through the course of pregnancy and (ii) oscillatory activity is rare and extremely weak during the early stages of pregnancy but increases in frequency and strength as one approaches labor.

While cooperative interactions primarily result in synchronization of activity between elements, other forms of couplings can result in a richer variety of collective dynamics. In **Chapter 3**, we have investigated systems where individual elements interact with their neighbors through lateral inhibition. In particular, we investigate the emergence of spatio-temporal patterns in an array of relaxation oscillators which are coupled through diffusion of the inactivating component of the local dynamics. These patterns can potentially arise in systems of coupled biochemical oscillators and thus, may be of interest to biologists. The simple model of coupled relaxation oscillators we have used helps explain different collective phenomena seen recently in chemical experiments such as anti-phase synchronized oscillations and heterogeneous oscillator death states with spatial patterns resembling Turing structures. The model also exhibits a chimera dynamical state in which part of the system is oscillating whereas other regions show negligible temporal activity.

In addition, we observe traveling waves of phase defect-like structures that behave like particles and have nontrivial interactions with each other. The complex spatio-temporal patterns produced by these interactions are reminiscent of those observed in the well-known cellular automata "Game of Life". As the latter has been shown to be capable of universal computation, it suggests the possibility that propagating defects in chemical media may be used for performing complex logical operations.

In **Chapter 4**, we have explored the effect of simultaneous action of excitatory and inhibitory coupling in continuous dynamical systems. Specifically, we have investigated collective behavior in a system of coupled Wilson-Cowan (WC) oscillators, that model the dynamics of local regions in the brain, connected using excitatory and inhibitory connections arranged in various topologies. As this model system provides a mesoscopic description of brain activity, our results may give insights into the genesis of observed patterns in large-scale cortical oscillations. We have first analyzed the different dynamical behavior seen for a pair of coupled WC oscillators, and then extended our study to a globally coupled network of WC oscillators. We show the existence of novel collective states, including those characterized by oscillator clusters, where each cluster is distinguished by its amplitude or frequency. As each oscillator is identical in terms of both intrinsic dynamics and connectivity, this indicates that the homogeneous system of WC oscillators undergoes spontaneous symmetry breaking. We also investigate the effect of removing a small fraction of connections, making the system marginally sparse. A surprising aspect is that although this densely connected system is effectively identical to the mean-field description, the dynamical properties are radically altered in response to extremely minor deviations from the fully connected situation.

In the preceding chapters we have considered continuous dynamical systems. An important question we consider next is whether coupled discrete dynamical systems can exhibit equally intriguing collective phenomena. In **Chapter 5**, we investigate spin systems, where the individual elements can switch between a finite number of possible states

at discrete time intervals. As the orientation of a spin can be interpreted as one of a number of mutually exclusive choices, such models have been applied to understand social phenomena involving coordination among agents, e.g., the adoption of innovations and consensus formation. The simplest case one can consider is that of binary choice where the spin flips between two states (Ising spins) depending on the interactions with its neighbors. The ferromagnetic Ising model having positive spin-spin coupling, such that each spin tries to align itself with its neighbors, can become globally ordered under suitable conditions. In social context this corresponds to complete consensus, i.e., each agent agrees with everyone else. However, in real social situations, there can also be antagonistic interactions between agents and systems having both types of interactions can exhibit a variety of complex behavior. In particular, we have investigated the consequences of cooperative coupling operating over short range and antagonistic coupling at longer range. In equilibrium, the system is divided into two oppositely aligned clusters with spins within each cluster oriented in the same direction. The social analogy would be two extremely polarized groups holding opposite convictions on various issues. However, we show analytically that in the presence of an external field nontrivial equilibrium behavior can occur, with one of the clusters being ordered while the other is disordered. We call this "chimera" state in analogy with similar phenomena recently seen in systems of coupled oscillators. We have also numerically established the existence of chimera order in 3-dimensional spin systems resembling layered magnetic materials thereby suggesting possible experimental observation of such states.

While the results described so far gives an indication of the rich variety of collective behavior in complex systems that emerge from their structure of the interactions among their elements, for many many natural systems these interactions themselves evolve over time in response to the dynamics of the components. In **Chapter 6** we investigate the coevolution of the interaction strengths with the dynamics on the nodes of a network. As in the preceding chapter, we consider a discrete dynamical system on each node, which can be in one of a finite number of states. In particular, we use the two-state Ising spin

to represent the state of each node, which allows us to study the evolution of structural balance in the model system. Structural balance, a concept that has been introduced in the context of social systems, is a property of signed networks. It corresponds to complete absence of conflicting constraints (referred to as frustration in the context of spin models in statistical physics), which results from incompatibilities between the states of the nodes and the sign of the links connecting them. We have considered networks, each of whose links are associated with a sign and a weight, corresponding to the nature and strength of interactions respectively. These links evolve using an adaptation rule, inspired by Hebb's principle, i.e., the link weights change in proportion to the correlation between activity of the connected elements. While this dynamics leads to structural balance, in the presence of stochastic fluctuations in the nodal dynamics, the time required to converge to this state exhibits extreme variability under suitable conditions. This divergence in the relaxation time scales is characterized by a bimodal distribution, which is observed for a wide range of system parameters. As larger fraction of positive interactions reduces frustration while larger fraction of negative interactions increases it, we have also investigated the role of bias in the sign of the interactions on the nature of the balanced state and the time required to converge to it. Our work suggests the intriguing possibility that biological networks may also evolve so as to approach balance.

We conclude with a short discussion of the general implications of the results reported in this thesis and indicate possible future directions of research.

2

Self-Organized transition to coherent activity in disordered media

2.1 Introduction

Rhythmic behavior is central to the normal functioning of many biological processes [28] and the periods of such oscillators span a wide range of time scales controlling almost every aspect of life [29–32]. Synchronization of spatially distributed oscillators is of crucial importance for many biological systems [18]. For example, disruption of coherent collective activity in the heart can result in life-threatening arrhythmia [33]. In several cases, the rhythmic behavior of the entire system is centrally organized by a specialized group of oscillators (often referred to as *pacemakers*) [34] as in the heart, where this function is performed in the sino-atrial node [35]. However, no such special coordinating agency has been identified for many biological processes. A promising mechanism for the self-organized emergence of coherence is through coupling among neighboring elements. Indeed, local interactions can lead to order without an organizing center in a broad class of complex systems [36, 37].

In this chapter we consider the self-organized emergence of coherent activity. This work is inspired by studies of the pregnant uterus whose principal function is critically dependent on coherent rhythmic contractions that, unlike the heart, do not appear to be centrally coordinated from a localized group of pacemaker cells [38]. In fact, the uterus remains quiescent almost throughout pregnancy until at the very late stage when large sustained periodic activity is observed immediately preceding the expulsion of the fetus [39]. In the USA, in more than 10 % of all pregnancies, rhythmic contractions are initiated significantly earlier, causing preterm births [40], which are responsible for more than a third of all infant deaths [41]. The causes of premature rhythmic activity are not well understood and at present there is no effective treatment for preterm labor [39].

We investigate here the emergence of coherence using a modeling approach that stresses the role of coupling in a system of heterogeneous entities. Importantly, recent studies have not revealed the presence of pacemaker cells in the uterus [42]. The uterine tissue has a heterogeneous composition, comprising electrically excitable smooth muscle cells (uterine myocytes), as well as electrically passive cells (fibroblasts and interstitial Cajal-like cells [ICLCs]) [43,44]. Cells are coupled in tissue by gap junctions that serve as electrical conductors. In the uterine tissue, the gap junctional couplings have been seen to markedly increase during late pregnancy and labor, both in terms of the number of such junctions and their conductances (by an order of magnitude [45,46]), which is the most striking of all electrophysiological changes the cells undergo during this period. The observation that isolated uterine cells do not spontaneously oscillate [42], whereas the organ rhythmically contracts when the number of gap junctions increases, strongly suggests a prominent role of the coupling. The above observations have motivated our model for the onset of spontaneous oscillatory activity and its synchronization through increased coupling in a mixed population of excitable and passive elements. While it has been shown earlier that an excitable cell connected to passive cells can oscillate [47–49], we demonstrate that coupling such oscillators with different frequencies (because of varying numbers of passive cells) can result in the system having a frequency *higher* than its constituent elements. We have

also performed a systematic characterization for the first time of the dynamical transitions occurring in the heterogeneous medium comprising active and passive cells as the coupling is increased, revealing a rich variety of synchronized activity in the absence of any pacemaker. Finally, we show that the system has multiple coexisting attractors characterized by distinct mean oscillation periods, with the nature of variation of the frequency with coupling depending on the choice of initial state as the coupling strength is varied. Our results provide a physical understanding of the transition from transient excitations to sustained rhythmic activity through physiological changes such as increased gap junction expression [50].

2.2 The Model

The dynamics of excitable myocytes can be described by a model having the form

$$C_m \dot{V}_e = -I_{ion}(V_e, g_i)$$

where V_e(mV) is the potential difference across a cellular membrane, C_m (= 1 μF cm^{-2}) is the membrane capacitance, I_{ion} (μA cm^{-2}) is the total current density through ion channels on the cellular membrane and g_i are the gating variables, describing the different ion channels. The specific functional form for I_{ion} varies in different models. To investigate the actual biological system we have first considered a detailed, realistic description of the uterine myocyte given by Tong *et al.* [51]. However, during the systematic dynamical characterization of the spatially extended system, for ease of computation we have used the phenomenological FitzHugh-Nagumo (FHN) system [33] which exhibits behavior qualitatively similar to the uterine myocyte model in the excitable regime. In the FHN model, the ionic current is given by

$$I_{ion} = F_e(V_e, g) = AV_e(V_e - \alpha)(1 - V_e) - g,$$

where g is an effective membrane conductance evolving with time as

$$\dot{g} = \epsilon(V_e - g),$$

$\alpha(= 0.2)$ is the excitation threshold, $A(= 3)$ specifies the fast activation kinetics and $\epsilon(= 0.08)$ characterizes the recovery rate of the medium (the parameter values are chosen such that the system is in the excitable regime and small variations do not affect the results qualitatively). The state of the electrically passive cell is described by the time-evolution of the single variable V_p [52]:

$$\dot{V}_p = F_p(V_p) = K(V_p^R - V_p),$$

where the resting state for the cell, V_p^R is set to 1.5 and $K(= 0.25)$ characterizes the time-scale over which perturbations away from V_p^R decay back to it. We model the interaction between a myocyte and one or more passive cells by:

$$\dot{V}_e = F_e(V_e, g) + n_p\, C_r(V_p - V_e), \tag{2.1a}$$

$$\dot{V}_p = F_p(V_p) - C_r(V_p - V_e), \tag{2.1b}$$

where $n_p(= 1, 2, \ldots)$ passive elements are coupled to an excitable element via the activation variable $V_{e,p}$ with strength C_r. Here, we have assumed for simplicity that all passive cells are identical having the same parameters V_p^R and K, as well as, starting from the same initial state. We observe that the coupled system comprising a realistic model of uterine myocyte and one or more passive cells exhibits oscillations (Fig. 2.1 (a)) qualitatively similar to the generic FHN model (Fig. 2.1 (b)), although the individual elements are incapable of spontaneous periodic activity in both cases. In Fig. 2.1 (a-b), the range of n_p and excitable-passive cell couplings for which limit cycle oscillations of the coupled system are observed is indicated with a pseudocolor representation of the period (τ). We also look at how a system obtained by diffusively coupling two such “oscillators" with

distinct frequencies (by virtue of having different n_p) behaves upon increasing the coupling constant D between V_e (Fig. 2.1 (c)). A surprising result here is that the combined system may oscillate *faster* than the individual oscillators comprising it.

To investigate the onset of spatial organization of periodic activity in the system we have considered a 2-dimensional medium of locally coupled excitable cells, where each excitable cell is connected to n_p passive cells [Fig. 2.1 (d)], n_p having a Poisson distribution with mean f. Thus, f is a measure of the density of passive cells relative to the myocytes. Our results reported here are for $f = 0.7$; we have verified for various values of $f \geq 0.5$ that qualitatively similar behavior is seen. The dynamics of the resulting medium is described by:

$$\frac{\partial V_e}{\partial t} = F_e(V_e, g) + n_p\, C_r(V_p - V_e) + D\nabla^2 V_e,$$

where D represents the strength of coupling between excitable elements (passive cells are not coupled to each other). Note that, in the limit of large D the behavior of the spatially extended medium can be reduced by a mean-field approximation to a single excitable element coupled to f passive cells. As f can be non-integer, n_p in the mean-field limit can take fractional values [as in Fig. 2.1 (a-b)].

We discretize the system on a square spatial grid of size $L \times L$ with the lattice spacing set to 1. For most results reported here $L = 64$, although we have used L up to 1024 to verify that the qualitative nature of the transition to global synchronization with increasing coupling is independent of system size. The dynamical equations are solved using a fourth-order Runge Kutta scheme with time-step $dt \leq 0.1$ and a standard 5-point stencil for the spatial coupling between the excitable elements. We have used periodic boundary conditions in the results reported here and verified that no-flux boundary conditions do not produce qualitatively different phenomena. Frequencies of individual elements are calculated using FFT of time-series for a duration 2^{15} time units. The behavior of the model for a specific set of values of f, C_r and D is analyzed over many (~ 100) realizations of

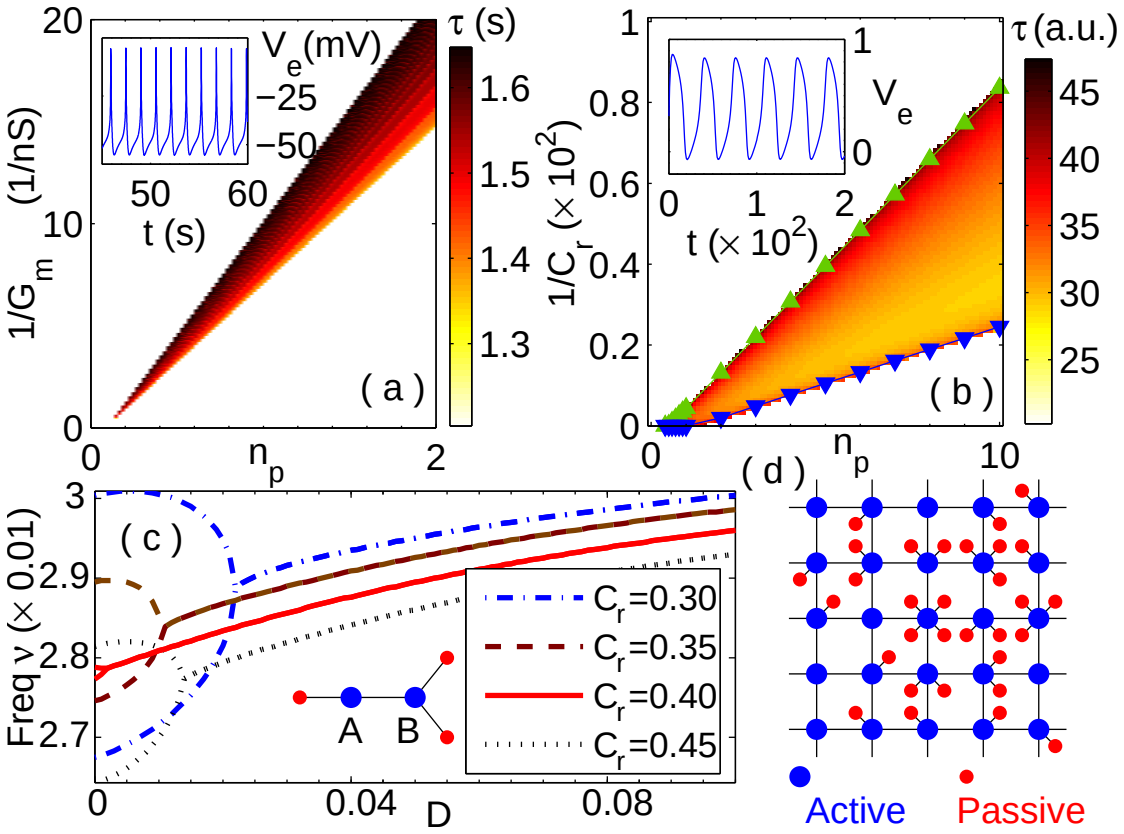

Figure 2.1: Oscillations through interaction between excitable and passive elements. A single excitable element described by (a) a detailed ionic model of an uterine myocyte and (b) a generic FHN model, coupled to n_p passive elements exhibits oscillatory activity (inset) with period τ for a specific range of gap junctional conductances G_m in (a) and coupling strengths C_r in (b). The triangles (upright and inverted) enclosing the region of periodic activity in (b) are obtained analytically by linear stability analysis of the fixed point solution of Eq. (2.1a). (c) Frequency of oscillation for a system of two "oscillators" A and B (each comprising an excitable cell and n_p passive cells with $n_p^A = 1$ and $n_p^B = 2$) coupled with strength D. Curves corresponding to different values of C_r show that the system synchronizes on increasing D, having a frequency that can be *higher* than either of the component oscillators. (d) Uterine tissue model as a 2-dimensional square lattice, every site occupied by an excitable cell coupled to a variable number of passive cells.

the n_p distribution with random initial conditions.

2.3 Results

To quantitatively analyze the dynamical transitions as the inter-cellular coupling is increased, we focus on the differences in the oscillatory behavior of individual elements in the simulation domain. In Fig. 2.2 (a) we see that at low D elements can have different periods, indicating the co-existence of multiple oscillation frequencies in the medium. This is explicit from the power spectral density of local activity at different sites [Fig. 2.2 (b)], which shows that there are multiple clusters in the domain, each being characterized by a principal frequency, ν [Fig. 2.2 (c)]. As all elements belonging to one cluster have the same period, we refer to this behavior as *cluster synchronization* (CS). Note that quiescent regions of non-oscillating elements, indicated in white in Fig. 2.2 (c), coexist with the clusters. As the coupling is increased the clusters merge [Fig. 2.2 (d)], thereby reducing the spread in the distribution of oscillation frequencies present in the medium, $P(\nu)$, eventually resulting in a single frequency for all oscillating elements (as seen for $D = 0.3$). As there are still a few local regions of inactivity, we term this behavior as *local synchronization* (LS). Further increasing D results in *global synchronization* (GS) characterized by *all* elements in the medium oscillating at the same frequency.

We can also interpret the dynamical transitions observed upon increasing the coupling between neighboring excitable elements as being coordinated by waves traveling over increasingly longer range in the system. Fig. 2.3 (first row) shows spatial activity in the system at different values of D after long durations ($\sim 2^{15}$ time units) starting from random initial conditions. As the coupling D between the excitable elements is increased, we observe a transition from highly localized, asynchronous excitations to spatially organized coherent activity that manifests as propagating waves. Similar traveling waves of excitation have indeed been experimentally observed *in vitro* in myometrial tissue from

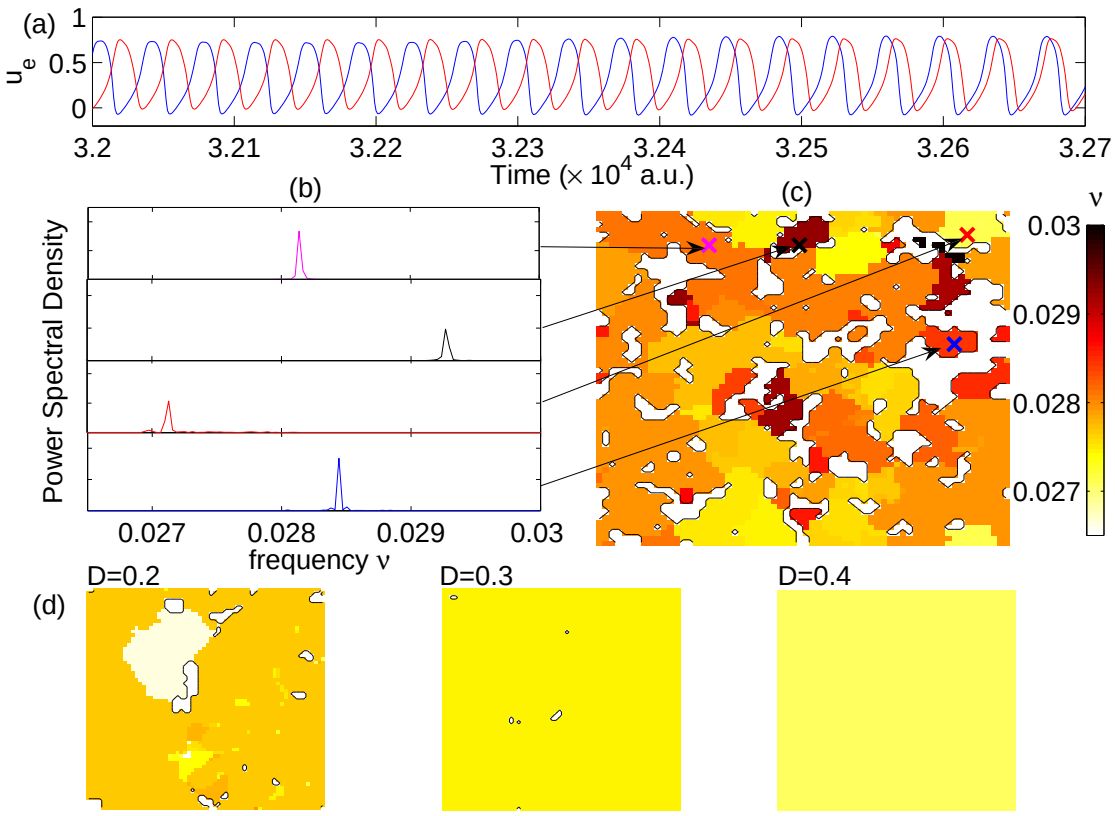

Figure 2.2: Synchronization via cluster merging. (a) Time-series of fast activation variable u_e for two excitable cells in the domain exhibiting distinct oscillation frequencies. (b) Power spectral density of u_e from four different sites [location shown in (c)] in a two-dimensional simulation domain with $L = 64$ ($f = 0.7, C_r = 1, D = 0.1$). (c) Pseudocolor plot indicating multiple clusters, each consisting of oscillators synchronized at a distinct frequency, i.e. cluster synchronization (white corresponding to absence of oscillation). (d) Increasing D from 0.1 in (c) to 0.2 in the left panel results in decreasing the number of clusters with distinct oscillation frequencies. Increasing D further to 0.3 results in local synchronization where all oscillators have the same frequency with a few patches showing absence of oscillation. When $D = 0.4$, all elements in the domain oscillate with same frequency (i.e. global synchronization).

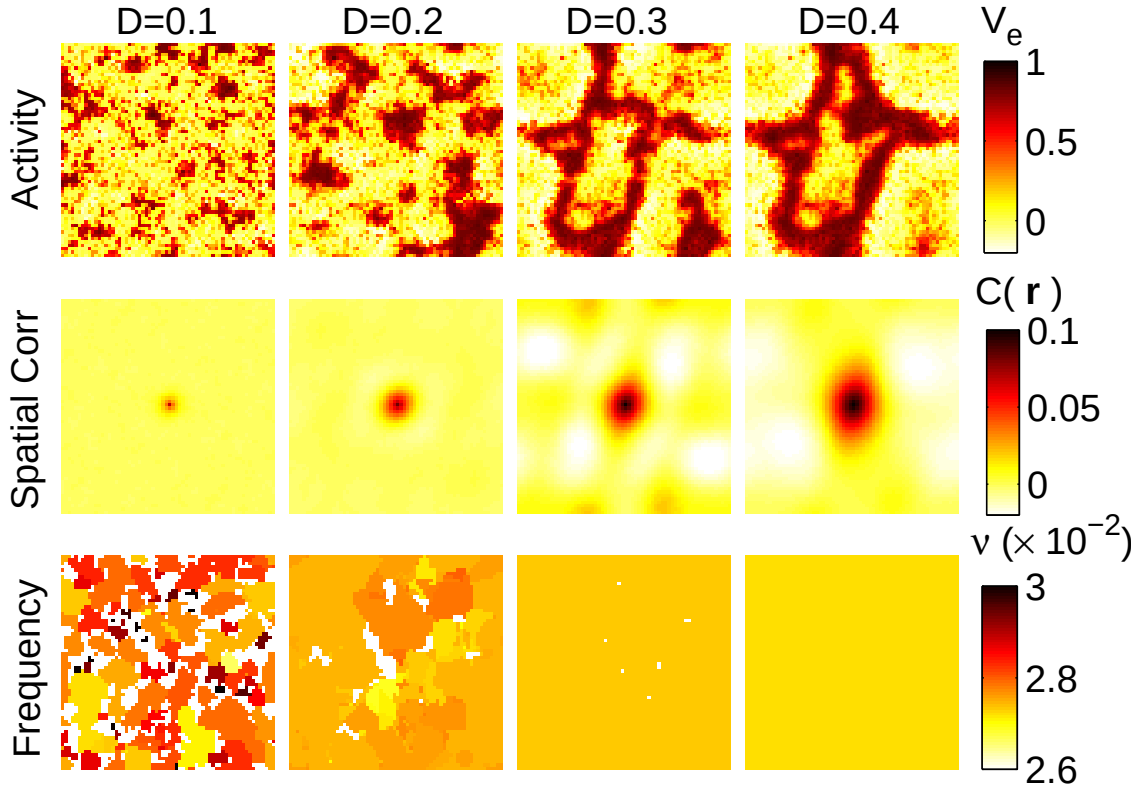

Figure 2.3: Emergence of synchronization via propagation of activity waves with increased coupling. Snapshots (first row) of the activity V_e in a two-dimensional simulation domain ($f = 0.7, C_r = 1, L = 64$) for increasing values of coupling D (with a given distribution of n_p). The corresponding time-averaged spatial correlation functions C($\mathbf{r}$) are shown in the middle row. The size of the region around $\mathbf{r} = 0$ (at center) where C($\mathbf{r}$) is high provides a measure of the correlation length scale which is seen to increase with D. The last row shows pseudocolor plots indicating the frequencies of individual oscillators in the medium (white corresponding to absence of oscillation). Increasing D results in decreasing the number of clusters with distinct oscillation frequencies, eventually leading to global synchronization characterized by spatially coherent, wavelike excitation patterns where all elements in the domain oscillate with same frequency.

the pregnant uterus [53]. The different dynamical regimes observed during the transition are accompanied by an increase in spatial correlation length scale (Fig. 2.3, middle row) and can be characterized by the spatial variation of frequencies of the constituent elements (Fig. 2.3, last row). For low coupling ($D = 0.1$), multiple clusters each with a distinct oscillation frequency ν coexist in the medium (CS). Note that there are also quiescent regions of non-oscillating elements indicated in white. With increased coupling the clusters merge, reducing the variance of the distribution of oscillation frequencies eventually resulting in a single frequency for all oscillating elements (LS, seen for $D = 0.3$). On increasing the coupling to even higher values ($D = 0.4$), a single wave traverses the entire system resulting in GS where *all* elements in the medium are oscillating at the same frequency. Our results thus help in causally connecting two well-known observations about electrical activity in the pregnant uterus: (a) there is a remarkable increase in cellular coupling through gap junctions close to onset of labor [45] and (b) excitations are initially infrequent and irregular, but gradually become sustained and coherent towards the end of labor [38].

The above observations motivate the following order parameters that allow us to quantitatively segregate the different synchronization regimes in the space of model parameters D and C_r [Fig. 2.4 (a)]. The CS state is characterized by a finite width of the frequency distribution as measured by the standard deviation, σ_ν, and the fraction of oscillating elements in the medium, $0 < f_{osc} < 1$. Both LS and GS states have $\sigma_\nu \to 0$, but differ in terms of f_{osc} (< 1 in LS, $\simeq 1$ in GS). Fig. 2.4 (b-c) shows the variation of the two order parameters $\langle \sigma_\nu \rangle$ and $\langle f_{osc} \rangle$ with the coupling D, $\langle\ \rangle$ indicating ensemble average over many realizations. Varying the excitable cell-passive cell coupling C_r together with D allows us to explore the rich variety of spatio-temporal behavior that the system is capable of [Fig. 2.4 (a)]. In addition to the different synchronized states (CS, LS and GS), we also observe a region where there is no oscillation (NO) characterized by $f_{osc} \to 0$, and a state where all elements oscillate with the same frequency and phase which we term coherence (COH). COH is identified by the condition that the order parameter $F \equiv \max_t[f_{act}(t)] \to 1$

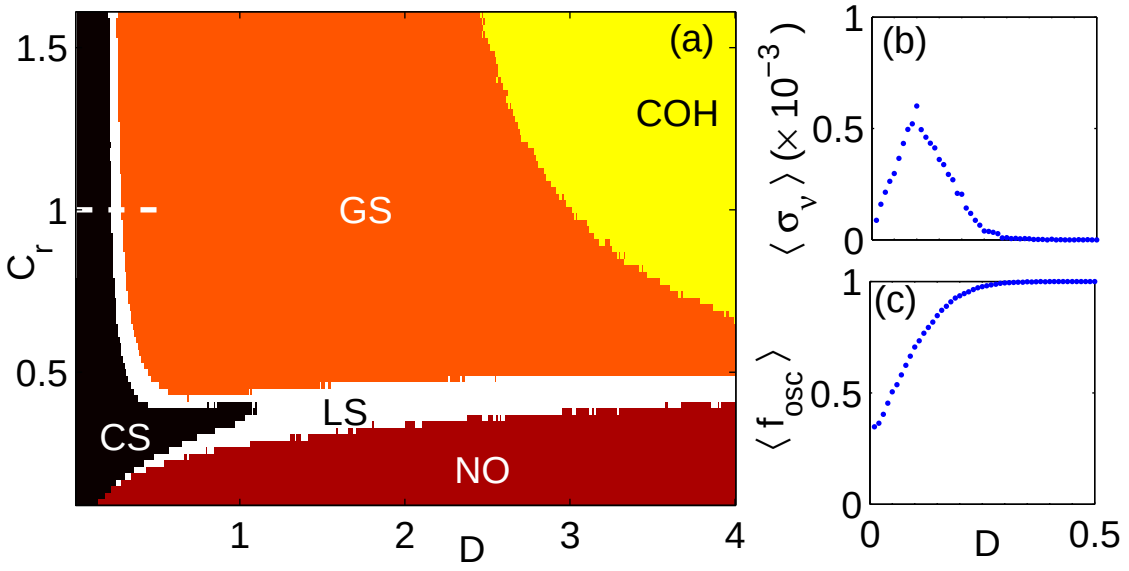

Figure 2.4: (a) Different dynamical regimes of the uterine tissue model (for $f = 0.7$) in $D - C_r$ parameter plane indicating the regions having (i) complete absence of oscillation (NO), (ii) cluster synchronization (CS), (iii) local synchronization (LS), (iv) global synchronization (GS) and (v) coherence (COH). (b-c) Variation of (b) width of frequency distribution $\langle \sigma_v \rangle$ and (c) fraction of oscillating cells $\langle f_{osc} \rangle$ with coupling strength D for $C_r = 1$ [i.e., along the broken line shown in (a)]. The regimes in (a) are distinguished by thresholds applied on order parameters $\langle \sigma_v \rangle$, $\langle f_{osc} \rangle$ and $\langle F \rangle$, viz., NO: $\langle f_{osc} \rangle < 10^{-3}$, CS: $\langle \sigma_v \rangle > 10^{-4}$, LS: $\langle \sigma_v \rangle < 10^{-4}$ and $\langle f_{osc} \rangle < 0.99$; GS: $\langle f_{osc} \rangle > 0.99$ and COH: $\langle F \rangle > 0.995$. Results shown are averaged over many realizations.

where $f_{act}(t)$ is the fraction of elements that are active ($V_e > \alpha$) at time t. In practice, the different states are characterized by thresholds whose specific values do not affect the qualitative nature of the results.

To further characterize the state of the system, we determined the mean frequency $\bar{\nu}$ by averaging over all oscillating cells for any given realization of the system. Fig. 2.5 (a) reveals that several values of the mean frequency are possible at a given coupling strength. When the initial conditions are chosen randomly for each value of the coupling (broken curve in Fig. 2.5 (a)), the mean frequency decreases with increasing D. On the other hand, $\bar{\nu}$ is observed to *increase* with D when the system is allowed to evolve starting from a random initial state at low D, and then adiabatically increasing the value of D. The abrupt jumps correspond to drastic changes in the size of the basin of an attractor at certain values of the coupling strength, which can be investigated in detail in future studies. This suggests a multistable attractor landscape of the system dynamics, with the basins of the multiple attractors shown in Fig. 2.5 (d) [each corresponding to a characteristic spatiotemporal pattern of activity shown in Fig. 2.5 (e)] having differing sizes. They represent one or more plane waves propagating in the medium and are quite distinct from the disordered patterns of spreading activity (Fig. 2.5 (b-c)) seen when random initial conditions are used at each value of D. We note that the period of recurrent activity in the uterus decreases with time as it comes closer to term [50] in conjunction with the increase in number of gap junctions. This is consistent with our result in Fig. 2.5(a) when considering a gradual increase of the coupling D.

As previously mentioned, the above results are for a fixed value of f, the mean number of passive cells per excitable cell. To investigate how varying the density of passive cells affects the spatial coherence in activity, we have considered a special case of the passive cell distribution to define another spatially extended, 2-dimensional lattice model for the uterine tissue. Here, an excitable cell, located at each lattice site, can be connected to either one or no passive cells (Fig. 2.6, left). This has the simplifying feature that the

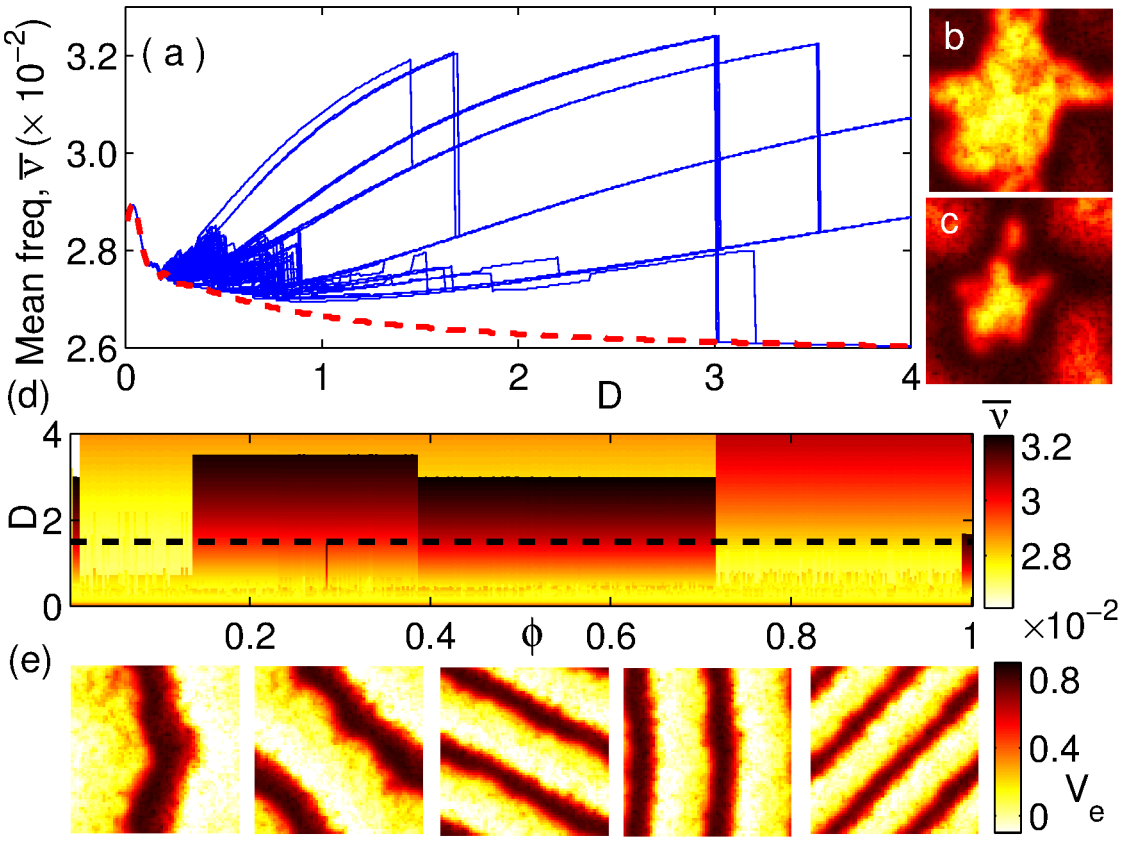

Figure 2.5: (a) Variation of mean oscillation frequency $\overline{\nu}$ with coupling strength D in the uterine tissue model ($f = 0.7$) for 400 different initial conditions at $C_r = 1$. Continuous curves correspond to gradually increasing D starting from a random initial state at low D, while broken curves (overlapping) correspond to random initial conditions chosen at each value of D. (b-c) Snapshots of activity in the medium at $D = 1.5$ for a random initial condition seen at intervals of $\delta T = 5$ time units. (d) Variation of the cumulative fractional volumes ϕ of the basins for different attractors corresponding to activation patterns shown in (b-c) and (e), as a function of the coupling strength D. (e) Snapshots of topologically distinct patterns of activity corresponding to the five attractors at $D = 1.5$ [shown by a broken line in (d)] when D is increased.

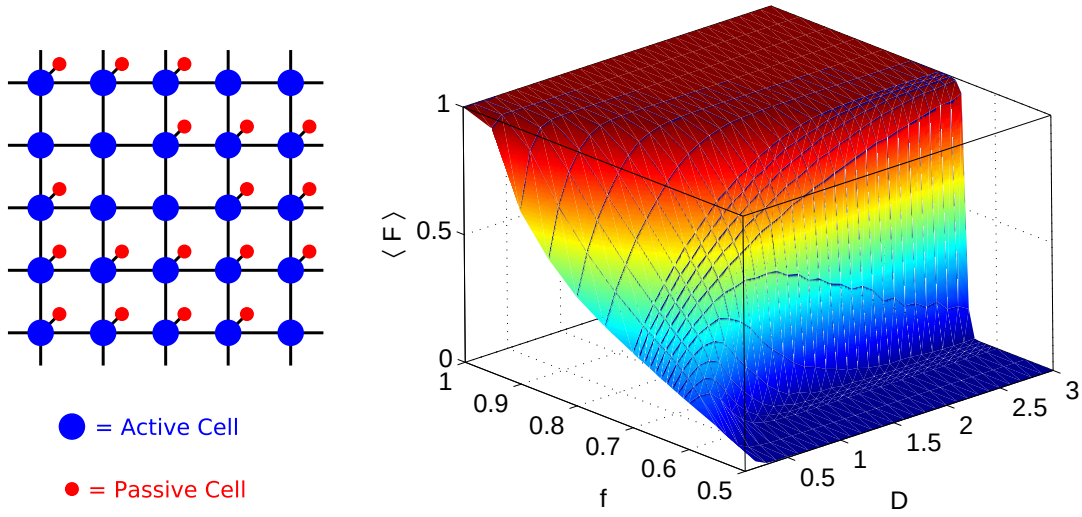

Figure 2.6: (left) A 2-dimensional square lattice model for uterine tissue where individual excitable cells (located at each site) can couple to either one or no passive cell. (right) Variation of the mean value of the order parameter, $\langle F \rangle$, characterizing coherence (COH) shown as a function of the passive cell density (f) and the coupling strength D between the excitable cells, for $C_r = 0.6$.

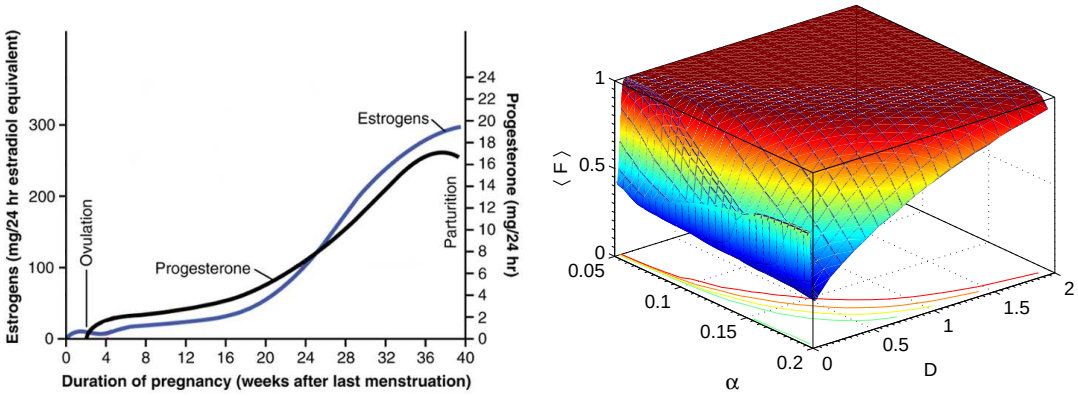

Figure 2.7: (left) Rate of production of human pregnancy-related hormones estrogen and progesterone over the course of pregnancy (adapted from Ref. [54]). (right) Variation of the mean value of the order parameter, $\langle F \rangle$, characterizing coherence (COH) shown as a function of the excitation threshold (α) and the coupling strength D between the excitable cells, for $C_r = 0.6$.

individual lattice sites either don't oscillate or oscillate at the same frequency in isolation. In this scenario, the passive cell density, f, which is the same as the fraction of oscillators in the lattice, varies between 0 and 1. When $f = 1$, the system corresponds to a *homogeneous* oscillatory medium. As the coupling between the excitable elements is increased, we observe that for high value of f the system becomes coherent (COH) as in the lattice model used earlier. At low passive cell density, increasing D results in cessation of oscillation (NO) [Fig. 2.6 (right)]. The transition to coherence can also be observed as a function of increasing passive cell density. For lower coupling, this exhibits a gradual rise, while at higher coupling there is an abrupt change in the order parameter characterizing coherence. This can be explained as a result of the system dynamics approaching that expected in the mean-field limit as the coupling D is increased.

An important biological factor that is believed to regulate the onset of uterine activity is the secretion of different hormones, such as estrogen and progesterone [54]. Estrogen increases the excitability of the myometrium, while pregesterone reduces it [55], so that altering the balance between the two can result in the uterus being quiescent or undergoing contractions. As seen from Fig. 2.7 (left), the rate of secretion of both these hormones increase during the course of pregnancy. However, close to term, the progesterone rate falls slightly while that of estrogen keeps increasing. This presumably results in a large increase in the myometrium excitability resulting in stimulation of uterine contractions. In our model, the role of such hormones can be incorporated by simply altering the value of the threshold of the excitable cells, α. Increasing ratio of estrogen to progesterone production rates can be modeled as reducing α which has the effect of making the medium more excitable. Fig. 2.7 (right) shows that coherence is achieved by either increasing excitability (i.e., reducing α) or increasing the coupling strength D between excitable cells or both. Thus, we believe that the role of hormones essentially amplifies quantiatively the coherence that is achieved in our model through increased coupling.

2.4 Discussion and Conclusion

Our results explain several important features known about the emergence of contractions in uterine tissue. Previous experimental results have demonstrated that the coupling between cells in the myometrium increases with progress of pregnancy [45]. This suggests that the changes in the system with time amounts to simultaneous increase of D and C_r, eventually leading to synchronization as shown in Fig. 2.4 (a). Such a scenario is supported by experimental evidence that disruption of gap-junctional communication is associated with acute inhibition of spontaneous uterine contractions [56]. The mechanism of synchronization discussed here is based on a very generic model, suggesting that our results apply to a broad class of systems comprising coupled excitable and passive cells [57, 58]. A possible extension will be to investigate the effect of long-range connections [59, 60].

To conclude, we have shown that coherent periodic activity can emerge in a system of heterogeneous cells in a self-organized manner and does not require the presence of a centralized coordinating group of pacemaker cells. A rich variety of collective behavior is observed in the system under different conditions; in particular, for intermediate cellular coupling, groups of cells spontaneously form clusters that oscillate at different frequencies. With increased coupling, clusters merge and eventually give rise to a globally synchronized state marked by the genesis of propagating waves of excitation in the medium. Our model predicts that a similar set of changes occur in the uterus during late stages of pregnancy.

3

Spatiotemporal pattern formation in homogeneous system of relaxation oscillators

3.1 Introduction

The problem of understanding pattern formation across a variety of chemical and biological contexts [10, 61] has stimulated much theoretical and experimental activity since the early work of Turing [16, 62, 63]. Studying the dynamics of coupled biochemical oscillators interacting through reaction-diffusion mechanisms constitutes a particularly promising approach to understanding the genesis of patterns in natural systems [64]. Generalizations of such processes involving differential excitatory and inhibitory interactions between elements as represented by the coupling terms, have been used to represent a variety of complex systems [65–67]. They have also been proposed recently as a possible mechanism for computation in biological and chemical systems [68, 69].

The stationary patterns exhibited by the models mentioned above represent only a frac-

tion of the variety seen in nature, many of which exhibit periodic activity. Thus, extending ideas underlying reaction-diffusion mechanisms to systems of interacting relaxation oscillators should permit investigation of spatio-temporal patterns in biological systems, where oscillations are observed across many spatial and temporal scales, ranging from the periodic variations of intracellular molecular concentrations [70, 71] to changes in the activity levels of different brain areas [72]. The coherent dynamics of these oscillators can produce functionally important collective behavior such as synchronization [73] yielding different biological rhythms [74]. However, synchronized oscillations constitute only one of a number of possible collective phenomena that can emerge from such interactions. For example, a recent set of experiments on coupled chemical oscillators in a microfluidic device [75, 76] have shown that anti-phase synchronization as well as spatially heterogeneous oscillator death states [77] can occur in this system under different conditions. Extending the mechanism of coupling by lateral inhibition (e.g., via a rapidly diffusing inhibitory chemical species) to arrays of relaxation oscillators, used for modeling biological periodic activity, can be expected to reveal the underlying mechanism for a variety of spatio-temporal phenomena seen in natural systems.

In this chapter, we study a generic model of relaxation oscillators, each comprising activator and inactivating components, coupled to nearest neighbors through lateral inhibition via diffusion of the inactivating component (in line with the experiments mentioned above). Our model is capable of exhibiting a variety of spatio-temporal patterns which may be observed experimentally, while its simplicity allows an analytical understanding of their genesis. We provide a simple theoretical demonstration of the existence and stability of an anti-phase synchronized state for coupled relaxation oscillators. In addition to reproducing some patterns reported earlier, we also observe novel states, such as attractors corresponding to spatially co-existing dynamically distinct configurations, which we term chimera states. Although homogeneous arrays of generic relaxation oscillators have been studied extensively, our observation of these spatially heterogeneous attractors for such systems is new to the best of our knowledge. We characterize basins of attraction for

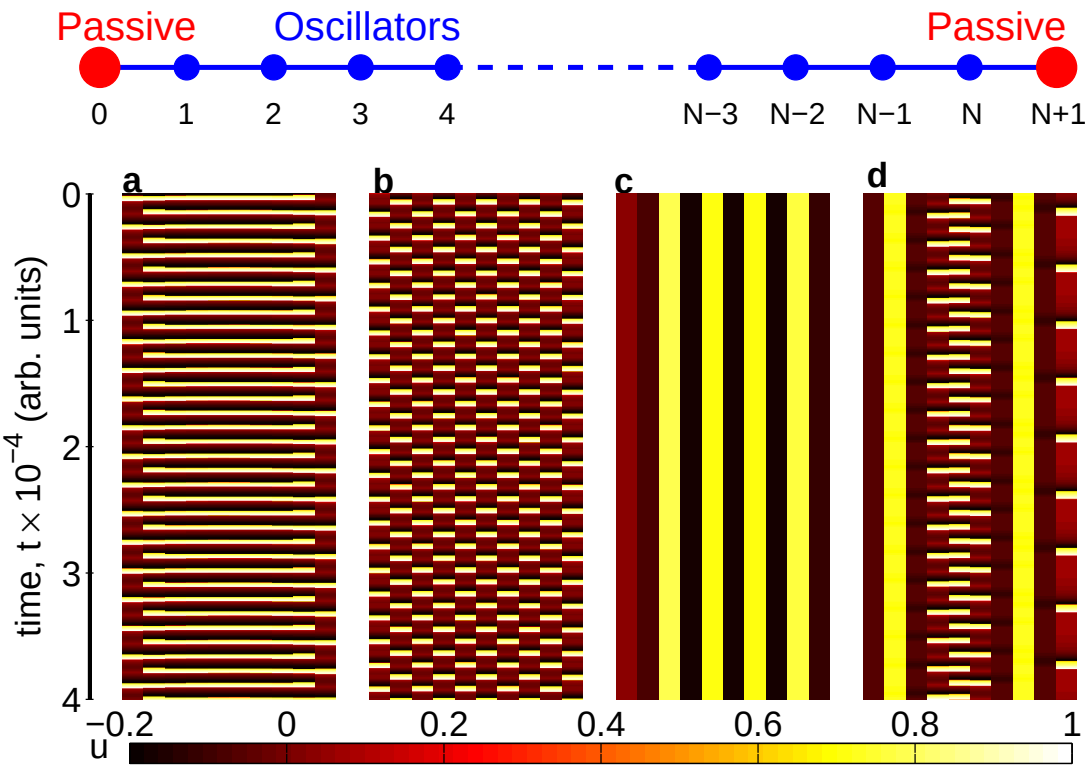

Figure 3.1: Spatio-temporal evolution of a 1-dimensional array of coupled relaxation oscillators ($N = 10$) with passive elements at the boundaries [model system shown schematically on top]. Pseudocolor plots of the activation variable u indicate different regimes characterized by (a) synchronized oscillations (SO), (b) anti-phase synchronization (APS), (c) spatially patterned oscillation death (SPOD) and (d) chimera state (CS), i.e., co-occurrence of spatial patches with dynamically distinct behavior.

various patterns seen in the model, also demonstrating an unexpected robustness of the chimera states. This robustness suggests that the states we describe can be reproduced in suitably designed experiments. We report phase defect-like discontinuities moving ballistically through the system, producing complex patterns on collision with each other. We observe analogous structures in two-dimensional media that bear a striking resemblance to persistent configurations in cellular automata (CA) [80], which have been linked to the universal computation capabilities of such systems [81–83].

3.2 The Model

Our model system comprises N relaxation oscillators interacting with each other in a specific topology. For the dynamics of individual relaxation oscillators we use the phenomenological FitzHugh-Nagumo (FHN) equations, which are a generic model for such systems. Each oscillator is described by a fast activation variable u and a slow inactivation variable v:

$$\begin{aligned} \dot{u} &= f(u,v) = u\,(1-u)\,(u-\alpha) - v, \\ \dot{v} &= g(u,v) = \epsilon\,(k\,u - v - b), \end{aligned} \tag{3.1}$$

where $\alpha = 0.139$, $k = 0.6$ are parameters describing the kinetics, $\epsilon = 0.001$ characterizes the recovery rate of the medium and b is a measure of the asymmetry of the oscillator (measured by the ratio of the time spent by the oscillator at high and low value branches of u). Parameter values are chosen such that the system is in the oscillatory regime. We have checked that small variations in the values do not affect our results qualitatively. To investigate spatial patterns generated by interaction between the oscillators, we arrange them in a 1-dimensional chain [Fig. 3.1 (top)]. In the chemical experiments, the beads containing the reactive solution are suspended in a chemically inert medium which allows passage of only the inhibitory chemical species [75]. In our model, the oscillators are diffusively coupled via the inactivation variable v. The boundary conditions for the chain take into account the inert medium by including non-reactive passive elements at each end that are diffusively coupled to the neighboring oscillators. The inert medium between the oscillators is not considered explicitly, its volume being relatively small compared to the reservoirs at the boundary. We have verified that inclusion of intermediate non-reactive cells diffusively coupling each pair of oscillators does not affect the fixed-point equilibria of the system or their stability, once the diffusion constant is suitably scaled.

The dynamics of the resulting system is described by

$$\begin{aligned}
\dot{u}_i &= f(u_i, v_i) + D_u\,(u_{i-1} + u_{i+1} - 2\,u_i), \\
\dot{v}_i &= g(u_i, v_i) + D_v\,(v_{i-1} + v_{i+1} - 2\,v_i), \\
\dot{v}_0 &= D_v\,(v_1 - v_0), \qquad \dot{v}_{N+1} = D_v\,(v_N - v_{N+1}),
\end{aligned} \tag{3.2}$$

where $i = 1, 2, \ldots, N$ and the diffusion constants D_u, D_v represent the strength of coupling between neighboring relaxation oscillators through their activation and inactivation variables, respectively. For most results reported here we have considered only diffusion of the inactivation variable, i.e., $D_u = 0$. For the simulations of the model system we have mostly used either $N = 10$ or 20, although larger values of N upto 1000 have been used to verify that our results are not sensitively dependent on system size. We have verified that the boundary conditions do not affect the results significantly by also considering periodic boundaries and observing patterns qualitatively identical to those reported here. The dynamical equations are solved using an adaptive Runge-Kutta scheme. The behavior of the system for each set of parameter values b and D_v is analyzed over many (10^4) initial conditions, with each oscillator having a random phase chosen from a uniform distribution.

3.3 Results

Fig. 3.1 (a-d) shows a variety of asymptotic spatio-temporal patterns that we observe in the model system: (a) synchronized oscillations (SO) with all elements (except those at the boundary) having the same phase, (b) anti-phase synchronization (APS) with neighboring elements in opposite phase, (c) Spatially Patterned Oscillator Death (SPOD) regime where the oscillators are arrested in various stationary states and (d) Chimera States (CS) where oscillating regions co-exist with patches showing negligible temporal variation. However, these do not exhaust the range of possible spatio-temporal phenomena that are observed

including propagating structures that are discussed later. Both APS and SPOD states have been observed experimentally in chemical systems [75]. Although the latter has been referred to as "Turing patterns" in the literature, we stress that SPOD is distinct as it is not obtained through destabilization of a homogeneous equilibrium (Turing instability) but occurs through a process of oscillator death [77]. There is a simple mathematical reason why the mechanism involved in generating SPOD *cannot* be Turing instability: the Jacobian matrix corresponding to the stable fixed point of the FHN model has the structure

$$\begin{pmatrix} - & - \\ + & - \end{pmatrix}$$

from which it immediately follows that the fixed point cannot be destabilized by the Turing mechanism [14].

To investigate the robustness of the observed patterns in detail, we numerically estimate the size of their basins of attraction in the (b, D_v) parameter space (Fig. 3.2). To identify distinct pattern regimes in (b, D_v) space [Fig. 3.2 (a)] we introduce the following order parameters. The number of non-oscillating cells in the bulk of the system, N_{no}, i.e., cells for which the variance with respect ot time of the activation variable u, $\sigma_t^2(u_i)$, is zero, is used to characterize the SPOD ($N_{no} = N$) and CS regimes ($0 < N_{no} < N$). Both SO and APS states have all elements in the bulk oscillating. However, SO is distinguished by having all oscillators in the same phase as measured by the variance of the activation variables u, $\langle \sigma_i^2(u) \rangle_t = 0$, where $\langle\ \rangle_t$ represents time average. We can also define the synchronization among the oscillators in two distinct (even, odd) sub-lattices, as measured by the time-averaged variance of the activation variable, viz., $\langle \sigma_{even}^2(u) \rangle_t$ and $\langle \sigma_{odd}^2(u) \rangle_t$. This pair of order parameters is zero for both SO and APS states; however, if $\langle \sigma_i^2(u) \rangle_t > 0$, it signifies the APS regime. In practice, different regimes are characterized by thresholds whose specific values do not affect the qualitative nature of the results. Fig. 3.2 (a) indicates the parameter regions where SO, APS, SPOD and CS states are observed for more than 50% of initial conditions (i.e., they have the largest basin). As mentioned earlier, the

system also exhibits other regimes apart from the above ones, which occur in regions of (b, D_v) parameter space shown in white.

While diffusive coupling in a homogeneous system of oscillators is expected to promote the SO state [18], a striking observation from this phase diagram is that the APS state has a very large basin of attraction in certain regions [Fig. 3.2(b)]. The existence of APS is somewhat counter-intuitive as for diffusively coupled identical isochronous oscillators the only stable attractors are synchronized oscillations or oscillator death [18]. To understand the origin of such anti-phase oscillations we consider a simple model that captures the essence of relaxation oscillation phenomena and can be solved exactly. We consider the relaxation limit ($\epsilon \to 0$ in FHN system) and extreme asymmetry where the limit cycle has a slow segment in which the system spends the entire duration of the oscillation period (the remaining segment of the cycle being traversed extremely fast). In this limit, we obtain the one-dimensional dynamical system: $\dot{x} = \omega(x)$, where x parameterizes the slow part of the limit cycle and can be redefined to belong to the interval $(0, 1)$. Fig. 3.3 (a) shows a schematic diagram of the trajectory of the limit cycle, where the system spends almost its entire oscillation period on the solid branch (the return from $x = 1$ to $x = 0$, shown by the broken line, is considered to be instantaneous). The model can be exactly solved if $\omega(x)$ is a constant ($= \omega$, say), although the geometrical argument is valid for any arbitrary positive definite function defined over the interval $(0, 1)$. By appropriate choice of time scale we set the period $\omega^{-1} = 1$. A system of two such diffusively coupled oscillators can be described by

$$\dot{x}_1 = 1 + D\,(x_2 - x_1), \quad \dot{x}_2 = 1 + D\,(x_1 - x_2). \tag{3.3}$$

Given the values of x_1, x_2 at some arbitrary initial time t', the solution of Eqn. (3.3) at a

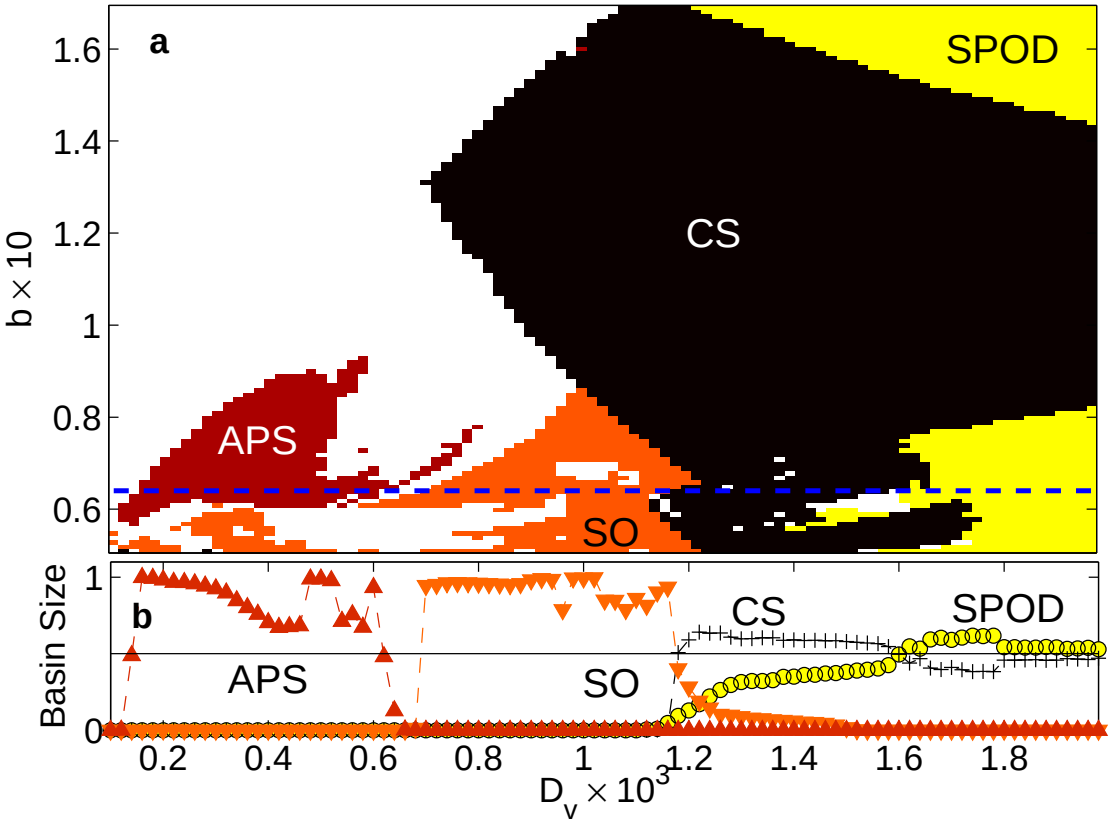

Figure 3.2: Different dynamical regimes of a 1-dimensional array of coupled relaxation oscillators ($N = 10$) in the $D_v - b$ parameter plane showing regions where the majority ($> 50\%$) of initial conditions result in synchronized oscillations (SO), anti-phase synchronization (APS), spatially patterned oscillator death (SPOD) and chimera state (CS). (b) Variation of the attraction basin size for the different regimes mentioned above (measured as fraction of initial states reaching the attractor) with coupling strength D for $b = 0.064$ [i.e., along the broken line shown in (a)]. In practice, the regimes are distinguished by thresholds applied on the order parameters $\sigma_t^2(u_i)$, $\langle\sigma_i^2(u)\rangle_t$, $\langle\sigma_{even}^2(u)\rangle_t$ and $\langle\sigma_{odd}^2(u)\rangle_t$, which have been taken to be 0.05 for the present figure. Basin sizes have been estimated using 10^4 initial conditions.

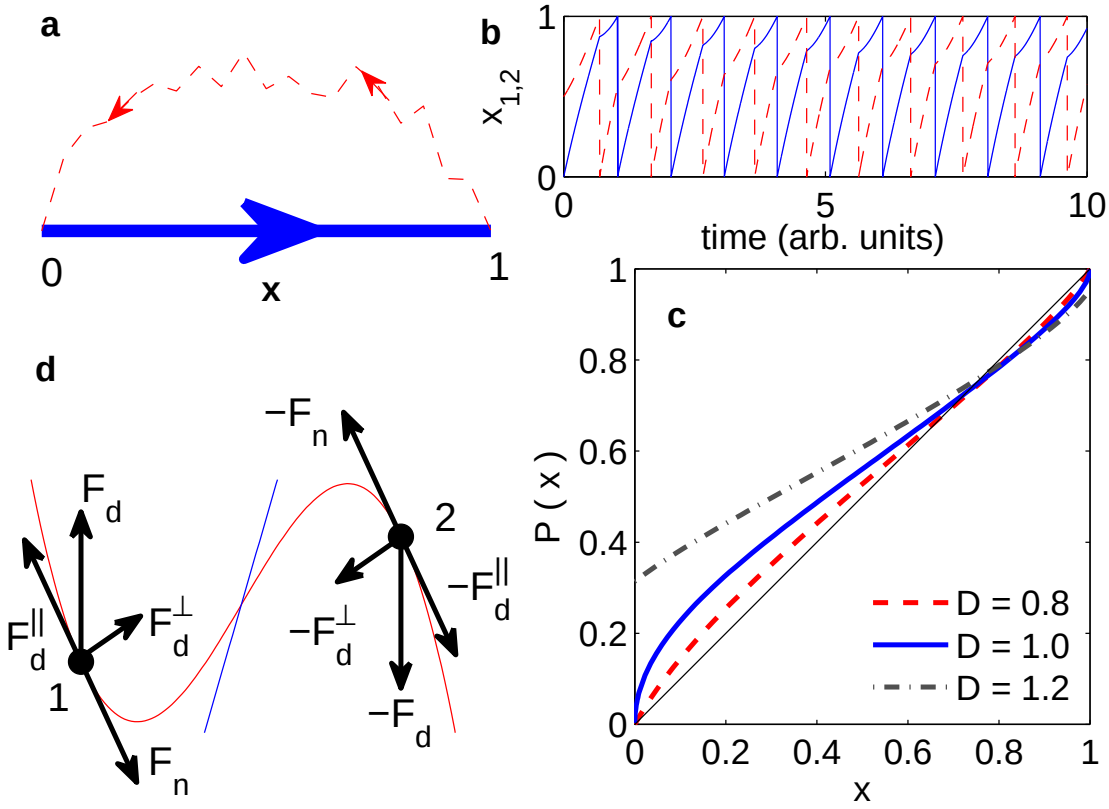

Figure 3.3: (a) Schematic diagram of a limit cycle trajectory for an oscillator in the relaxation limit ($\epsilon \to 0$) and extreme asymmetry (for details see text) such that the oscillator is on the solid line ($0 < x < 1$) for almost its entire period. (b) Time-series of two such coupled oscillators [Eqn. (3.3) with $D = 1$] and (c) the Poincare map for the system at different coupling strengths D showing stable anti-phase synchronization. (d) Phase-plane diagram indicating the general mechanism (see text) for oscillator death in a system of two coupled oscillators (1 and 2).

later time t follows the relations:

$$\begin{aligned} x_1(t) + x_2(t) &= x_1(t') + x_2(t') + 2(t - t'), \\ x_1(t) - x_2(t) &= [x_1(t') - x_2(t')]\ \exp[-2D(t - t')], \end{aligned} \tag{3.4}$$

till time t'' when $max(x_1, x_2)$ reaches $x = 1$. After this the larger of (x_1, x_2) is mapped back to $x = 0$ (because of the instantaneous nature of the remaining segment of the limit cycle) and t' is replaced by t''. Using the above exact solution of the coupled system (3.3), its Poincare map $P(x)$ is constructed in two steps. First, if x_1 starts at 0 and x_2 starts at some point $0 < x < 1$, we find the location of $x_1[= f(x)]$ at some time t when $x_2 = 1$

(which is then immediately mapped to $x_2 = 0$). Now, starting with $x_2 = 0$ and $x_1 = f(x)$, when $x_1 = 1$ we find the location of x_2: $x' = f(f(x)) = P(x)$. Using solution (3.4), with $x_1(t') = 0$, $x_2(t') = x$, $x_1(t) = f(x)$ and $x_2(t) = 1$, we get

$$f(x) = 1 + D^{-1}\, W[-Dx\, \exp\{D(x-2)\}],$$

where W is the Lambert W-function. Fig. 3.3 (c) shows the Poincare map $P(x) = f(f(x))$ for different values of the coupling strength D. The map has one stable and one unstable fixed point, which correspond to the anti-phase synchronized (APS) and synchronized oscillating (SO) states, respectively. Thus, for the model (3.3) we find that APS is the only stable state. Relaxing the extremal conditions under which this was derived may allow a stable SO state to coexist with the stable APS state [84]. This is a fundamental mechanism for generating APS states in any system of diffusively coupled oscillators exhibiting anti-phase oscillations.

When the coupling D_v between oscillators in the array is increased to very high values, we observe that the oscillatory regimes (e.g., SO and APS) are replaced by stationary spatial patterns such as SPOD (Fig. 3.2). To understand the genesis of SPOD at strong coupling, we can again focus on a pair of coupled relaxation oscillators in the relaxation limit ($\epsilon \to 0$). The parameter b is chosen such that the v-nullcline is placed symmetrically between the two branches of the u-nullcline with the oscillator taking equal time to traverse each branch [Fig. 3.3 (d)]. When the two oscillators (1 and 2) are in opposite branches (as shown in the schematic diagram), the two opposing forces acting on each oscillator, corresponding to the coupling [$F_d = D_v(v_2 - v_1)$] and the intrinsic kinetics (F_n) respectively, can exactly cancel when the coupling is strong resulting in oscillator death. Symmetry ensures that the force due to the intrinsic kinetics for the two oscillators is identical in magnitude but oppositely directed in the steady state. The occurrence and stabilization of this *heterogeneous* stationary state is the key to the occurrence of SPOD at strong coupling.

At intermediate values of coupling D_v in large arrays, the competition of the above mechanism with the intrinsic oscillatory dynamics dominant at low coupling, may give rise to chimera states. This CS regime is especially interesting as the system exhibits a remarkable heterogeneous dynamical state in spite of the bulk being homogeneous. The occurrence of CS is not dependent on boundary conditions as it is also reproduced with periodic boundaries. The observation of such states in a generic model of relaxation oscillators suggests that they should be present in a wide class of systems; similar phenomena have been recently reported in a specific chemical system model [85]. The chimera state described here comprises regions with dynamically distinct behavior, as opposed to its recent usage referring to the co-occurrence of coherent and non-coherent domains [78, 79].

Aside from the spatio-temporal patterns in Fig. 3.1 (a-d) we also observe attractors having point-like “phase defects” (i.e., with a discontinuity of phase along the oscillator array at this point), moving in the background of system-wide oscillations. As seen from a typical example of such states [Fig. 3.4 (a)], after initial transients these defects move in the medium with interactions between two such entities resulting in either the two being deflected in opposite directions, or either both or only one getting annihilated. This is unlike the situation of oppositely charged defects in non-oscillatory media which typically annihilate on collision [86]. While the boundary for systems with passive elements at the ends is a source of new defects entering the medium, similar persistent structures are also seen in systems with periodic boundary conditions where, in the steady state, a conserved number of defects can reflect off each other indefinitely [Fig. 3.4 (b)].

To observe how these propagating defects manifest in higher dimensional systems, we consider a 2-dimensional array of coupled oscillators defined on a torus. The system can have extremely complicated transient phenomena, and for simplicity we discuss only its asymptotic behavior. For a square lattice, we observe that there is a specific configuration of four sites that persists indefinitely (reminiscent of the *glider* configurations in the 2-dimensional CA “Game of Life" [80]). These structures can move in horizontal or vertical

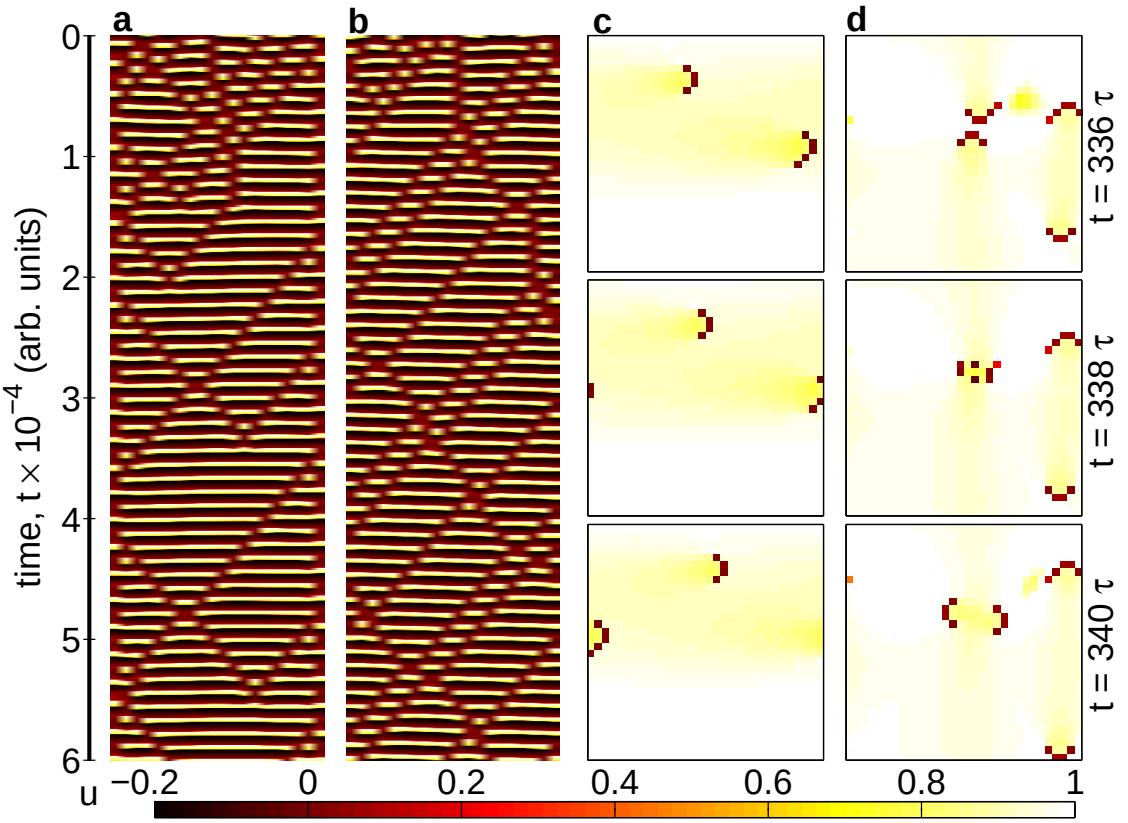

Figure 3.4: (a-b) Spatio-temporal evolution of a system of coupled relaxation oscillators showing traveling waves of phase defects in (a) a linear array with passive elements at the boundaries and (b) with periodic boundary conditions. (c-d) Propagating defects in two-dimensional media with periodic boundary condition showing (c) two horizontally moving “gliders" and (d) collision of two “gliders". For clear visualization of the motion of the spatially extended defects, snapshots of the two-dimensional medium are taken at intervals which are multiples of the oscillation period for the mean activity of the system τ.

directions [Fig. 3.4 (c)]. The interaction of such “gliders” can produce complex spatio-temporal patterns, e.g., Fig. 3.4 (d) which shows two “gliders” that on collision move off in directions perpendicular to their incident ones.

So far we have assumed that only the inactivation variable v can diffuse as this is the situation in the experimental system that motivated our study. However, in principle, one can conceive of a system where both activation and inactivation variables can diffuse through the medium. To investigate the effect of such interactions on the collective dynamics of the system of coupled oscillators, we have considered the simplest case $D_u = D_v = D$,

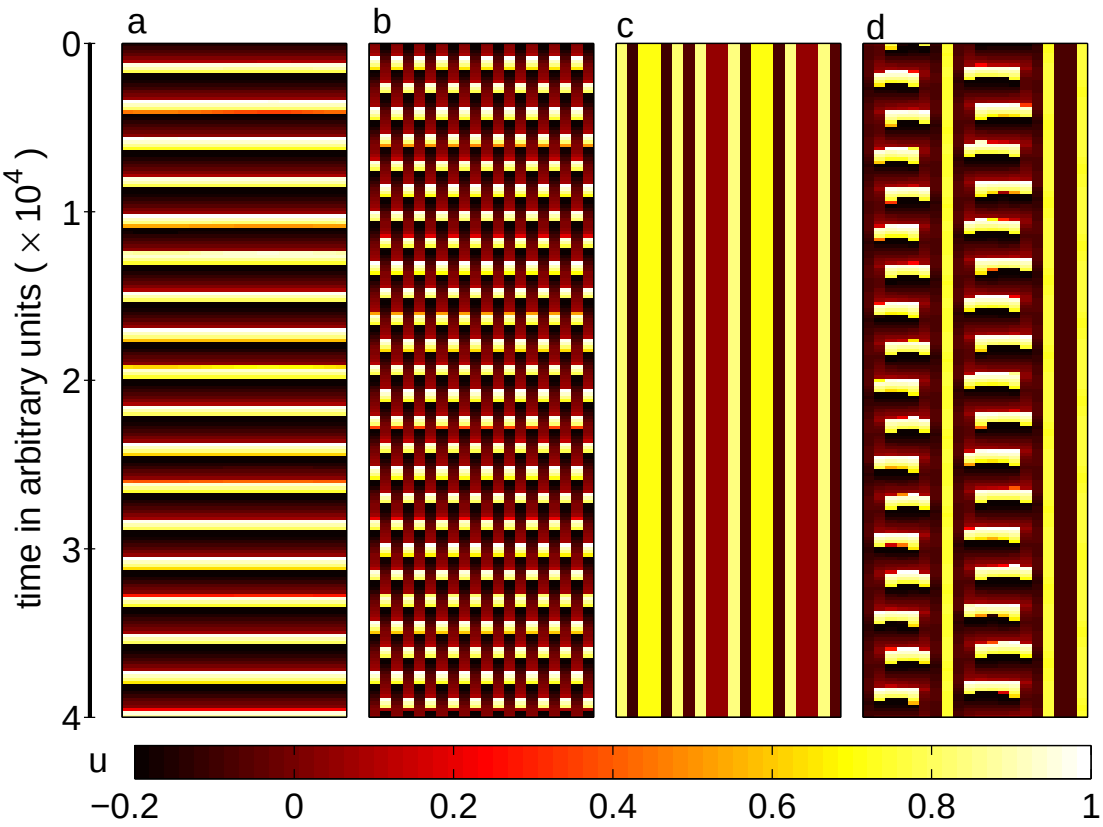

Figure 3.5: Spatio-temporal evolution of a 1-dimensional array of coupled relaxation oscillators ($N = 20$) with $D_u = D_v$ and periodic boundary conditions, exhibiting patterns similar to those seen in systems that allow diffusion of only inactivation variable. Pseudo-color plots of the activation variable u indicate different regimes characterized by (a) synchronized oscillations (SO), (b) anti-phase synchronization (APS), (c) spatially patterned oscillation death (SPOD) and (d) chimera state (CS, corresponding to co-occurrence of spatial patches with dynamically distinct behavior).

i.e., the coupling strengths for both variables are the same. Also, to avoid the edge effects introduced by the passive reservoirs at each end, periodic boundary conditions have been imposed on the system. Figures 3.5 and 3.6 show a representative selection of the asymptotic spatio-temporal patterns observed at different values of b and D. We observe that the system exhibits all the patterns (SO, APS, SPOD, CS and propagating defects) discussed in detail earlier in the context of diffusion in only the inactivation variable. As a consequence of using periodic boundary conditions we also observe variants of these patterns with a spatial gradient. For example, Fig. 3.6 shows SO and APS with such gradients that we refer to as gradient synchronization (GS) and gradient anti-phase synchronization

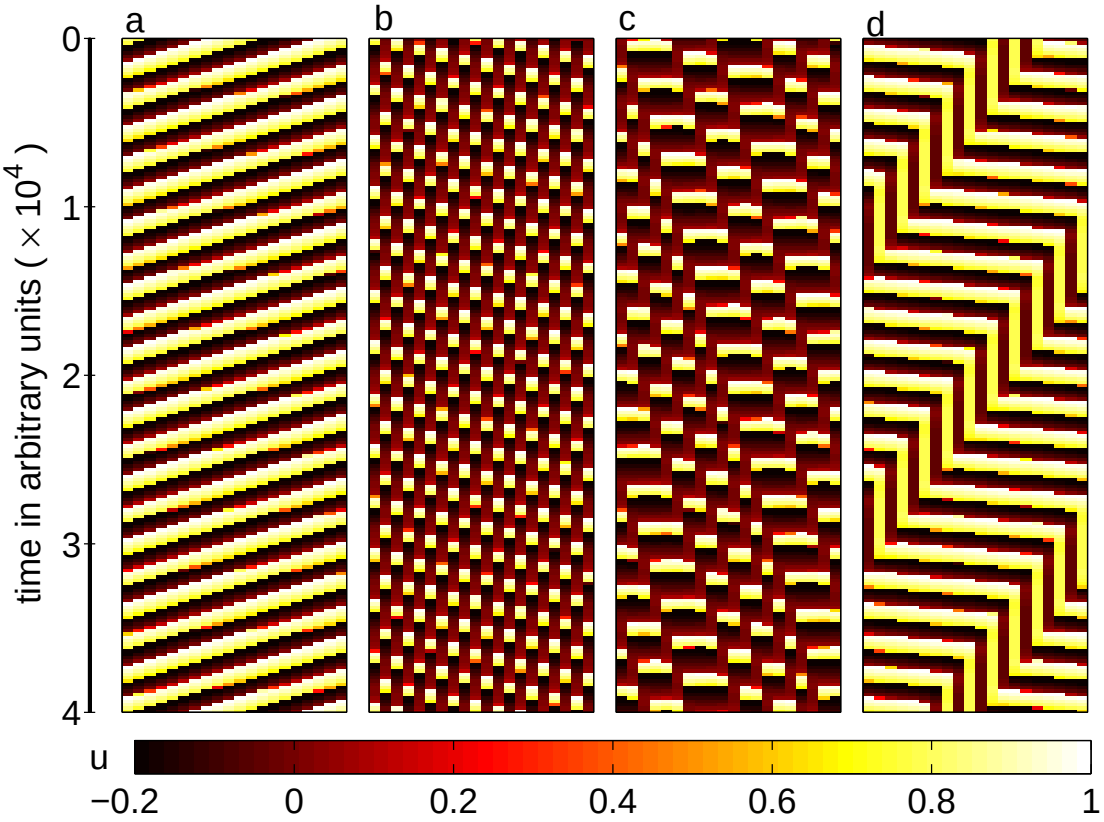

Figure 3.6: Spatio-temporal evolution of a 1-dimensional array of coupled relaxation oscillators ($N = 20$) with $D_u = D_v = D$ and periodic boundary conditions, showing patterns that have a spatial gradient. Pseudocolor plots of the activation variable u indicate different regimes characterized by (a) gradient synchronization (GS), (b) gradient anti-phase synchronization (GAPS), (c) traveling defects and (d) traveling chimera state (region with SPOD propagating over a background of GS).

(GAPS). The manifestation of spatial gradient in CS results in a propagating region of SPOD traveling against a background in GS, which we can term as a traveling chimera state. The different pattern regimes observed for this system are indicated in (b, D) space shown in Fig. 3.7.

3.4 Discussion and Conclusion

To conclude, we have shown that a simple model of relaxation oscillators interacting via lateral inhibition-like coupling yields a variety of striking spatio-temporal patterns. Our

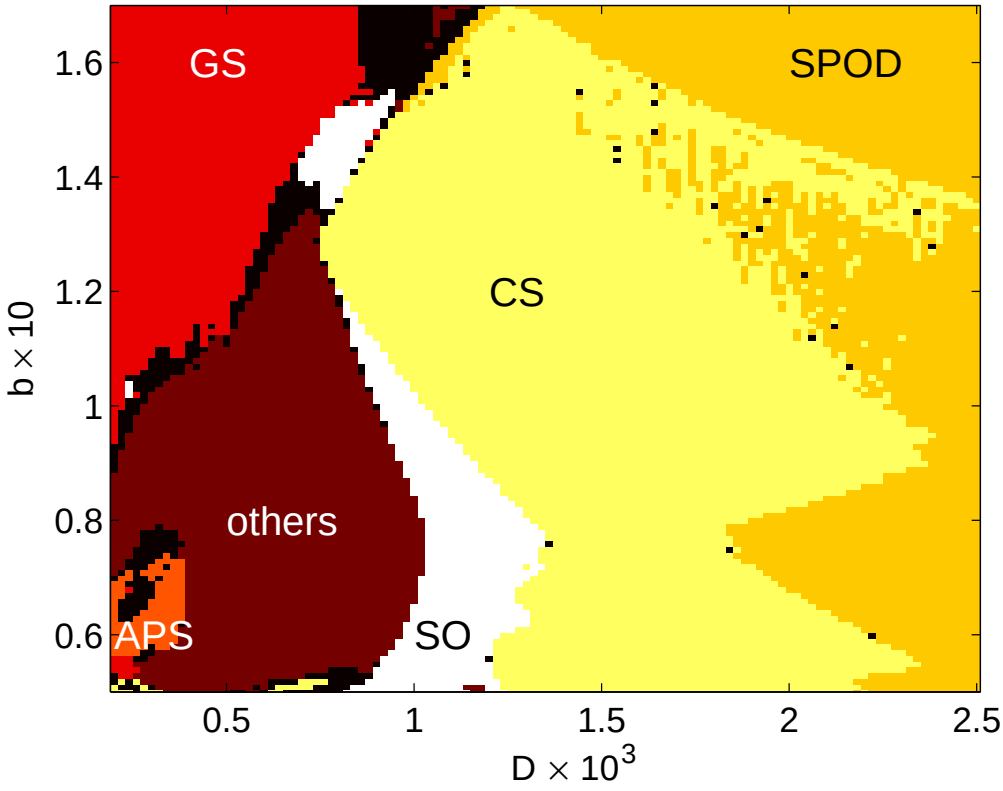

Figure 3.7: Different dynamical regimes of a 1-dimensional array of coupled relaxation oscillators ($N = 20$) in the $D - b$ parameter plane (with $D_u = D_v = D$) and periodic boundary conditions, showing regions where the majority ($> 50\%$) of initial conditions result in synchronized oscillations (SO), gradient synchronization (GS), anti-phase synchronization (APS), spatially patterned oscillation death (SPOD) and chimera state (CS). The region marked "others" exhibit patterns that do not belong to any of the ones mentioned above (e.g., gradient anti-phase synchronization and traveling defects).

model is simple and generic, suggesting that the patterns we predict may be observed in a range of experiments. These include coupled electronic circuits implementing relaxation oscillators [87] and Pt wire undergoing CO oxidation where the system is in an oscillatory regime [88] as well as the microfluidic chemical systems mentioned earlier. It will also be of great interest to see whether similar patterns occur in well-known generic models of chemical oscillators such as the Brusselator [89]. Recent theoretical work on trapped ions [90] suggest yet another system where such patterns can be found experimentally. Our initial exploration of propagating configurations in 2-dimensional media suggests that systems of higher dimensions may exhibit yet more striking features. The possibil-

ity of using the propagating defects for computation is an intriguing one, especially as analogous entities have been used to construct logic gates in CA [80].

4

Emergence of complex patterns through spontaneous symmetry breaking in dense homogeneous networks of neural oscillators

4.1 Introduction

Collective dynamics of coupled oscillators, in particular, synchronization [18], is integral to many natural phenomena [91] and is especially important for several biological processes [28, 29, 74], such as brain function [72, 92–95]. While very large-scale synchronization of neuronal activity is considered pathological, as in epilepsy [96], the brain is capable of exhibiting a variety of complex spatiotemporal excitation patterns that may play a crucial role in information processing [97]. Understanding the dynamics of these patterns at the scale of the entire brain (imaged using techniques such as fMRI) is of fundamental importance, as interaction between widely dispersed brain regions are responsible for significant behavioral changes, such as loss of consciousness caused by disruption

of communication between different areas of the cerebral cortex [98]. As detailed simulation of each individual neuron in the brain is computationally expensive [99, 100], when studying the dynamics of the entire system it is useful to focus on the network of interactions between brain regions. It has also been explicitly shown that the collective response of a large number of connected excitatory and inhibitory neurons, which constitute such regions, can be much simpler than the dynamics of individual neurons [101]. Indeed, each region can be described using phenomenological models in terms of a few aggregate variables [102].

Using anatomical and physiological data obtained over several decades, the networks of brain regions for different animals have been reconstructed [103–105], where the individual nodes correspond to large assemblies ($10^3 - 10^6$) of neurons [106, 107]. The connectivity C (i.e., fraction of realized links) of these networks ($C \sim 10^{-1}$) is significantly higher than that among neurons ($C \sim 10^{-6}$) [108]. A schematic representation of a network of the Macaque brain regions (adapted from Ref. [105]) is shown in Fig. 4.1 (a). The collective activity of such networks can result in complicated nodal dynamics, including temporal oscillations at several scales that are known to be functionally relevant [72, 111, 112]. Each of these nodes can be described using neural field models of localized neuronal population activity, which can have varying mathematical complexity and biological realism [113–115]. In this chapter, we use the well-known and pioneering model proposed by Wilson and Cowan (WC) [116, 117] to describe the activity of each brain region. We also discuss how our model may provide insights into recent experimental findings related to the communication between brain areas during the transition to loss of consciousness [98, 118, 119].

The complex collective dynamics obtained using this model for the Macaque network, shown in Fig. 4.1 (b), are reminiscent of experimentally recorded activity of brain regions [72]. The range of behaviors observed in this system at different connection strengths [Fig. 4.2 (a)-(b)], can arise from an interplay of several factors, which makes their anal-

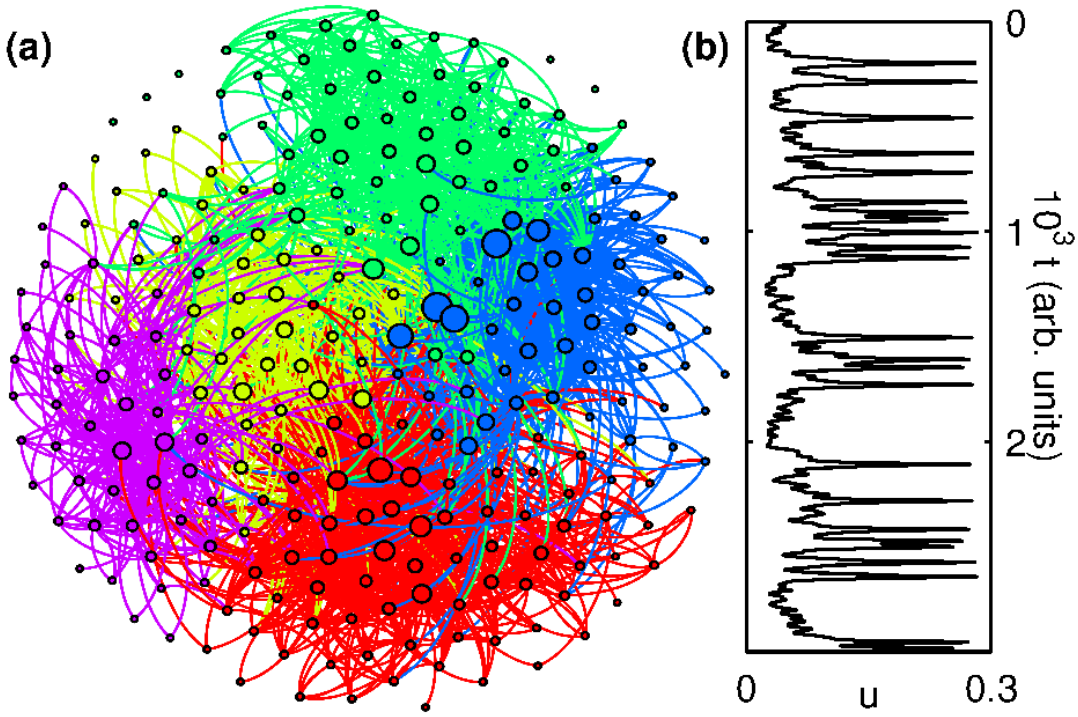

Figure 4.1: (a) The directed network of connections between regions of the Macaque brain, adapted from Ref. [105]. The size of each node is proportional to its total degree and the colors distinguish the modules (characterized by significantly higher intra-connection density and obtained using a partitioning algorithm [110]). The color of each link corresponds to that of the source node. (b) Time series of the excitatory component of a typical node in this network with coupling strength $w = 500$, where each node is modeled as a Wilson-Cowan oscillator.

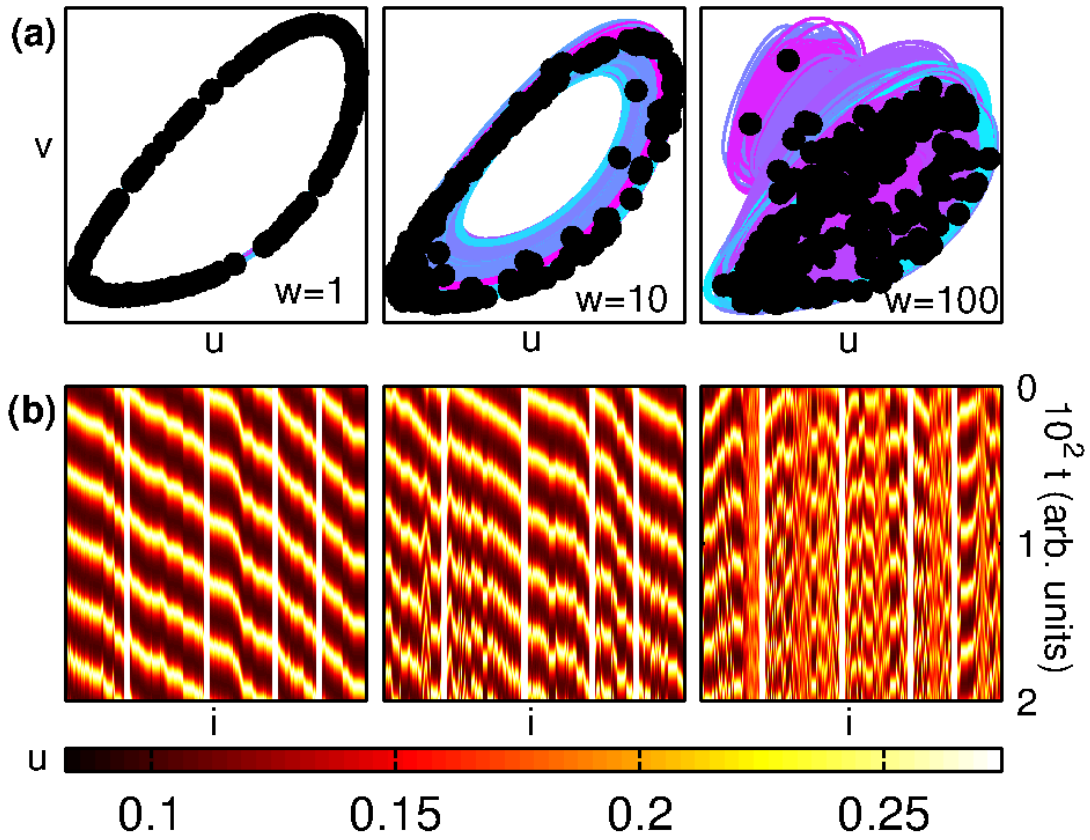

Figure 4.2: (a) Phase space projections of the oscillators connected to each other using the connection topology of the Macaque brain network, with different coupling strengths. The filled circles represent the location of each oscillator at a time instant. The panels here are scaled individually for better visualization. (b) Time-series of the excitatory component u, for the corresponding values of w used in the panels directly above. The nodes i are arranged according to their modules (demarcated by white lines).

ysis difficult. A possible approach to understand the genesis of these patterns is to focus on the dynamics of the nodes interacting in the simplified setting of a homogeneous, globally coupled system, which is an idealization of the densely connected network. In this chapter we show that this simple system exhibits an unexpectedly rich variety of complex phenomena, despite lacking the detailed topological features of brain networks [e.g., Fig. 4.1 (a)], such as heterogeneity in degree (number of connections per node) and modular organization. In particular, we show the existence of novel collective states, including those characterized by oscillator clusters, where each cluster is distinguished by its amplitude or frequency. The occurrence of such clusters is surprising as each node is identical in terms of both intrinsic dynamics and connectivity, indicating that the homogeneous system of oscillators undergoes *spontaneous symmetry breaking*. In addition we observe patterns where the time-series for all oscillators are identical except for a non-zero phase difference between n_{cl} groups of exactly synchronized elements which we refer to as “phase clusters". On removing a few links from the network while preserving the structural symmetry of connections we observe even more dramatic situations such as the appearance of many (> 2) clusters having different amplitudes. In addition, oscillator death, which is seen over a substantial region of parameter space in the fully connected system, occurs in a drastically reduced region for such marginally sparse networks. As the behavior of a large, densely connected system is effectively identical to that of the corresponding mean-field model, it is remarkable that the dynamical properties of the system considered here are radically altered in response to extremely minor deviations from the fully connected situation.

4.2 The Model

The model we consider comprises a network of N oscillators, each described by the WC model whose dynamics results from interactions between an excitatory and an inhibitory

neuronal subpopulation. The average activity of each node i (u_i, v_i) evolves as:

$$\begin{aligned} \tau_u \dot{u}_i &= -u_i + (\kappa_u - r_u u_i)\, \mathcal{S}_u(u_i^{in}), \\ \tau_v \dot{v}_i &= -v_i + (\kappa_v - r_v v_i)\, \mathcal{S}_v(v_i^{in}), \end{aligned} \tag{4.1}$$

where, $u_i^{in} = c_{uu}u_i - c_{uv}v_i + \sum'(w_{ij}^{uu}u_j - w_{ij}^{uv}v_j) + I_u^{ext}$ and $v_i^{in} = c_{vu}u_i - c_{vv}v_i + \sum'(w_{ij}^{vu}u_j - w_{ij}^{vv}v_j) + I_v^{ext}$ represent the total input to the two subpopulations respectively. The time constants and external stimuli for the subpopulations are indicated by $\tau_{u,v}$ and $I_{u,v}^{ext}$ respectively, while $c_{\mu\nu}$ $(\mu, \nu = u, v)$ corresponds to the strength of interactions within and between the subpopulations of a node. The interaction strengths are represented by the weight matrices $W^{\mu\nu} \equiv \{w_{ij}^{\mu\nu}\}$ and the summation Σ' is over all network neighbors (for a globally coupled system, $\Sigma' \equiv \Sigma_{1\le j\le N, j\neq i}$). The function $\mathcal{S}_\mu(z) = [1 + \exp\{-a_\mu(z - \theta_\mu)\}]^{-1} + \kappa_\mu - 1$ has a sigmoidal dependence on z, with $\kappa_\mu = 1 - [1 + \exp(a_\mu\theta_\mu)]^{-1}$. The parameter values have been chosen such that each isolated node ($W^{\mu\nu} = 0$) is in the oscillatory regime, viz., $a_u = 1.3$, $\theta_u = 4$, $a_v = 2$, $\theta_v = 3.7$, $c_{uu} = 16, c_{uv} = 12, c_{vu} = 15, c_{vv} = 3, r_u = 1, r_v = 1, \tau_u = 8$, $\tau_v = 8$, $I_u^{ext} = 1.25$ and $I_v^{ext} = 0$. For the homogeneous systems considered here the links will have same strength, i.e., $w_{ij}^{\mu\nu} = w/k$ ($\mu, \nu = u, v$ and $i(\neq j) = 1, \ldots, N$; $w_{ii}^{\mu\nu} = 0$), where k is the degree of a node

The dynamical system (Eq. 4.1) is numerically solved using an adaptive-step Runge-Kutta integration scheme for different system sizes (N) and coupling strengths (w). Linear stability analysis is used to determine the stability of some of the patterns and identify the associated bifurcations. The behavior of the system for each set (w, N) is analyzed over many ($\sim$ 100) randomly chosen initial conditions. We have explicitly verified that our results are robust with respect to small variations in the parameters.

4.3 Results

We first examine the collective dynamics of a pair of coupled oscillators ($N = 2$) as a function of the interaction strength between them (Fig. 4.6). Fig. 4.4 (a)-(b) show that while exact synchronization (ES) of oscillator dynamics occurs at weak coupling ($w \lesssim 3.2$), a state of anti-phase synchronization (APS) is observed at higher values of w ($4.4 \lesssim w \lesssim 11$). For intermediate w, the co-existence of the dominant frequencies corresponding to ES and APS states [Fig. 4.5 (a)] indicates that the quasi-periodic (QP) behavior observed in this regime can be interpreted as arising through competition between the mechanisms responsible for the above two states. At $w \sim 11$, the system undergoes spontaneous symmetry-breaking, eventually giving rise to inhomogeneous in-phase synchronization (IIS), characterized by different phase-space projections and distinct amplitudes for the time-series of each oscillator [Fig. 4.4 (a)-(b), last panel]. The nature of the transition from APS to IIS is made explicit in Fig. 4.5 (b) [top panel], where the fixed points of one of the oscillators, obtained using numerical root finding, are shown over a range of w. At $w \approx 10.943$, a pair of heterogeneous unstable solutions related by permutation symmetry, corresponding to an inhomogeneous steady-state (ISS), emerge from a homogeneous unstable solution, beyond which all three solutions coexist. Thus, spontaneous symmetry breaking appears to arise in the system through a subcritical pitchfork bifurcation, with the number of positive eigenvalues corresponding to the homogeneous solution decreasing by unity (not shown). The ISS is stable over a very small range, $10.964 \lesssim w \lesssim 11.002$, as seen from their corresponding eigenvalues in Fig. 4.5 (b) [lower panel]. Note that stability is lost on either end of this interval through supercritical Hopf bifurcations (Fig. 4.6). For $w \gtrsim 700$, both oscillators converge to the inactive state $u_i = v_i = 0, \forall i$, corresponding to amplitude death (AD, not shown).

To understand how the patterns we observe for a pair of WC oscillators generalize for a larger system, we now increase the number of oscillators and examine the collective dynamics (Fig. 4.7). We observe that while the patterns seen for a pair of coupled oscil-

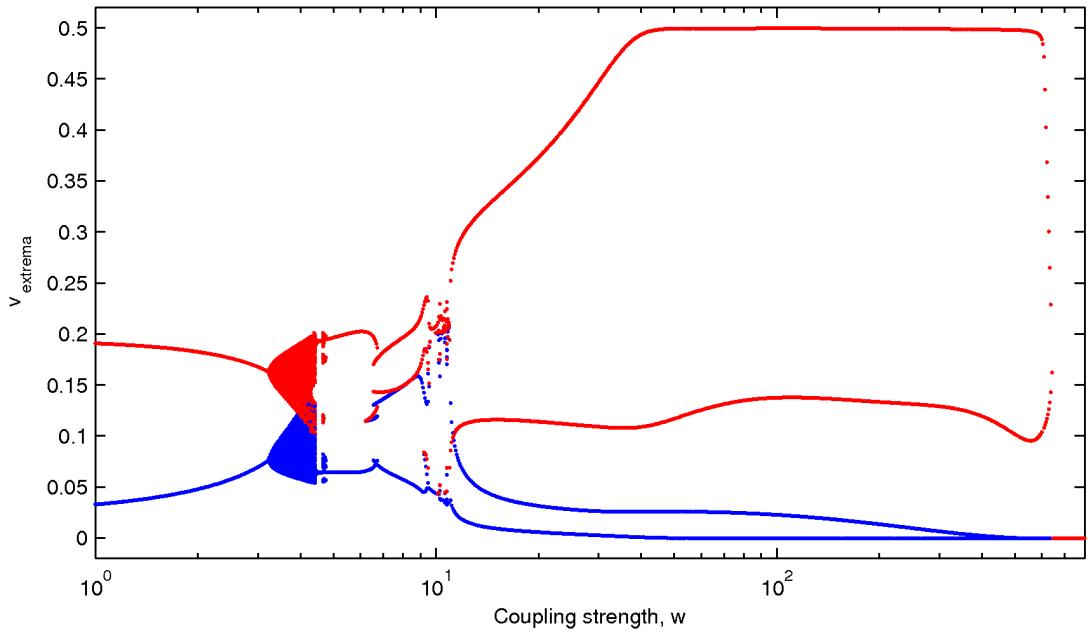

Figure 4.3: Bifurcation diagram for a pair of coupled WC oscillators with coupling strength w as the bifurcation parameter, obtained for a set of 20 random initial conditions (i.c.). Red dots represent the maxima of the inhibitory components v for each i.c., while blue dots represent the corresponding minima.

lators, namely ES, QP, ISS, IIS, APS and AD persist (first four shown in Fig. 4.8 (a)-(b) for $N = 20$) [1], qualitatively different states also emerge. As mentioned earlier, a new class of patterns characterized by the existence of phase clusters appears. The most robust of these, referred to as gradient synchronization (GS), has $n_{cl} \sim N$. Another new pattern comprises two oscillator clusters, each characterized by a unique frequency [Fig. 4.9 (a)]. This constitutes a dramatic instance of spontaneous breaking of permutation symmetry, as the oscillators are intrinsically indistinguishable for this completely homogeneous system. Thus, the appearance of multiple frequencies in a dynamical network need not imply heterogeneity in connectivity or node properties.

A third new pattern is a homogeneous steady state referred to as oscillator death (OD), in which the individual nodes have the same time-invariant, non-zero activity. This dynamical state appears over a large region in (w, N)-space as seen in the phase diagram,

[1] Note that APS, which for $N > 2$ has a very small basin of attraction, is a “phase cluster" state for which $n_{cl} = 2$.

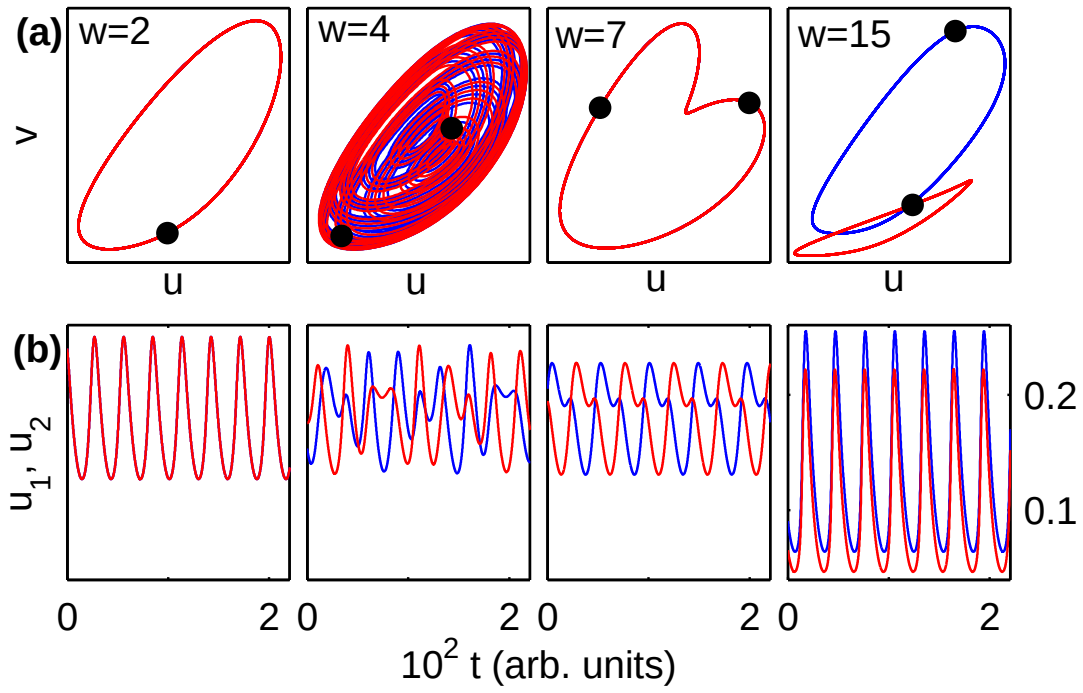

Figure 4.4: Collective dynamics of a system of two coupled WC oscillators. (a) Phase space projections of the trajectories and (b) time-series for each oscillator showing exact synchronization (ES, for coupling $w = 2$), quasiperiodicity (QP, $w = 4$), anti-phase synchronization (APS, $w = 7$) and inhomogeneous in-phase synchronization (IIS, $w = 15$). The filled circles represent the location of each oscillator in phase space at a time instant. The panels in (a) are scaled individually for better visualization.

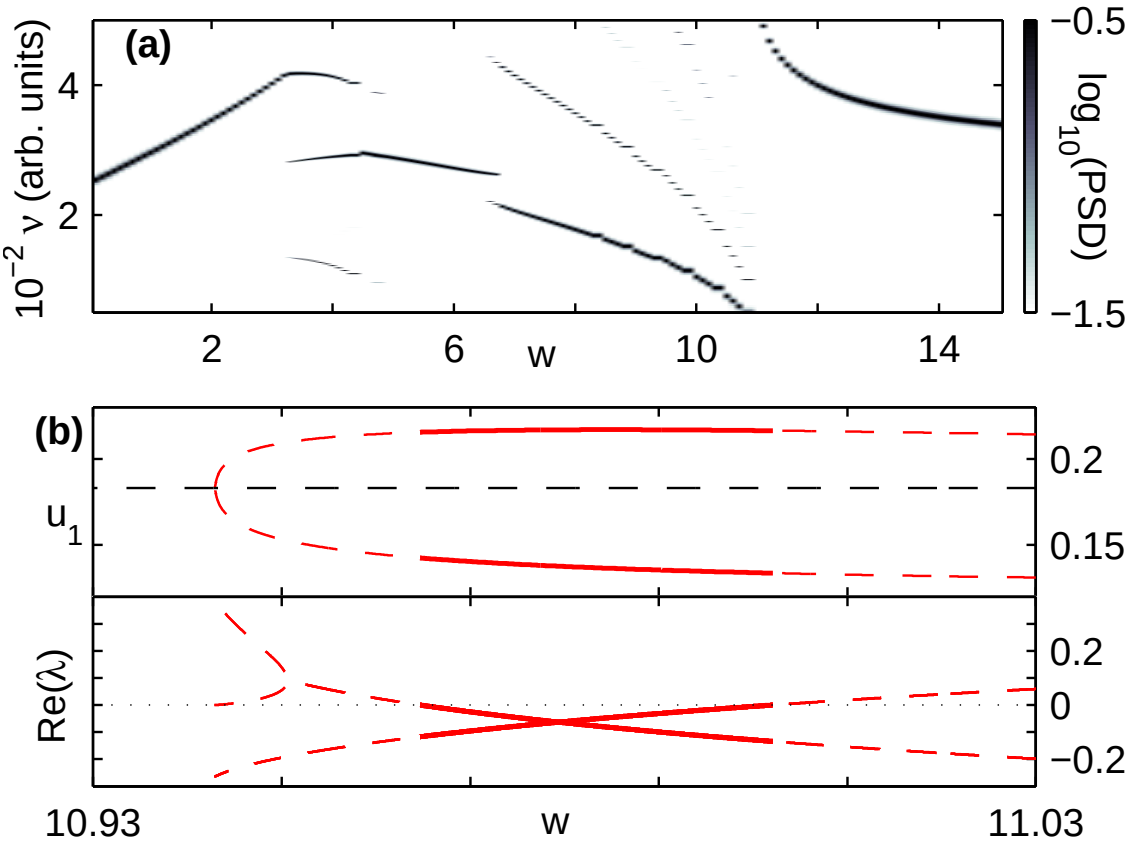

Figure 4.5: Dynamical bifurcations in a system of two coupled WC oscillators. (a) Power-spectral density (PSD) of the time-series for the *u* component of each oscillator, revealing the dominant frequencies as a function of *w*. (b) All fixed points of the system (upper panel) and the real parts of the eigenvalues corresponding to the heterogeneous fixed points (lower panel) showing the transitions between APS and IIS regimes. Solid (broken) lines represent stable (unstable) solutions. The horizontal broken line (upper panel) represents the unstable homogeneous solution.

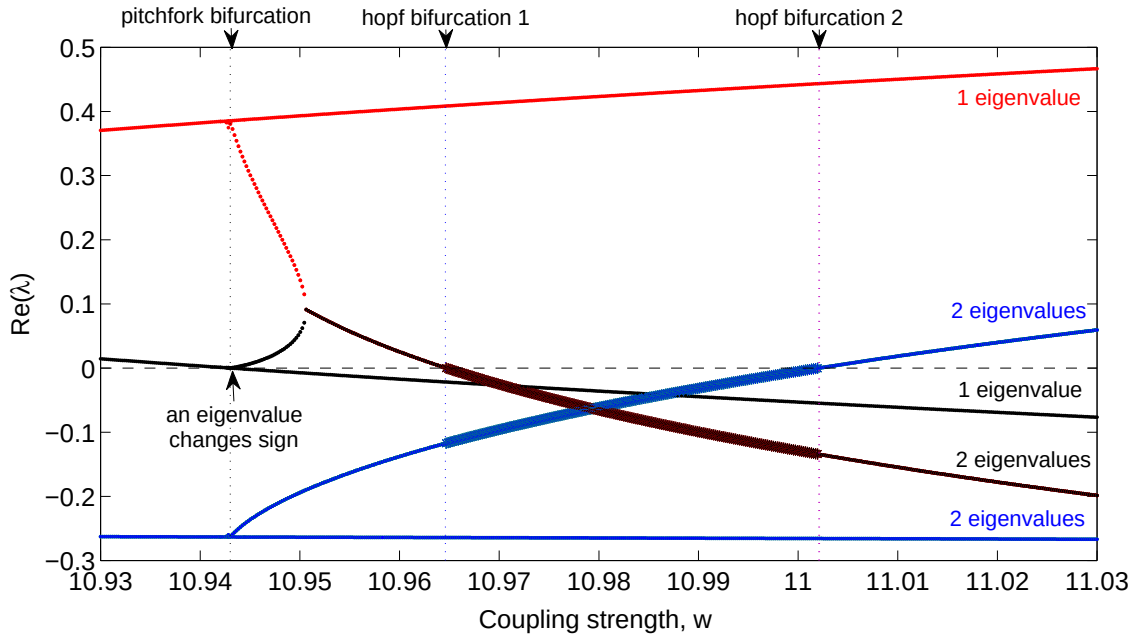

Figure 4.6: Real parts of the eigenvalues of all the fixed points for a pair of coupled WC oscillators, shown as a function of coupling strength w in the neighborhood of the transition between APS and IIS regimes. The vertical dotted lines indicate the locations where different bifurcations occur in this range of w. Thick lines between the two Hopf bifurcations represent stable solutions. Three of the branches shown correspond to a pair of eigenvalues, as indicated in the figure.

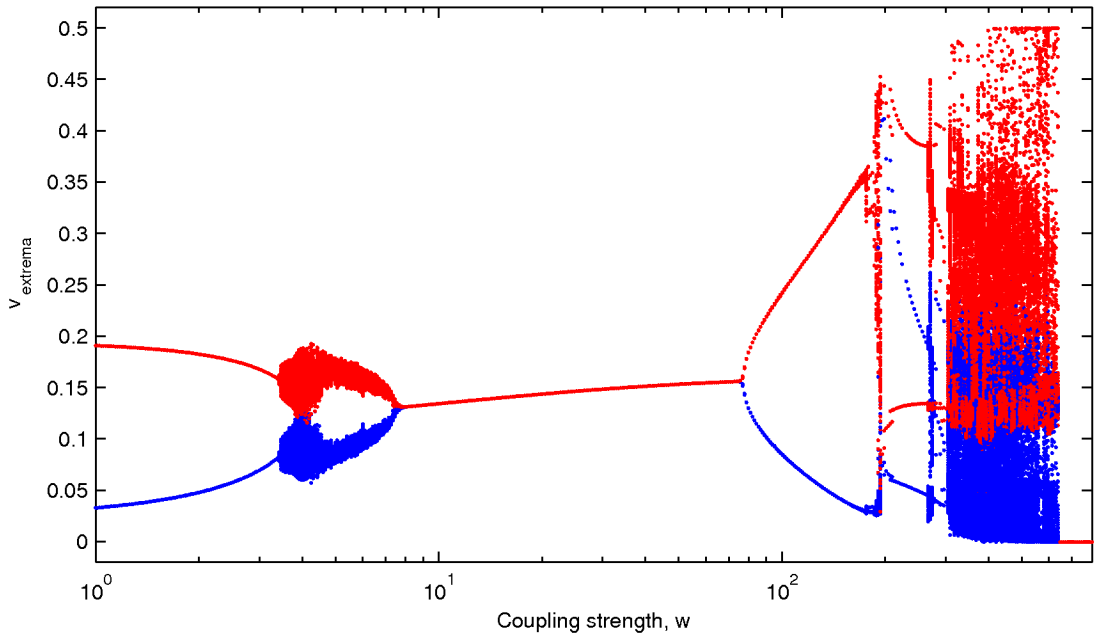

Figure 4.7: Bifurcation diagram for $N = 20$ globally coupled WC oscillators with coupling strength w as the bifurcation parameter, obtained for a set of 20 random initial conditions (i.c.). Red dots represent the maxima of the inhibitory components v for each i.c., while blue dots represent the corresponding minima.

Fig. 4.9 (b). To identify and segregate the regimes in this diagram, we use several order parameters (summarized in Table 4.1). The mean of the oscillation amplitude, measured as the variance (σ^2) with respect to time of one of the WC variables, v, averaged over all the nodes $\langle\sigma_t^2(v_i)\rangle_i$, is zero for all the non-oscillating states AD, OD and ISS. These are further distinguished by using the mean and variance with respect to all nodes of the time-averaged v, i.e., $\langle\langle v_i\rangle_t\rangle_i$ (=0 for AD) and $\sigma_i^2(\langle v_i\rangle_t)$ (=0 for OD and AD). To distinguish between the oscillating patterns, we consider the mean coherence, measured as $\langle\sigma_i^2(v_i)\rangle_t$, and the total space occupied by all the trajectory projections Δ, as measured by the number of non-zero bins of their histogram in (u, v)-space. ES is characterized by $\langle\sigma_i^2(v_i)\rangle_t = 0$ and IIS by $\sigma_i^2(\langle v_i\rangle_t) > 0$. The remaining patterns, GS and QP, are distinguished by $\Delta \sim 0$ for GS. Note that $\langle\rangle_t$ and $\langle\rangle_i$ represent averaging over time and all nodes, respectively. In practice, different regimes are characterized by thresholds whose specific values do not affect the qualitative nature of the results.

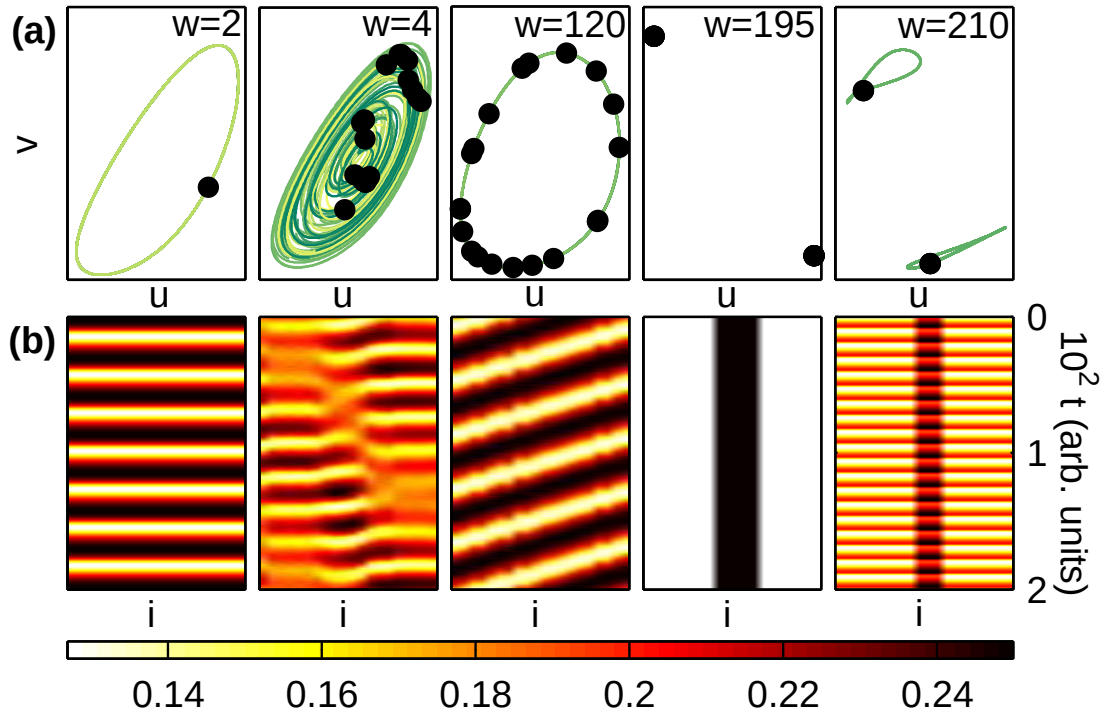

Figure 4.8: Collective dynamics of N globally connected WC oscillators. (a) Phase space projections of the trajectories and (b) time-series for $N = 20$ globally coupled oscillators, showing exact synchronization (ES, $w = 2$), quasiperiodicity (QP, $w = 4$), gradient synchronization (GS, $w = 120$), inhomogeneous steady-state (ISS, $w = 195$) and inhomogeneous in-phase synchronization (IIS, $w = 210$). The panels in (a) are scaled individually for better visualization.

Table 4.1: Order parameters used for identifying the different dynamical regimes of a homogeneous network of WC oscillators (as explained in the main text).

Pattern	$\langle\sigma_t^2(v_i)\rangle_i = 0$	$\langle\langle v_i\rangle_t\rangle_i = 0$	$\sigma_i^2(\langle v_i\rangle_t) = 0$	$\langle\sigma_i^2(v_i)\rangle_t = 0$	$\Delta > 0$
AD	✓	✓	✓	✓	
OD	✓		✓	✓	
ISS	✓				
ES			✓	✓	
QP					✓
IIS					
GS			✓		

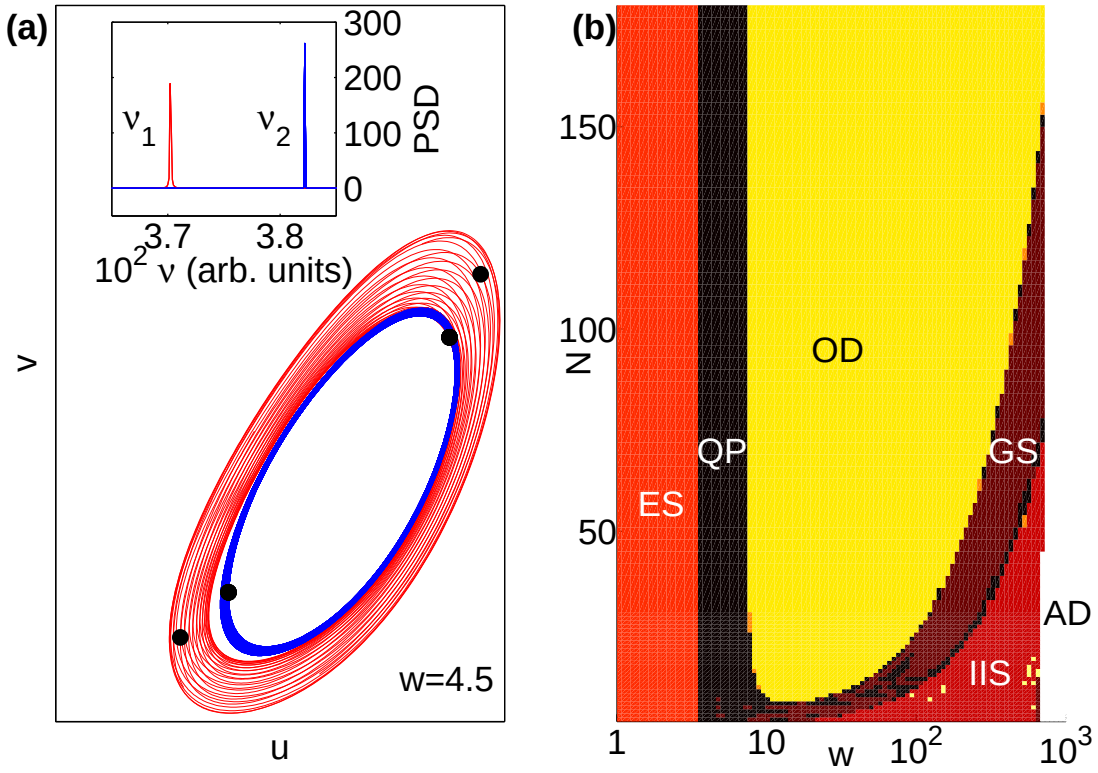

Figure 4.9: Dynamical regimes in a system of N globally coupled WC oscillators. (a) Phase space projections of the different oscillators ($N = 20$) for $w = 4.5$, which form two clusters with frequencies ν_1 and ν_2, indicated by the power-spectral density (PSD, inset). (b) Phase diagram for N WC oscillators globally coupled with strength w, indicating areas where the majority ($> 50\%$) of initial conditions result in ES, QP, GS, IIS, oscillator death (OD) and amplitude death (AD). Note that the w-axis is logarithmic.

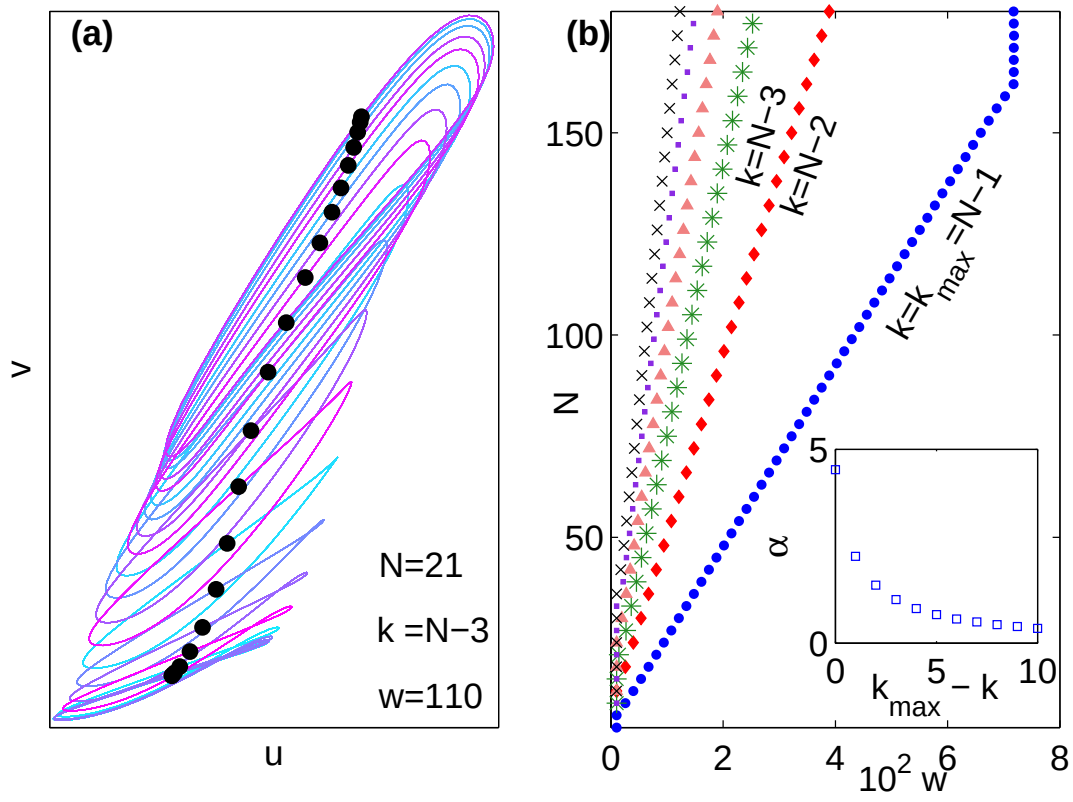

Figure 4.10: Effect of marginally sparse connection density on collective dynamics of WC oscillators. (a) As the degree k, i.e., the number of links per node, deviates slightly from the globally coupled case ($k_{max} = N-1$) to $N-3$, the trajectories of the IIS state split into many ($\sim N$) distinct projections ($N = 21, w = 110$). (b) The OD region in Fig. 4.9 (a) shrinks rapidly with the number of removed links, as seen from the slope of the upper boundary of OD (inset).

As a first step towards extending the results seen for the globally coupled system to brain networks of the type shown in Fig. 4.1 (a), we have investigated the consequences of gradually decreasing the connection density. To ensure that the degree reduction preserves as many of the existing symmetries as possible, we arrange the nodes on a circle and sequentially remove connections between nodes placed furthest apart. In addition to preserving degree homogeneity, this ensures that every node has the same neighborhood structure. As we deviate from the global coupling limit, we observe patterns similar to those shown in Fig. 4.8 (a-b), although the precise form of the attractors may differ and it is now the translational symmetry that is being spontaneously broken. For example, as seen in Fig. 4.10 (a), a reduction of just 2 links per node causes the trajectory in the IIS state to split into many more ($\sim N$) projections than seen for the fully connected case (~ 2). Also, while the phase diagram of the system remains qualitatively unchanged when the degree is decreased from $k_{max} = N - 1$, there is a dramatic quantitative reduction in the area corresponding to OD [Fig. 4.10 (b)] even with the reduction of one link per node. This is surprising, as one would expect that a marginal deviation from the global coupling limit in large systems will not result in a perceptible change from the mean-field behavior.

4.4 Discussion and Conclusion

Our result that weakening connections between nodes of a network can increase coherence in collective activity (viz., observation of ES at low w) suggests an intriguing relation between two recent experimental findings: (i) anaesthetic-induced loss of consciousness occurs through the progressive disruption of communication between brain areas [98] and (ii) functional connectivity networks reconstructed from EEG data become increasingly dense with the development of fatigue in sleep- deprived subjects [118, 119]. The latter study finds that the onset of sleep is accompanied by an increase in the degree of synchronization between brain areas, while the former result implies that the interaction strengths between these areas will concurrently get weaker. Although it may appear

counter-intuitive that decreased coupling strength would result in increased synchronization, our findings illustrate that these results are not incompatible.

Another important implication of this study follows from our demonstration that systems with simple connection topology are capable of exhibiting very rich dynamical behavior. In particular, many of the patterns seen in our simulations of the network of Macaque brain regions (Fig. 4.1) resemble those observed using much simpler connectivity schemes (Fig. 4.8). Hence, patterns seen in complex systems that are often attributed to their non-trivial connection structure, may in fact be independent of the details of the network architecture. With the availability of high-resolution data and increased computational power, it is now possible to model brain networks incorporating a high level of realistic detail [99, 100, 120]. While these studies are extremely important, we need to be careful while attributing observed dynamical features to the structural properties of the network, as such features might appear even with very simple connection topologies. Our findings provide a baseline for future studies on the specific role of the detailed aspects (degree heterogeneity, modular architecture, etc.) of brain networks on their collective dynamics.

To conclude, we have shown that the collective dynamics of a homogeneous system of oscillators, motivated by mesoscopic descriptions of brain activity, exhibits spontaneous symmetry breaking that gives rise to several novel patterns. Despite preserving the structural symmetry of connections, a marginal increase in the network sparsity, corresponding to an extremely small deviation from the mean-field, unexpectedly changes the robustness of certain patterns. Our results suggest that some of the complicated activity patterns seen in the brain can be explained even without complete knowledge of its wiring diagram.

5

Chimera ordering in spin systems

5.1 Introduction

Transition to states characterized by simple or complex ordered patterns is a phenomenon of central importance in equilibrium statistical physics as well as in dynamical systems far from equilibrium [91, 121]. Examples of simple ordering at thermal equilibrium include the aligned orientation of spins in Ising-like systems, while, in the context of nonlinear dynamics, this may be observed in the phase synchronization of coupled oscillators. However, more complex ordering behavior may also occur in various systems under different conditions, especially in the presence of heterogeneities. A surprising recent finding is that even *homogeneous* dynamical systems can exhibit a robust, partially ordered state characterized by the coexistence of incoherent, desynchronized domains with coherent, phase locked domains [122]. Such *chimera* states have initially been observed only in different types of oscillator populations, including complex Ginzburg-Landau equations, phase oscillators, relaxation oscillators, etc., arranged in various connection topologies [78, 123–131]. Given that “chimera" refers to the co-occurrence of incongruous elements, one can extend the concept of chimera-like states to include those characterized by simultaneous existence of strongly and weakly ordered regions in an otherwise homo-

geneous system. If such a state can occur as the global free-energy minimum of a system in thermal equilibrium, it may widen the scope of experimentally observing chimera-like order in physical situations.

It is with this aim in mind that we investigate chimera-like ordering in systems at thermal equilibrium. Specifically, we consider spin-models as they are paradigmatic for different complex systems comprising interacting components which can be in any of multiple discrete states. For example, simple Ising-like models consisting of binary-state elements are versatile enough to be used for understanding processes operating in a wide range of physical (e.g., magnetic materials [132–134]), biological (e.g., neural networks [135]) and social (e.g., opinion formation [27, 136]) systems. The nature and connection topology of the interactions between the spins decide whether the entire population reaches a consensus corresponding to a highly ordered state, or is in a weakly ordered state (including the case of complete disorder) that corresponds to the stable coexistence of contrary orientations. The existence of a chimera state in such situations would imply that even though every spin is in an identical environment, different regions of the system will exhibit widely different degrees of ordering.

In this chapter we report the novel occurrence of chimera order in spin systems. This is characterized for a system of Ising spins by the simultaneous occurrence of strongly and weakly ordered regions, as measured by the magnitude of local magnetizations. The specific system we consider in detail is globally coupled and comprises two sub-populations (or *modules*) with the nature of interactions between spins depending on whether they belong to the same or different groups. Our central result is that when subjected to a uniform magnetic field at a finite temperature, one of the sub-populations can become *highly ordered* while the other remains *weakly ordered*. This is surprising as both the interactions as well as the external field for the two modules are *identical*. Moreover, the chimera state is not a metastable state, but rather the global minimum of free energy for the system. The critical behavior of the system associated with the onset of chimera or-

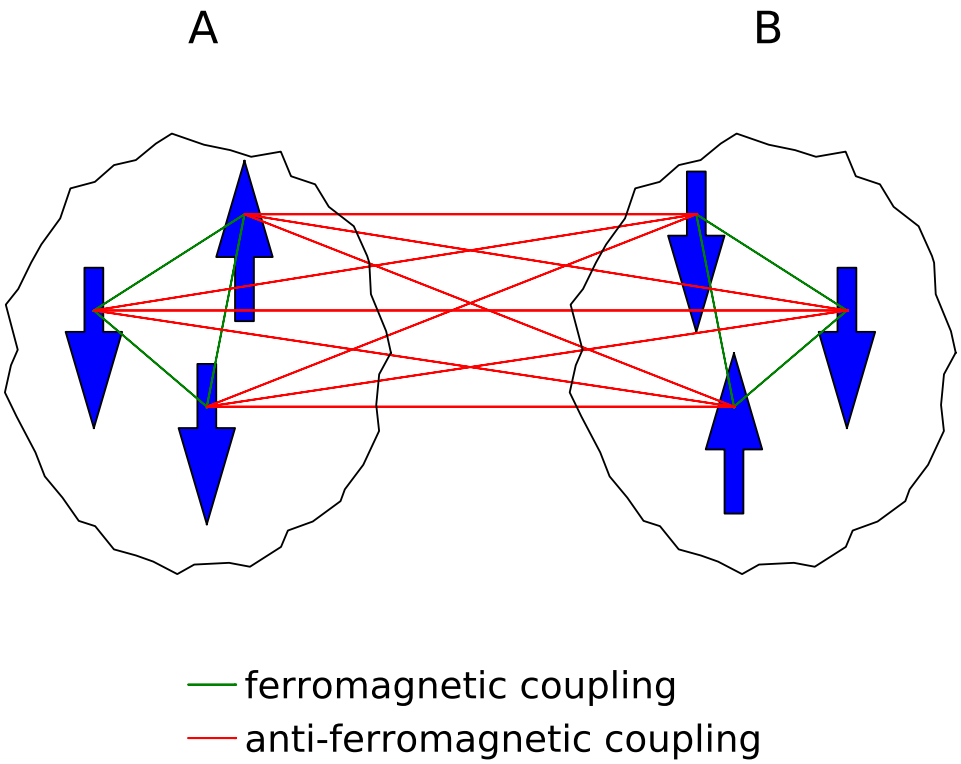

Figure 5.1: Schematic diagram of a system of $2N$ globally coupled Ising spins arranged into two subpopulations (A,B) of N spins each. Spins belonging to the same module interact with each other ferromagnetically, while those belonging to different modules have antiferromagnetic interactions.

dering is established in this chapter by an exact analytical treatment. We also demonstrate by Monte Carlo (MC) simulations the existence of similar complex ordering phenomena in three-dimensional spin systems with nearest neighbor interactions. This opens up the possibility of experimentally observing chimera states in layered magnetic systems, e.g., manganites [133, 134]. While the effect of noise on chimera state in coupled oscillators is not well-understood, the chimera order in spin systems reported here arise in the presence of (thermal) noise; thus, it is robust and likely to be seen in real physical situations.

5.2 The Model

We consider a system of $2N$ globally coupled Ising spins arranged into two sub-populations (Fig. 5.1), each having N spins, at a constant temperature T and subjected to a uniform external magnetic field $H(> 0)$. A dynamical system analogous to our model has recently been analyzed by Abrams *et al.* [126] where two clusters of identical oscillators, each maintaining a fixed phase difference with the others, was shown to possess a chimera state. The interaction between two spins belonging to the same module is ferromagnetic, having strength J (> 0), while that between spins belonging to different modules is antiferromagnetic with strength $-J'$ (where $J' > 0$). It is obvious that in the absence of an external field, the modules will be completely ordered in opposite orientations at zero temperature. As temperature is increased, the magnitude of the magnetizations for the two modules will decrease by the same amount, eventually becoming zero at a critical temperature, T_c. In the presence of an external field H that favors spins with +ve orientation, the module having negative magnetization will be subjected to competition between (i) the field H which attempts to align the spins along the +ve direction and (ii) the antiferromagnetic interaction J' which is trying to do the opposite. In the presence of a strong field $H > H_0$ (where H_0 is a threshold field), as the temperature is increased from zero, the spins in both modules initially remain ordered and are oriented in the *same* direction. We show below that beyond a certain critical temperature T_{c1}, one module becomes more disordered relative to the other. As the temperature increases further beyond a second critical temperature T_{c2}, the two modules again attain the same magnetization, which decreases gradually with T [Fig. 5.2 (a)]. The phase transitions at T_{c1} and T_{c2} are continuous and are characterized by critical exponents α and β which are derived exactly below. For $H < H_0$, the spins in the two modules are oriented at $T = 0$ in opposite directions, although having the same magnitude. At any finite temperature below T_{c2}, the module whose spins were initially oriented opposite to the direction of the field is seen to be more disordered than the other module. The same critical exponents as in the case of $H > H_0$ are observed

for the transition at T_{c2}, beyond which the magnetization of the two modules are same in magnitude and orientation.

5.3 Results

For the system described above, the energy for a given configuration of spins is

$$E = -J \sum_{\substack{i,j,s \\ i \neq j}} \sigma_{is}\sigma_{js} + J' \sum_{\substack{i,j,s,s' \\ s \neq s'}} \sigma_{is}\sigma_{js'} - H \sum_{i,s} \sigma_{is}, \tag{5.1}$$

where $\sigma_{is} = \pm 1$ is the Ising spin on the i-th node ($i, j = 1, 2, \cdots N$) in the s-th module ($s, s' = 1, 2$) and $J, J' > 0$. Since each spin is connected to every other spin, mean-field treatment is exact for our effectively infinite-dimensional system. Thus, the total free energy of the system can be expressed as:

$$F(m_1, m_2) = -aN(m_1^2 + m_2^2) + bNm_1m_2 - HN(m_1 + m_2) + Nk_BT\left[S(m_1) + S(m_2)\right], \tag{5.2}$$

where the magnetizations per spin of the two modules ($m_s = \frac{1}{N}\sum_{i=1}^{N} \sigma_{is}$) are the order parameters for the system,

$$S(m) = \frac{1}{2}[(1+m)\log(1+m) + (1-m)\log(1-m)] - \log 2$$

is the entropy term, and $a = J(N-1)/2$, $b = J'N$ are system parameters (k_B being the Boltzmann constant).

To find the condition for equilibrium at a temperature T, the free energy can be minimized with respect to m_1 and m_2 to obtain:

$$-2am_1 + bm_2 - H + \frac{k_BT}{2}\log\frac{1+m_1}{1-m_1} = 0, \tag{5.3}$$

$$-2am_2 + bm_1 - H + \frac{k_BT}{2}\log\frac{1+m_2}{1-m_2} = 0. \tag{5.4}$$

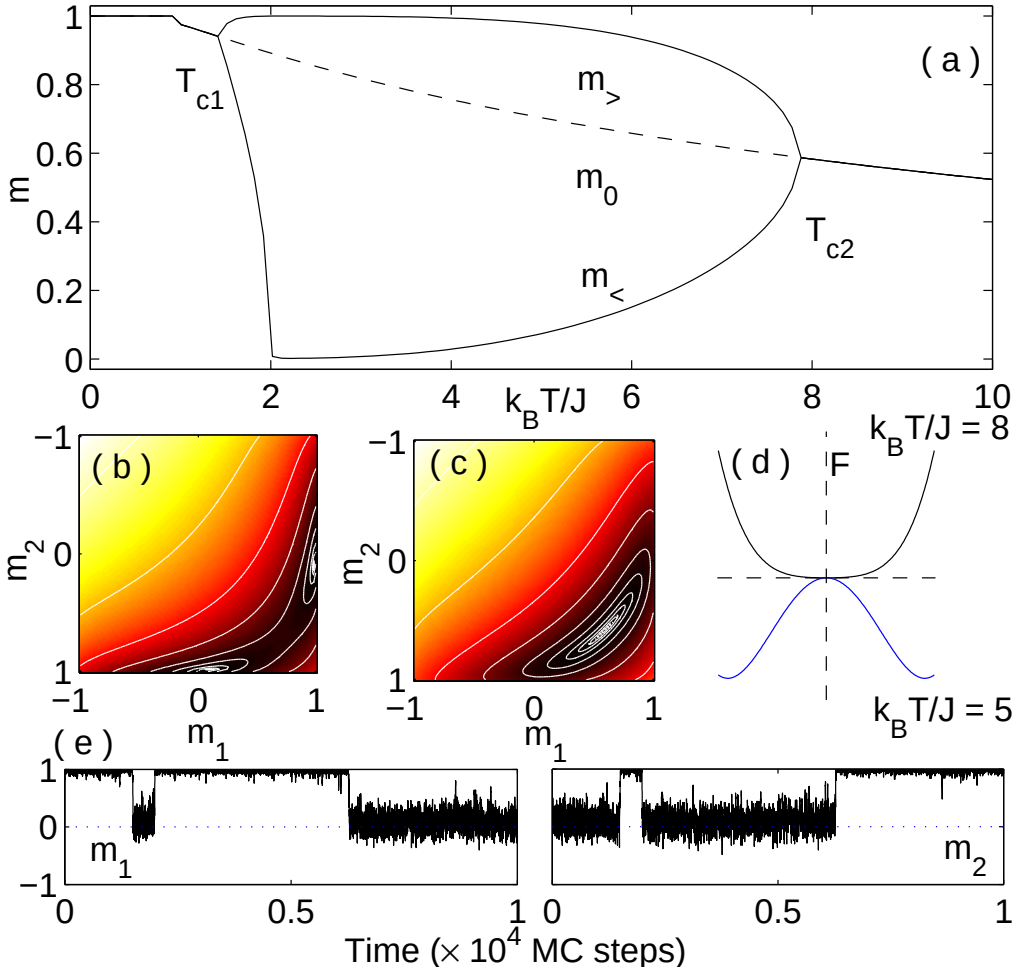

Figure 5.2: (a) Variation of magnetization per spin of the two modules (m_1, m_2) with temperature for $H > H_0$. Between the temperatures T_{c1} and T_{c2}, the magnetizations of the two modules are different, with the smaller value being called $m_<$ and the larger one $m_>$. The broken line indicates the saddle point of the free energy function corresponding to $m_1 = m_2 = m_0$ (see text). The free energy landscape corresponding to chimera order at $k_BT/J = 5$ (b) shows that there are two free-energy minima for $m_1 \neq m_2$ (the curves are iso-energy contours and darker shades correspond to lower energy), whereas outside the range $[T_{c1}, T_{c2}]$ there is only one free-energy minimum (m_0) on the $m_1 = m_2$ line as is seen for $k_BT/J = 8$ (c). This is seen explicitly in (d) when the free energy per spin F is observed along the curve of steepest descent from m_0 (for $T_{c1} < T < T_{c2}$) or along the curve of slowest ascent (for $T < T_{c1}$ or $T > T_{c2}$). All the results shown in (a-d) are obtained analytically. (e) Time-evolution of the magnetizations per spin of the two modules, m_1 and m_2, shown for MC simulations with $N = 100$ at $k_BT/J = 5$. In the chimera ordered state, the system switches due to thermal noise between the two free-energy minima corresponding to the two modules exchanging their magnetization states between $m_>$ and $m_<$. In all cases, $a = 1$ and $b = H = 10$.

Eqs. 5.3-5.4 may be expressed in the form $m_{1,2} = g(m_{2,1})$, where we define the one-dimensional map,

$$g(x) = \frac{1}{b}\left[2ax + H - \frac{k_B T}{2}\log\frac{1+x}{1-x}\right]. \tag{5.5}$$

Solutions of $g^2(x) \equiv g(g(x)) = x$ give the extrema m_1^* and m_2^* of the free-energy F (Eq. 5.2). Numerical solution for the extrema values shows that for suitable parameter values and $H > H_0$, the system has two critical temperatures T_{c1} and T_{c2}. For temperatures lower than T_{c1} and above T_{c2} the only fixed-point of the map g^2 is the unstable fixed point, $g(x) = x$, of Eq. (5.5). Thus, this solution corresponds to $m_1 = m_2 \equiv m_0$, where the free energy $F(m_1, m_2)$ has a minimum. The value for m_0 is obtained from

$$(-2a + b)m_0 - H + \frac{k_B T}{2}\log\frac{1+m_0}{1-m_0} = 0. \tag{5.6}$$

However, in the temperature range $T_{c1} < T < T_{c2}$, there are *two* types of fixed points of the twice-composed map g^2: (i) a stable fixed point $m_1 = m_2 = m_0$ [obtained from Eq. (5.6)] corresponding to a saddle point of the free energy function [shown by a broken line in Fig. 5.2 (a)], and (ii) the pair of unstable fixed points $m_1 \neq m_2$ which form a period-2 orbit of Eq. (5.5) corresponding to a minimum of the free energy F [shown by solid lines in Fig. 5.2 (a)]. As one of $(m_1\ ,\ m_2)$ is higher and the other low, we obtain a chimera state where one module is disordered ($m_<$) relative to the other module ($m_>$). The chimera state occurs through subcritical pitchfork bifurcations of the map g^2 as the temperature is increased above T_{c1} or decreased below T_{c2} [1]. For $H < H_0$, the system exhibits chimera ordering for $T > 0$ and it has a single critical temperature at T_{c2} above which the magnetizations of the two modules become same.

By observing the free-energy $F(m_1, m_2)$ landscape in the range $0 \leq m_1, m_2 \leq 1$, we obtain a clear physical picture of the transition to chimera ordering [Fig. 5.2 (b-c)]. The homogeneous state $m_1 = m_2 = m_0$ is a local extremum (i.e., $\partial F/\partial m_{1,2} = 0$) for the range

[1] It is of interest to note that the chimera state in oscillator arrays occur via saddle-node bifurcation [78, 126, 137].

of parameters considered here. However, its nature changes from a free-energy minimum to a saddle point as the temperature is increased beyond T_{c1} and again changes back to a minimum when temperature exceeds T_{c2}. This is seen by looking at the matrix of the second derivatives of free energy per site with respect to m_1, m_2:

$$\mathcal{H}\big|_{m_0} = \begin{pmatrix} A & b \\ b & A \end{pmatrix}, \tag{5.7}$$

where $A = -2a + k_B T \frac{1}{1-m_0^2}$. The eigenvalues of this matrix are $\lambda_+ = A + b$ along the $m_1 = m_2$ line and $\lambda_- = A - b$ in the direction perpendicular to it (parallel to $m_1 = -m_2$ line). Below T_{c1} and above T_{c2} both eigenvalues are positive indicating that m_0 is a minimum [Fig. 5.2 (c)]. The transition to chimera ordering occurs in the range $T_{c1} < T < T_{c2}$ when the smaller eigenvalue λ_- becomes negative while the other eigenvalue remains positive, indicating that m_0 is now a saddle point. This gives us an implicit relation for T_c as the temperature where $\lambda_- = 0$, which gives

$$k_B T_c = 2(2a + b)(1 - m_0^2).$$

Numerical investigation of the landscape indicates that this transition is accompanied by the creation of two minima away from the $m_1 = m_2$ line [Fig. 5.2 (b)]. These minima are symmetrically placed about the $m_1 = m_2$ line [as $F(m_1, m_2) = F(m_2, m_1)$] and correspond to the two coexisting chimera states $C_1 : m_1 = m_>, m_2 = m_<$ and $C_2 : m_1 = m_<, m_2 = m_>$. The two minima are separated by an energy barrier $\Delta = F(m_0, m_0) - F(m_>, m_<)$ which for a finite system can be crossed by thermal energy [Fig. 5.2 (d)]. This switching behavior between the two chimera states has a characteristic time $\tau \sim \exp(\Delta/k_B T)$ which is indeed observed from MC simulations in small systems [Fig. 5.2 (e)] [2] Note that each

[2]For $N = 100$, we observe that $\tau > 10^3$ MC steps for a range of temperatures. For larger systems, e.g., $N = 1000$, switching was not observed for the duration of our simulations, which is consistent with the exponential divergence of τ as one approaches the thermodynamic limit. This follows from the exponential dependence of τ on the energy barrier height, and the fact that free energy is proportional to N for given values of a, b, H and T as can be seen from Eq. (5.2).

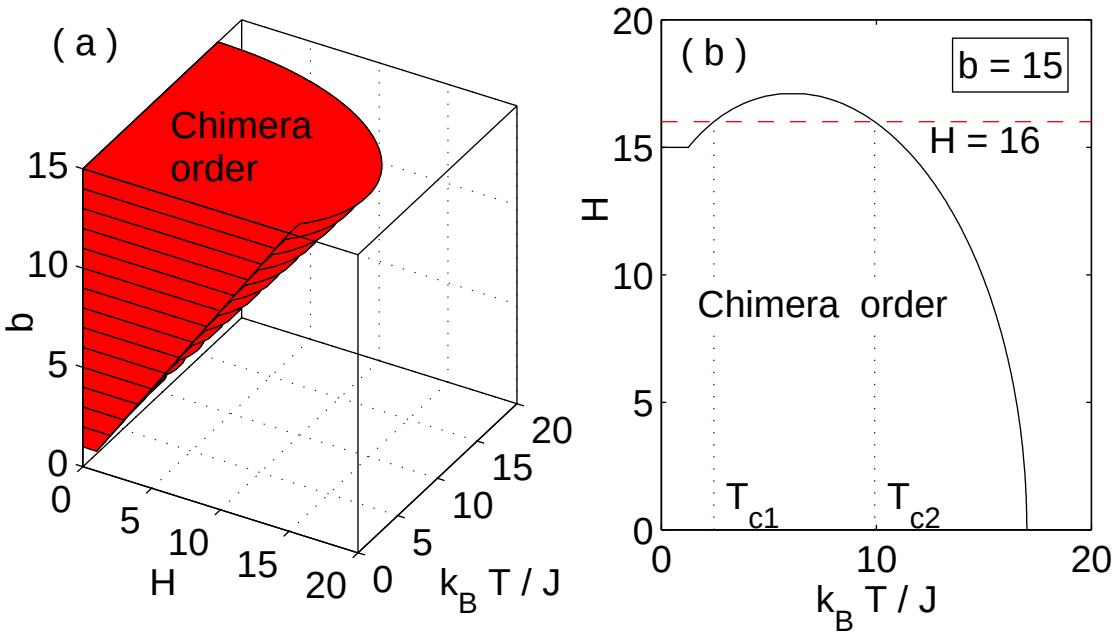

Figure 5.3: (a) Phase diagram in the magnetic field (H), temperature (k_BT/J) and antiferromagnetic coupling (b) parameter space obtained by numerical minimization of free energy for $a = 1$ with the region in which chimera ordering occurs being indicated. A cross-section along $H - T$ plane for $b = 15$ is shown in (b). The broken line indicates $H = 16$, for which the critical temperatures are shown by dotted lines.

minimum corresponds to a state having a specific arrangement of both highly ordered and weakly ordered regions, and hence is unlike the minima seen in phase-coexistence state of systems such as metamagnets, where each of the minima corresponds to a homogeneous phase (ordered or disordered) [3].

Fig. 5.3 shows the region in ($H - T - b$) parameter space where chimera ordering is observed in our system as obtained by numerical minimization of the free energy. Temperature induced transitions are always continuous whose exponents are analytically derived below. To investigate the critical behavior of the system around T_{c1} and T_{c2}, we shall use the order parameters:

$$p_1 = m_1 - m_2 \quad \text{and} \quad p_2 = 2m_0 - (m_1 + m_2).$$

[3] See, e.g., Section 4 of Ref. [133].

For $T_{c1} < T < T_{c2}$ where the chimera ordering is observed, as mentioned earlier the free-energy minima are at m_1 and m_2 while m_0 corresponds to a saddle point. The order parameters p_1 and p_2 are non-zero in this region and zero elsewhere. When p_1, p_2 are small, we solve for them using Eqs. (5.3), (5.4) and (5.6) by expressing m_1 and m_2 in terms of p_1, p_2, and obtain

$$p_1 \propto \mid T - T_c \mid^{1/2} \quad \text{and} \quad \mid p_2 \mid \propto \mid T - T_c \mid . \tag{5.8}$$

Thus, as $T \to T_{c1}^{+}$ or $T \to T_{c2}^{-}$, the order parameters vanish continuously with exponents $\beta = 1/2$ for p_1 and $\beta = 1$ for p_2. Similar calculations for the field induced transition at finite temperature yield identical critical exponents. Note that at zero temperature the field induced transition is of first order and its discontinuous nature can be shown exactly by analyzing the free energy. The values of the exponents for all continuous transitions have been confirmed by us numerically.

We have also analyzed the critical behavior of the specific heat $C = -T\frac{\partial^2 F_0}{\partial T^2}$ where F_0 is the equilibrium free energy at a given a, b, H and T. Although it involves both first and second order derivatives of p_1 and p_2, as the most dominant term is $\partial^2 p_1/\partial T^2$, the divergence at critical temperature is characterized by exponent $\alpha = 3/2 : C \propto \mid T - T_{c1,c2} \mid^{-3/2}$.

While the system we have considered so far has the advantage of being amenable to exact analytical treatment, we have also numerically analyzed spin models which are closer to real magnetic materials. We have performed MC simulation studies of a three-dimensional Ising spin model with nearest neighbor interactions having an anisotropic nature [Fig. 5.4 (a)]. The system emulates a layered magnetic system comprising multiple layers of two-dimensional spin arrays stacked on top of each other, with interactions along a plane being ferromagnetic (J) and those between planes anti-ferromagnetic ($-J'$). One example of such a system is $FeCl_2$ where the exchange integral between Fe electron clouds is such that the Fe atoms within the same layer interact ferromagnetically while those in different layers interact antiferromagnetically [133]. Fig. 5.4 (b-c) shows chimera

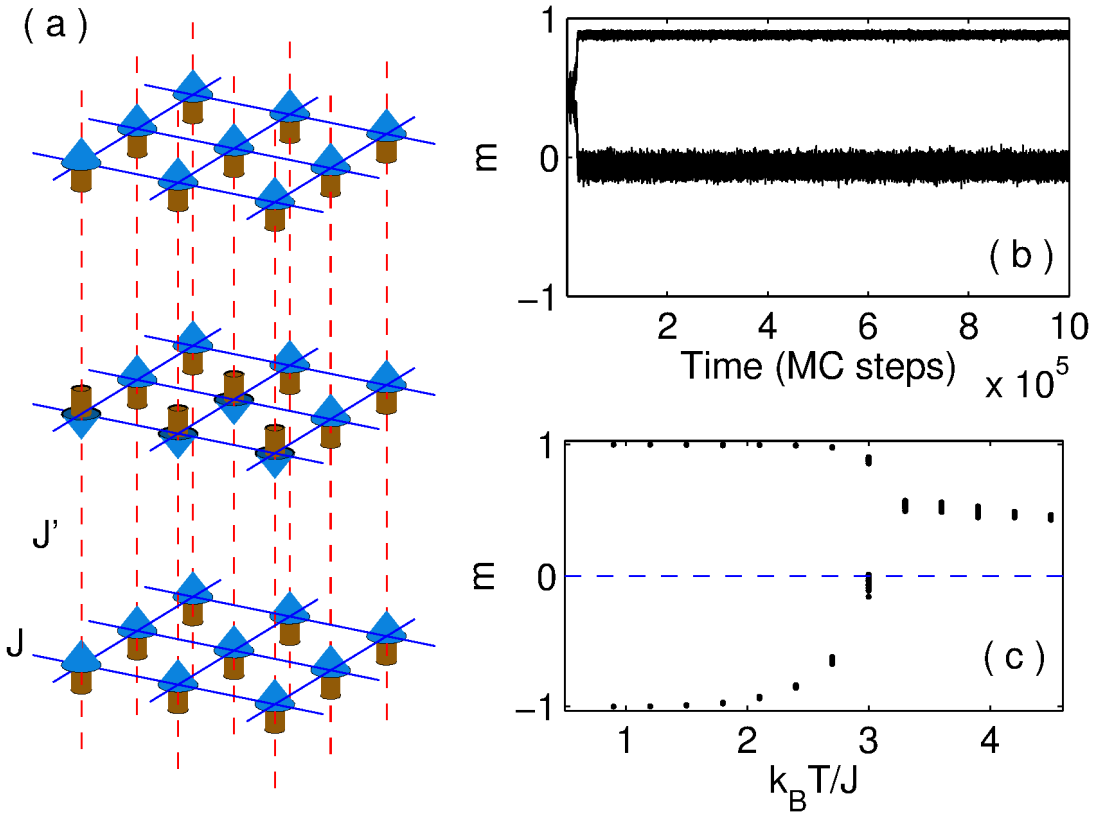

Figure 5.4: (a) Schematic diagram of the 3-dimensional layered spin system with ferromagnetic (anti-ferromagnetic) interactions within layers, J (between layers, J') indicated by continuous (broken) lines. In the chimera state alternate layers show strong and weak order. (b) The time-evolution in MC steps of the magnetization of each of the 32 layers of a 3-dimensional system, with every layer having 128×128 spins, showing chimera ordering for $k_BT/J = 3$. (c) The magnetizations of different layers of the $128 \times 128 \times 32$ spin system at different temperatures. Chimera ordering is manifested as different values of $|m|$ for alternate layers (e.g., at $k_BT/J = 3$). In all cases $J = J' = 1$ and $H = 1.8$.

ordering in such a 3-dimensional spin system with periodic boundary conditions and starting from random initial spin configurations. As seen from Fig. 5.4 (b), the chimera state appears relatively rapidly and persists for the duration of the simulation. Similar behavior was observed in other systems having different sizes, parameters and interaction structure, indicating that chimera ordering is a robust phenomenon that should be possible to observe in an experimental magnetic system. Note that in this system the chimera ordering is observed with nearest neighbor interactions, while, for systems of coupled oscillators, chimera states have so far been observed only with spatially non-local coupling.

5.4 Discussion and Conclusion

In summary, we have shown the existence of a novel complex ordering behavior that we term chimera order in analogy with the simultaneous occurrence of coherent and incoherent behavior in dynamical systems. For a system of two clusters of Ising spins, where the spins are coupled ferromagnetically (anti-ferromagnetically) to all spins in the same (other) cluster, subjected to a uniform external magnetic field at a given temperature, chimera ordering is manifested as a much higher magnetization in one cluster compared to the other. To illustrate the wider implication of our result we can use the analogy of two communities of individuals who are deciding between a pair of competing choices. The interactions of an agent with other members of its own community strongly favor consensus while that with members of a different community are antagonistic. Thus, given that every individual is exposed to the same information or external environment, we would expect that unanimity about a particular choice in one community will imply the same for the contrary choice in the other community. However, the occurrence of chimera order suggests that under certain conditions, when given the same external stimulus we may observe consensus in one community while the other is fragmented.

While chimera states (defined in the original context of oscillators) have been recently

observed in experiments [138–140], extension of the concept of chimera state as defined here suggests an alternative approach to experimentally observe such states in physical systems. Our demonstration of chimera order in a three-dimensional spin system with nearest neighbor interactions indicate that a possible experimental example can be layered magnetic materials (e.g., manganites) having different types of interactions between and within layers [133, 134]. Although in this chapter we look at the case of two competing choices, it is possible to extend the analysis to q-state Potts spin dynamics. Given the wider applicability of spin models for studying ordering in different contexts, one can consider other connection topologies as well as mesoscopic features such as the occurrence of multiple modules (> 2) and hierarchical organization.

6

Extreme variability in convergence to structural balance in frustrated dynamical systems

6.1 Introduction

Many complex systems that arise in biological, social and technological contexts can be represented as a collection of dynamical elements, interacting via a non-trivial connection topology [141, 142]. A variety of critical behavior has been observed in such systems, both in the collective dynamics taking place on the network, as well as in the evolution of the network architecture itself [26]. The interplay between changes to the connection topology (by adding, removing or rewiring links) and nodal dynamics has also been investigated in different contexts [143–149]. While the coevolution of network structure and nodal activity has mostly been studied in the simple case where the links are either present or absent, many naturally occurring networks have links with heterogeneously distributed properties. Connections in such systems can differ quantitatively by having a distribution of weights (which may represent the strength of interaction) [150–152] and/or qualita-

tively through the nature of their interactions, viz., positive (cooperative or activating) and negative (antagonistic or inhibitory) [153]. The presence of negative links in signed networks can introduce frustration through the presence of inconsistent relations within cycles in the system [154, 155]. Networks whose positive and negative links are arranged such that frustration is absent are said to be *structurally balanced* – a concept that was originally introduced in the context of social interactions [156]. A classic result in graph theory is that a balanced network can be always represented as comprising two subnetworks, with only positive interactions within each subnetwork, while links between the two are exclusively negative [157]. Networks of dynamical elements with such structural organization can exhibit non-trivial collective phenomena, e.g., “chimera" order [79].

Recently, the processes through which structural balance can be achieved in networks has received attention from scientists and quantitative models for understanding their underlying mechanisms have been proposed. Evolving networks where the sign of links are flipped to reduce frustration have been shown to reach balance; however, introduction of constraints can sometimes result in jammed states which prevent convergence to the balanced state [158, 159]. Another approach, using coupled differential equations for describing link adaptation [160], has been analytically demonstrated to result in balance [161, 162].

While most studies on structural balance have been done in the context of social networks, an important question is whether other kinds of networks, in particular, those that occur in biology, exhibit balance. The recent observation that the resting human brain is organized into two subnetworks that are dynamically anti-correlated (with the activity within each subnetwork being correlated) [163] point to the intriguing possibility that the underlying network may in fact be balanced. As connections in the brain evolve according to long-term potentiation which embodies Hebb’s principle [164, 165], i.e., the link weights change in proportion to the correlation between activity of the connected elements, it suggests a novel process for achieving structural balance. Thus, signed and

weighted networks can remove frustration by adjusting the weights associated with the links in accordance with the dynamical states of their nodes. Such a local adaptation process has an intuitive interpretation in social systems, viz., agents that act alike have their ties strengthened, while those behaving differently gradually develop antagonistic relations. In fact, Hebb's rule may apply more broadly to a large class of systems, for example, in gene regulation networks where it has been suggested that co-expression of genes can lead to co-regulation over evolutionary time-scales [166, 167].

In this chapter, we show that such a link-weight adaptation dynamics can in fact lead to structural balance (shown schematically in Fig. 6.1), using only local information about the correlation between dynamical states of the nodes. The temporal behavior of the approach to balance shows unexpected features. In particular, we observe that the system exhibits a high degree of variability in the time required to converge to the balanced state when stochastic fluctuations are present in the nodal dynamics. This relaxation time has a bimodal distribution for a range of adaptation rates and noise strengths. Finite-size scaling of the transition from fast to slow relaxation shows that the variation of the scaling exponent is related to the qualitative nature of the way the bimodal distribution emerges. As a larger fraction of positive (negative) interactions reduces (promotes) frustration, we also investigate the role of bias in the sign of interactions on the nature and rate of convergence to the balanced state.

6.2 Model

We consider a system of N globally coupled Ising spins $\sigma_i = \pm 1$ ($i = 1, \ldots, N$), the energy for a given configuration of spins being

$$\mathcal{E} = -\sum_{i \neq j} J_{ij}\sigma_i\sigma_j \tag{6.1}$$

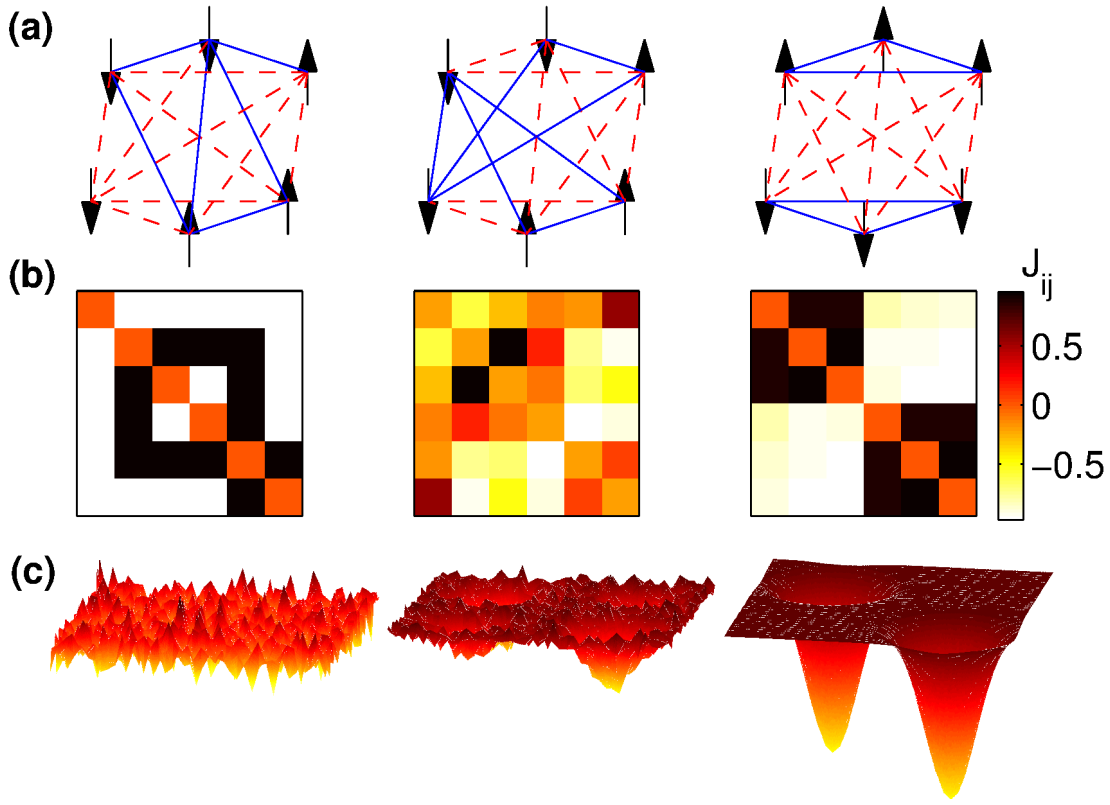

Figure 6.1: Coevolution of coupling strength with the dynamics on the node starting from a disordered state of spin orientations and interaction strengths randomly selected to be ±1. (a) The spin configurations in the initial (left), intermediate (center) and final, i.e., after convergence to structural balance (right), states for a system of $N = 6$ spins. Solid (broken) lines represent positive (negative) interactions between spins. The corresponding coupling matrices J are shown in (b) while the schematic energy landscapes are represented in (c). The two minima in the balanced state correspond to the pair of degenerate ground states related by reversal of each spin.

where $J_{ij}(= J_{ji})$ is the symmetric bond, representing interaction strength between the spin pair (i, j). Structural balance in real social networks have been recently investigated using a similar energy function [168, 169]. The balanced state corresponds to the situation where the interactions are consistent with the corresponding spin pairs, i.e., J_{ij} and $\sigma_i\sigma_j$ have the same sign. Starting from a disordered spin configuration and random distribution of interactions, the state of the spins are updated stochastically at discrete time-steps using the Metropolis Monte Carlo (MC) algorithm with temperature T. The interaction strengths also evolve after every MC step according to the following deterministic adaptation dynamics:

$$J_{ij}(t+1) = (1-\epsilon)J_{ij}(t) + \epsilon\sigma_i(t)\sigma_j(t), \tag{6.2}$$

where ϵ governs the rate of change of the interaction relative to the spin dynamics. The J_{ij} dynamics alters the energy landscape on which the state of the spin system evolves. The *relaxation time* for the system is defined as the characteristic time scale in which the balanced state is reached. Note that the form of Eq. (6.2) ensures that the relaxation time $\sim 1/\epsilon$ in the absence of any thermal fluctuation (i.e., at $T = 0$). Also, it restricts the asymptotic distribution of J_{ij} to the range $[-1, 1]$, independent of whether the system converges to a balanced state. In many real systems the signature of the link cannot change, although the magnitude of the link weight can. We have also considered a variant of Eq. (6.2) for which the dynamics is constrained such that the sign of each J_{ij} cannot change from the initially chosen value. As a result several of the interactions can go to zero when the system relaxes.

In our simulations the initial state of the system for each realization is constructed by choosing the spins σ_i to be ± 1 with equal probability. For most results shown here, each initial J_{ij} is chosen from a distribution with two equally weighted δ function peaks at ± 1, i.e., $P(z;\mu) = [(1+\mu)/2]\delta(z-1) + [(1-\mu)/2]\delta(z+1)$ where the mean $\mu = 0$. We have verified that the results do not change qualitatively if the initial distribution has a non-zero mean, or has a different functional form (e.g., a uniform distribution in $[-1, 1]$),

provided that the system is initially far from balance. For each set of parameters (T, ϵ), 10^4 different realizations have been used to statistically quantify the relaxation behavior of the system, which is identified using the energy per bond [Eq.(6.1)] normalized by the number of connections, i.e., $E = \mathcal{E}/\binom{N}{2}$, as the order parameter. The number of spins has been chosen to be $N = 64$ for most of the figures shown here, although we have verified that the results are qualitatively unchanged for N upto 512. Simulating larger systems is computationally very expensive as the system is globally coupled and disordered with time-varying interactions.

6.3 Results

In the absence of thermal fluctuations (i.e., at $T = 0$), the dynamics of the system can be understood intuitively. Starting from a random initial state, the spin dynamics stops when the system gets trapped in local energy minimum within a few MC steps ($\sim 1/\epsilon$, as mentioned above). The subsequent evolution of the interaction strengths makes this configuration a global minimum. However, at finite temperature, the stochastic fluctuations of the spins may prevent the system from remaining in a metastable state for sufficiently long. This does not allow the J_{ij} dynamics to alter the energy landscape sufficiently to make the configuration the global minimum. Thus, an extremely long time may be required to reach structural balance, and the relaxation time diverges due to the stronger fluctuations on increasing temperature.

Fig. 6.2 (a) shows the time-evolution of the order parameter E for several typical runs for different initial conditions and realizations of a system with $T = 15, \epsilon = 0.05$. The order parameter of the system initially corresponds to that for a maximally disordered state (≈ 0) but eventually relaxes to a balanced state ($E = -1$). The time required for reaching balance, referred to as *relaxation time*, τ, is estimated by measuring the duration starting from the initial state after which E decreases below $-1/2$ [Fig. 6.2 (a)]. For a large

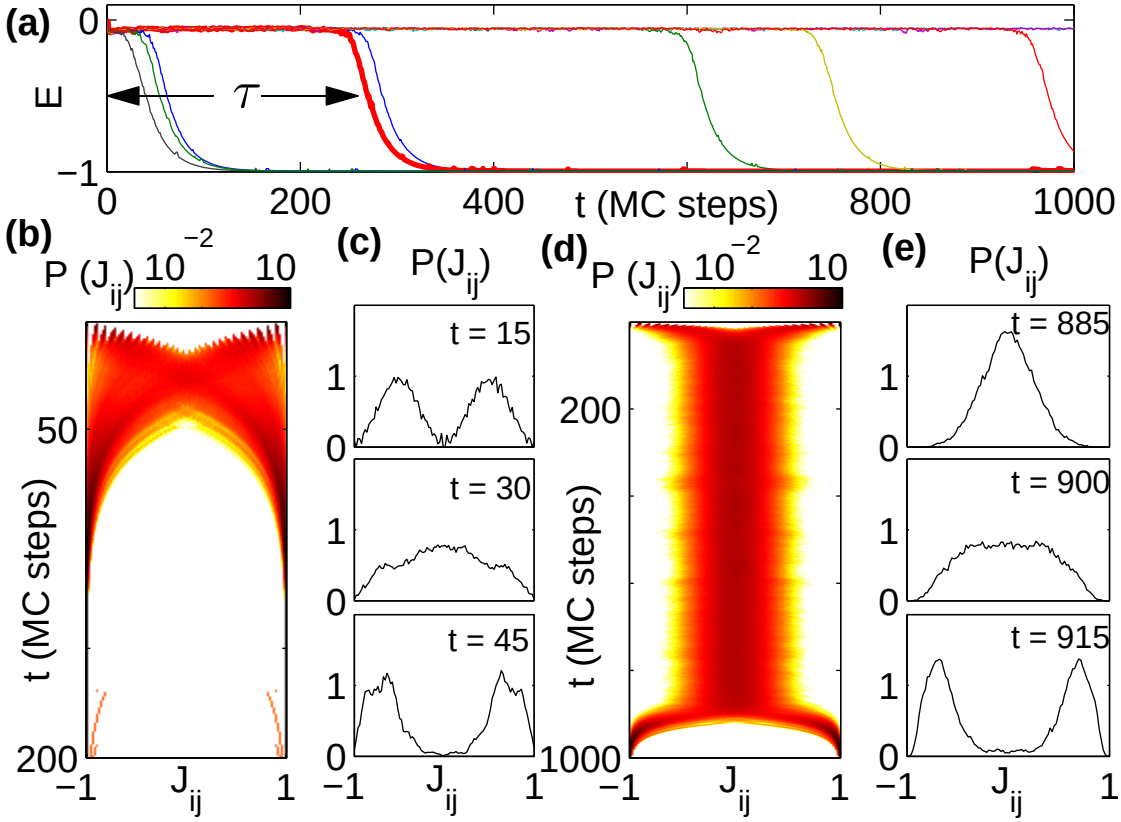

Figure 6.2: (a) Typical time-evolution of the energy per bond E for a system of N spins starting from different initial conditions. The relaxation time τ indicated in the figure is the duration after which E decreases below -0.5. (b-e) Time-evolution of the distributions for the interaction strength J_{ij} shown for two cases: (b-c) when the system relaxes rapidly and (d-e) when convergence takes much longer. Snapshots of the J_{ij} distribution at specific times immediately before, during and immediately after the convergence are shown for the two cases in (c,e) respectively. For all figures $N = 256$ with $T = 51$, $\epsilon = 0.05$.

range of parameters, we observe two very distinct types of behavior: in one, the system relaxes rapidly, while in the other this takes a longer time. In both cases, once the order parameter starts decreasing (i.e., after time τ), it reaches a balanced state within a time-interval $\sim 1/\epsilon$. As this is typically much shorter than the relaxation time for the second case, the transition to the balanced state can appear rather suddenly for the latter. Before the onset of the convergence to the balanced state, the order parameter fluctuates over a very narrow range around zero, and there is little indication as to when the transition will happen. Characteristic time-evolution corresponding to these two types of behavior are shown in Fig. 6.2 (b-e). When the system relaxes rapidly, smaller peaks emerge from the two peaks of the initial J_{ij} distribution (located at ± 1) and eventually cross each other to reach the opposite ends asymptotically, converging to a two-peaked distribution again [Fig. 6.2 (b-c)], indicating that all interactions are now balanced. However, in the case where convergence takes significantly longer [Fig. 6.2 (d-e)], the initial distribution is first completely altered to a form resembling a Gaussian distribution with zero mean. After a long time, the system abruptly converges towards a balanced state with a corresponding transformation of the J_{ij} distribution to one having peaks at ± 1. Note that even with the same initial spin configuration and realization of J_{ij} distribution, different MC runs generate distinct trajectories that are similar to those shown in Fig. 6.2 (a). This implies that knowledge of the initial conditions is not sufficient to decide whether the system will relax rapidly or not.

To quantitatively characterize the distinction between the two types of relaxation behavior, we focus on the statistics of τ (Fig. 6.3). Fig. 6.3 (a) shows the distribution of the relaxation time for a given set of (T, ϵ) where cases of both fast and slow convergences are seen. The resulting bimodal nature is clearly observed with the peak at lower τ ($\sim$ 100 MC steps) corresponding to fast convergence to balanced state while that occurring at a higher value ($\sim 10^7$ MC steps) arises from the instances of slow relaxation. The distribution decays exponentially at very high values of τ. Fig. 6.3 (b) shows the temperature dependence of the distribution of $\log_{10}(\tau)$ for two different values of ϵ. For the smaller ϵ

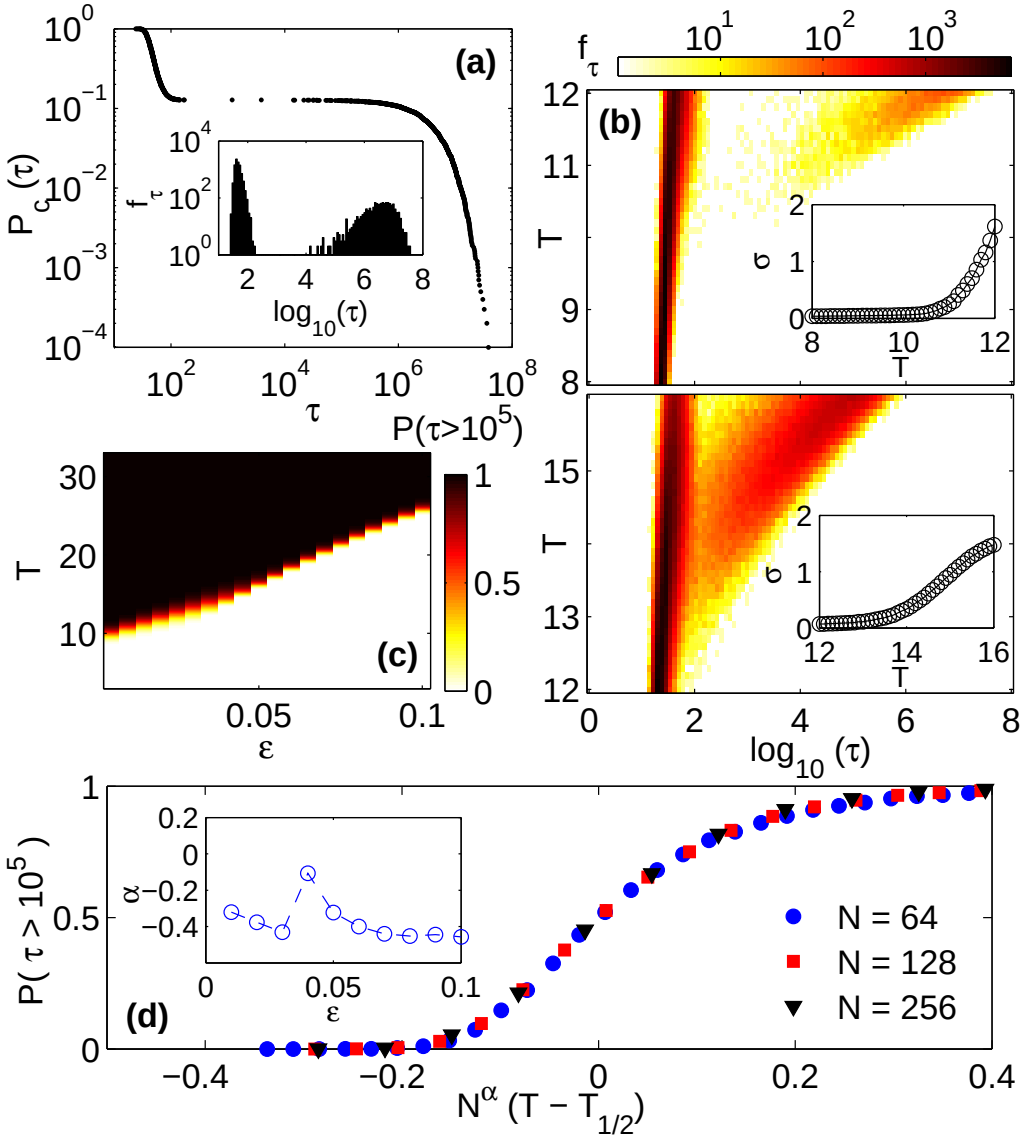

Figure 6.3: (a) The cumulative distribution of relaxation time τ for system of $N = 64$ spins with $T = 12, \epsilon = 0.03$ shows a gap implying a bimodal nature for the distribution. The inset showing the corresponding frequency distribution f_τ for $\log_{10}(\tau)$ clearly indicates this bimodal nature. (b) Probability distributions of $\log_{10}(\tau)$ shown as a function of temperature T for $\epsilon = 0.03$ (top) and 0.05 (bottom) indicates the onset of bimodal behavior at higher values of temperature, e.g., for $T \gtrsim 10$ in (top). Bimodality appears around the temperature where the standard deviation of $\log_{10}(\tau)$ starts increasing appreciably from an almost constant value (insets). (c) The probability that relaxation takes longer than 10^5 MC steps, $P(\tau > 10^5)$ shown as a function of ϵ and T. The point of transition from fast to slow convergence can be quantified by $T_{1/2}(\epsilon)$, i.e., the temperature at which $P(\tau > 10^5)$=1/2 for a given value ϵ (indicated by boundary between the dark and light regions). (d) Finite size scaling of the probability that relaxation takes longer than 10^5 MC steps, $P(\tau > 10^5)$, with $N^\alpha(T - T_{1/2})$ for different system sizes N ($\epsilon = 0.05$). The temperature at which $P(\tau > 10^5)$ becomes half is represented as $T_{1/2}$. A scaling exponent value of $\alpha \approx -0.32$ shows reasonable data collapse. The inset shows the scaling exponents for the best data collapse at different values of ϵ.

(= 0.03), the second peak is well-separated from the first when bimodality first appears, while for the larger ϵ (= 0.05) the second peak appears close to the first one. To estimate the temperature where the second peak appears, we plot the standard deviation of $\log_{10}(\tau)$ as a function of T (inset), as bimodality is characterized by an increase in the dispersion of relaxation times. To observe how the distribution is affected by variation in both T and ϵ, we show in Fig. 6.3 (c) how the probability that the relaxation takes a long time (viz., $\geq 10^5$ MC steps) varies as a function of these two parameters. As we know that the system relaxes rapidly when the temperature is decreased close to zero, we expect this probability to be negligible at very low values of T. On the other hand, when temperature is increased to very high values, the relaxation takes increasingly longer, so that the probability $P(\tau > 10^5)$ approaches 1. We indeed observe a monotonic increase in this probability from 0 to 1 as the temperature is increased for a given value of ϵ. We can define a transition temperature $T_{1/2}(\epsilon)$ as the value of T at which this probability is equal to $1/2$. We observe that $T_{1/2}(\epsilon)$ increases with ϵ, which implies that the relaxation to the balanced state requires a longer duration as the interaction dynamics becomes slower. For a given ϵ, we study the variation of the probability $P(\tau > 10^5)$ with T for different system sizes. Finite-size scaling shows data collapse with a scaling exponent α [Fig. 6.3 (d)] that varies with ϵ (inset). Depending on the value of ϵ, we observe that there may be different types of bimodal distribution of the relaxation times, e.g., one where the second peak is clearly separated from the first, and the other where they are joined [Fig. 6.3 (b)]. The variation of α with ϵ appears to reflect this change from one type of bimodality to another (inset).

So far we have assumed that the initial J_{ij} distribution is unbiased (i.e., $\mu = 0$). However, having a higher fraction of interactions of a particular sign can have significant consequences for both the structure of the final balanced state and the time required to converge to it. To investigate the role of this initial bias among the interaction strengths, we consider a distribution with two differently weighted δ function peaks at ± 1 (i.e., $\mu \neq 0$). Fig. 6.4 (a) shows the distribution of the relaxation times as μ is varied over the inter-

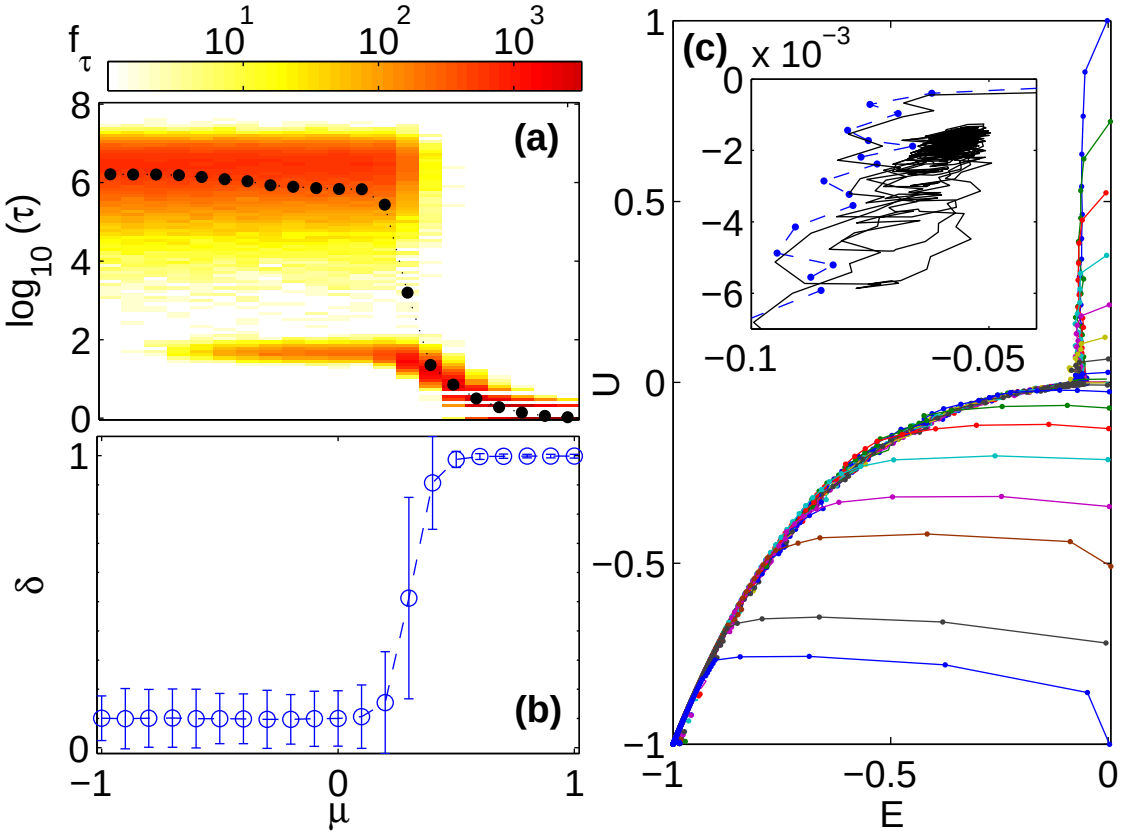

Figure 6.4: (a) Probability distribution of $\log_{10}(\tau)$ shown as a function of the mean μ of the initial distribution for J_{ij} for $T = 17$, $\epsilon = 0.05$. The filled circles represent the average of $\log_{10}(\tau)$ for different values of μ. The distribution does not change much for small bias ($|\mu|$); however the lower peak disappears as μ approached -1 while the the relaxation behavior occurs faster as μ approaches $+1$. (b) Scaled size difference $\delta = (C_1 - C_2)/N$ between the two clusters of aligned spins shown as a function of μ. As μ increases from negative values to 1, δ increases from values close to 0 towards 1. (c) Trajectories representing the time-evolution of the system ($N = 256$) in the (E, U) order parameter space for different values of μ (from top to bottom, μ increases from -1 to 1 in steps of 0.1). After transients, all trajectories converge to a single curve independent of the time required to converge to the balanced state. A magnified view (inset) compares the trajectory corresponding to a long relaxation time (solid curve), which appears to be trapped in this region, with the one corresponding to a short relaxation time (broken curve) for $\mu = 0$.

val $[-1, 1]$ with the parameters T, ϵ chosen such that there is a clear bimodal nature of the relaxation time distribution for the unbiased case ($\mu = 0$). If all the interactions are anti-ferromagnetic ($\mu = -1$), the system is extremely frustrated and the relaxation to a balanced state may take a long time, whereas in the case where the interactions are all ferromagnetic ($\mu = 1$), the system is balanced to begin with. Thus, with increasing μ, we expect the relaxation time to decrease, which is indeed observed; in addition, the peak at higher values of τ disappears as μ approaches 1. On the other hand, when μ approaches -1, the peak corresponding to shorter relaxation times is no longer present. The two clusters that comprise the final balanced state can have very different size distributions depending on the bias in the initial distribution of J_{ij}. For the unbiased case, the two clusters are approximately of the same size. We observe from Fig. 6.4 (b) that this property holds for the entire range of negative values for μ. As μ increases from 0, the size difference between the two clusters start increasing, eventually leading to a single cluster where all the spins interact with each other ferromagnetically ($\mu \simeq 1$). Note that if the system initially has a very low degree of frustration [e.g., $\mu \geq 0.4$ in Fig. 6.4 (a,b)], the system relaxes almost immediately to a balanced state where the larger cluster comprises almost the entire system. To visualize the coevolving dynamics in the link weights and spin orientations as the system approaches balance for different values of μ, we use an additional order parameter [158, 159] that measures the frustration in a signed network in terms of the fraction of triads deviating from balance (a triad being balanced if the product of its link weights approaches +1), $U = -\sum_{i,j,k} J_{ij}J_{jk}J_{ki}/\binom{N}{3}$. Fig. 6.4 (c) shows that the trajectories corresponding to different values of μ converge to a single curve after transients, eventually reaching the balanced state at $(E = -1, U = -1)$. For $\mu < 0$, the initial trajectory is approximately vertical indicating that it is dominated by the adaptation dynamics (Eq. 6.2), whereas for $\mu > 0$, it has strong horizontal component implying that it is governed primarily by the MC update of the spin states. Realizations in which the system takes a long time to relax to the balanced state are distinguished by trajectories that appear to be trapped in a confined region in the (E, U) space for a considerable period

[Fig. 6.4 (c), inset].

We can qualitatively understand the appearance of short relaxation times as follows. In the initial state, when the system has a random assignment of interaction strengths, the energy landscape is extremely rugged, resembling that of a spin glass [154]. The system starts out in a potential well corresponding to one of the many initially available local minima. As the state of the system evolves, the J_{ij} dynamics (Eq. 6.2) lowers the energy of the state by making the interactions consistent with the spin orientations of the system, while the spin dynamics (updated according to the MC algorithm) can either result in a further lowering of energy as the state moves towards the bottom of the potential well, or is ejected from the initial local minima due to thermal fluctuations. The probability of escaping from the well at the t-th iteration, $p(t)$, depends on the potential barrier height with neighboring wells. If the state cannot escape in the first few iterations from the local minimum from which it starts, successive lowering of the energy of this well by the J_{ij} dynamics results in the minima becoming deeper, so that the probability of escape is reduced further. Eventually, the system relaxes to the balances state with a time-scale of $\sim \epsilon^{-1}$, when the well becomes the global minimum of a smooth energy landscape. On the other hand, if the state escapes from the initial well within the first few iterations, when the J_{ij} dynamics has not yet been able to significantly reduce the energy of a particular well, the barrier heights separating the different local minima are all relatively low. As a result, the system can jump from one well to another with ease, corresponding to frequent switching of the spin orientations. As J_{ij} moves towards $\sigma_i\sigma_j$ at any given time (Eq. 6.2), rapid changes in the sign of the latter implies that there is effectively no net movement of J_{ij} towards ± 1. In fact, in this case, we observe that the initial distribution of J_{ij}, comprising delta-function peaks at ± 1, transforms within a few iterations to one resembling a Gaussian peaked at zero [Fig. 6.2 (d-e)]. Once the system reaches such a state, it can only attain a balanced state through a low-probability event which corresponds to the state remaining in the same local minimum for several successive time steps. As such an event will only happen after extremely long time, this will lead to a very large relaxation time for a range of T and

ϵ. Let us assume for simplicity that when the system is in the state corresponding to frequent spin flips and low interaction strengths, the probability of escaping from a local minimum is approximately a constant ($p(t) \approx p$). Then the probability that the system jumps between different minima for t steps and gets trapped in the $t+1$-th step is $p^t(1-p)$. This results in the distribution of the relaxation times (under the simplifying assumption of constant p) having an exponential tail, which is indeed observed [Fig. 6.3 (a)].

6.4 Discussion and Conclusion

To conclude, we have shown that a link adaptation dynamics inspired by the Hebbian principle can result in an initially frustrated network achieving structural balance. However, in the presence of fluctuations, we observe that the system exhibits a large dispersion in the time-scale of relaxation to the balanced state, characterized by a bimodal distribution. This extreme variability of the time required to converge to the balanced state is a novel phenomenon that requires further investigation. Our result suggests that even when a system has the potential of attaining structural balance, the time required for this process to converge may be so large that it will not be observed in practice. Although we have considered a globally connected network of binary state dynamical elements, it is possible to extend our analysis to sparse networks [27, 170] and different kinds of nodal dynamics (e.g., q-state Potts model). As many networks seen in nature have directed links, a generalization of the concept of balance to directed networks and understanding how it can arise may provide important insights on the evolution of such systems.

7

Conclusions

> *A complex system is exactly that; there are many things going on simultaneously. If you search carefully, you can find your favorite toy: fractals, chaos, self-organized criticality, Lotka-Volterra predator-prey oscillations, etc., in some corner, in a relatively well developed and isolated way. But do not expect any single simple insight to explain it all.*
>
> – Rolf Landauer, as quoted in Ref. [8]

The work described in this thesis form part of a research program aimed at revealing the general principles underlying the dynamical behavior of complex systems. We view a complex system as comprising relatively large number of components coupled to each other via various types of connection topologies and nature of interactions, such that new phenomena emerge at the systems level that are absent in the dynamics of individual elements. While this definition is sufficiently broad to cover a large variety of natural, technological and social systems, our research strategy involves systematically varying the complexity at the level of the dynamics of the individual elements and in the nature of connections to uncover universal features underlying the dynamics of apparently very different complex systems, ranging from spin models to opinion formation and from the

pregnant uterus to microarray of chemical oscillators. In the following subsections, the important results and conclusions reported in the thesis are summarized. We conclude with a brief discussion of possible future extensions of our results.

7.1 Summary of main results

Self-organization of coherent activity in heterogeneous system of coupled excitable and passive cells

Synchronized oscillations are of critical functional importance in many biological systems. In this thesis we have shown that such oscillations can arise without centralized coordination in a disordered system of electrically coupled excitable and passive cells. Increasing the coupling strength results in waves that lead to coherent periodic activity, exhibiting cluster, local and global synchronization under different conditions. Our results may explain the self-organized transition in a pregnant uterus from transient, localized activity initially to system-wide coherent excitations just before delivery.

Collective phenomena in a homogeneous system of diffusively coupled relaxation oscillators

A variety of complex spatial patterns relevant to chemical and biological systems can be generated through reaction-diffusion mechanisms. In this thesis, we have shown that diffusive coupling through the inactivating component in a system of relaxation oscillators extends such complexity to the temporal domain, generating remarkable spatiotemporal phenomena. We provide analytic explanations of the antiphase synchronization and spatially patterned oscillatory death regimes. We report a chimera state where patches with distinct dynamics coexist and also observe propagating phase defects resembling persis-

tent structures in cellular automata that may be used for computation.

Pattern formation through spontaneous symmetry-breaking in dense, homogeneous networks of neural oscillators

Recent experiments have highlighted how collective dynamics in networks of brain regions affect behavior and cognitive function. In this thesis, we have shown that a simple, homogeneous system of densely connected oscillators representing the aggregate activity of local brain regions can exhibit a rich variety of dynamical patterns emerging via spontaneous breaking of permutation or translational symmetry. Our results connect recent experimental findings and suggest that a range of complicated activity patterns seen in the brain can be explained even without a full knowledge of its wiring diagram.

Chimera order in spin systems

It has recently been shown that a population of oscillators having identical environments can exhibit a heterogeneous phase topology termed as chimera state. In this thesis, we have generalized this phenomenon to the broader perspective of order-disorder transitions in physical systems with discrete states. By an exact analytic treatment we show that chimera states can occur in a system of Ising spins in thermal equilibrium. We also numerically establish the existence of chimera ordering in 3-dimensional models of layered magnetic materials (such as manganites) suggesting possible means of experimentally observing it.

Dynamics of convergence to structural balance in frustrated dynamical systems

In many complex systems, the dynamical evolution of the different components can result in adaptation of the connections between them. In this thesis, we have considered the problem of how a fully connected network of discrete-state dynamical elements which can interact via positive or negative links, approaches structural balance by evolving its links to be consistent with the states of its components. The adaptation process, inspired by Hebb's principle, involves the interaction strengths evolving in accordance with the dynamical states of the elements. We observe that in the presence of stochastic fluctuations in the dynamics of the components, the system can exhibit large dispersion in the time required for converging to the balanced state. This variability is characterized by a bimodal distribution, which points to an intriguing non-trivial problem in the study of evolving energy landscapes.

7.2 Outlook

In this thesis, we have addressed several problems that can contribute to a general understanding of spatio-temporal pattern formation in a broad class of natural systems. A natural extension of the work presented here would be to develop theoretical techniques to understand the different types of spatio-temporal phenomena that have been observed in connection with epidemics [171]. In particular travelling waves of contagion has been observed during measles epidemics [172], dengue haemorrhagic fever in Thailand [173] and infestations of larch budmouth [174], while synchronization between different regions have been observed in the spread of influenza [175] as well as for measles and whooping cough [176]. Traditional compartmental models in epidemiology have strong resemblance to the phenomenological models of excitable and oscillatory media that I have worked with: for instance, the susceptible, infected and recovered compartments

in an epidemic model directly correspond to the resting, excited and recovering states of an excitable/oscillatory element. It is therefore of interest to see whether the theoretical models I have investigated for explaining spatio-temporal pattern formation in excitable/oscillatory media can be fruitfully applied to understand the epidemiological patterns mentioned above. In particular, the dependence of the different pattern regimes on the nature of coupling as well as other model parameters could give us insights about the conditions under which waves or synchronization of epidemics will take place.

Investigating the dynamics of contagia propagation is sufficiently general to cover a large range of phenomena including how ideas spread across society while also being of immense practical interest in connection with understanding how epidemics of infectious diseases occur. In view of the recurrent pandemics which have emerged in the recent past, it would be fascinating to see if efficient intervention strategies can be designed based on complex systems theoretical approaches. The availability of data on incidence of such diseases will also provide a crucial reality check on theoretical models being developed.

Another topic in epidemic modeling which builds on the present research is the role of temporal evolution of the interactions between neighboring elements on the spreading dynamics of contagia. This will be an intriguing application of a novel theoretical approach involving descriptions of continuum media where the diffusion is evolving at a time-scale slower than that of the local dynamics. The approach can be generalized to other connection topologies such as complex networks, where the above problem can be connected to the phenomenon of learning in networks of the brain (through modification of the synaptic strengths) and evolution and development in gene expression networks (through changes in the role of specific transcription factors). While a general theory explaining how slowly evolving coupling strength can affect the dynamics of these systems would be a crucial component for the projected general theory of complex systems, the implications of such a theory in the context of epidemics may be used to explain the efficacy of procedures that isolate different regions or subpopulations during an epidemic (e.g., through quarantine).

Another direction would be to explore the possibility of developing infection spreading models that take into account factors that have traditionally not been considered in detail, such as, changes in the pattern of interactions among agents as an epidemic propagates [177]. This would require developing atomistic models of reaction-diffusion systems in evolving networks and apply them to understand the propagation of infections on a network of interactions that are slowly evolving. Once there is some insights about the emergent properties of such models, we can try to develop analytical understanding of these features. These studies would help us figure out fundamental properties of real infection spreading and help us develop effective intervention strategies. Ideally, using such models one should be able to compare the efficacy of different strategies such as quarantine and mass vaccination.

Another topic that can be studied in future is the modeling of competing contagia [178]. While most epidemiological models tend to study an infectious disease in isolation, in reality a population is subject to a large variety of pathogens simultaneously. While in some cases being infected with one type of disease increases the risk of being infected by another (cooperative interaction between contagia), it is also possible that being infected by one can provide immunity against another (antagonistic interaction between contagia). Exploration of this problem fits naturally into the overall program of exploring complex systems dynamics where the individual entities can interact with each other through either cooperative or antagonistic interactions. It would also be important to model the competing infections on an evolving network of interaction as these models would be better representation of the situation in the real world and insights gained from the study can have practical implications.

Bibliography

[1] L. Wolpert *et al.*, *Principles of Development* (3rd Ed., Oxford University Press, Oxford, 2007).

[2] S. Kondo, in *Systems Biology: The Challenge of Complexity*, edited by S. Nakanishi *et al.* (Springer, Tokyo, 2009), p. 37.

[3] A. T. Winfree, *When Time Breaks Down* (Princeton University Press, Princeton, 1987).

[4] J. T. Bonner, *The Social Amoebae: The Biology of Cellular Slime Molds* (Princeton University Press, Princeton, 2009).

[5] I. R. Epstein and J. A. Pojman, *An Introduction to Chemical Dynamics: Oscillations, Waves, Patterns, and Chaos* (Oxford University Press, New York, 1998).

[6] B. P. Belousov, Compilation of Abstracts on Radiation Medicine **147**, 145 (1959).

[7] M. F. Crowley and I. R. Epstein, J. Phys. Chem. **93**, 2496 (1989).

[8] P. Ball, *The Self-Made Tapestry: Pattern Formation in Nature* (Oxford University Press, New York, 1999).

[9] P. Ball, *Nature's Patterns: a Tapestry in Three Parts* (Oxford University Press, New York, 2009).

[10] M. C. Cross and P. C. Hohenberg, Rev. Mod. Phys. **65**, 851 (1993).

[11] M. Cross and H. Greenside, *Pattern Formation and Dynamics in Nonequilibrium Systems* (Cambridge Univ. Press, Cambridge, 2009).

[12] R. C. Desai and R. Kapral, *Dynamics of Self-Organized and Self-Assembled Structures* (Cambridge Univ. Press, Cambridge, 2009).

[13] H. Meinhardt, *Models of Biological Pattern Formation* (Academic Press, California, 1982).

[14] J. Murray, *Mathematical Biology* (Springer, 2003), Vol II.

[15] E. Schöll, *Nonlinear Spatio-Temporal Dynamics and Chaos in Semiconductors* (Cambridge Univ. Press, Cambridge, 2001).

[16] A. M. Turing, Phil. Trans. R. Soc. Lond. B **237**, 37 (1952).

[17] A. A. Andronov, A. A. Vitt and S. E. Khaykin, *Theory of Oscillators* (Gostekhizdat, Moscow, 1937, in Russian).

[18] A. Pikovsky, M. Rosenblum and J. Kurths, *Synchronization* (Cambridge Univ. Press, Cambridge, 2003).

[19] C. Huygens (Hugenii), *Horologium Oscillatorium*, (Apud F. Muguet, Parisiis, 1673). English translation: *The Pendulum Clock*, (Iowa State University Press, Ames, 1986).

[20] J. Rayleigh, *The Theory of Sound* (Dover Publishers, New York, 1945).

[21] W. H. Eccles and J. H. Vincent, British Patent Spec. clxiii p.462 (1920).

[22] E. Kaempfer, *The History of Japan (With a Description of the Kingdom of Siam)* (Sloane, London, 1727). Posthumous translation; reprint by McLehose, Glasgow, 1906.

[23] E. V. Appleton, Proc. Cambridge Phil. Soc. (Math. and Phys. Sci.) **21**, 231 (1922).

[24] B. van der Pol, Phil. Mag. **3**, 64 (1927).

[25] E. Ising, Z. Phys. **31**, 253 (1925).

[26] S. N. Dorogovtsev, A. V. Goltsev and J. F. F. Mendes, Rev. Mod. Phys. **80**, 1275 (2008).

[27] S. Dasgupta, R.K. Pan and S. Sinha, Phys. Rev. E **80**, 025101 (2009).

[28] L. Glass, Nature (London) **410**, 277 (2001).

[29] M. U. Gillette and T. J. Sejnowski, Science **309**, 1196 (2005).

[30] M. Golubitsky, I. Stewart, P.-L. Buono and J. J. Collins, Nature (London) **401**, 693 (1999).

[31] A. T. Winfree, *The Geometry of Biological Time* (Springer, New York, 2000).

[32] V. Hakim and N. Brunel, Neural Comput. **11**, 1621 (1999).

[33] J. Keener and J. Sneyd, *Mathematical Physiology* (Springer, New York, 1998).

[34] T. R. Chigwada, P. Parmananda and K. Showalter, Phys. Rev. Lett. **96**, 244101 (2006).

[35] R. W. Tsien, R. S. Kass and R. Weingart, J. Exp. Biol. **81**, 205 (1979).

[36] G. Grégoire and H. Chaté, Phys. Rev. Lett. **92**, 025702 (2004).

[37] T. Vicsek, A. Czirók, E. Ben-Jacob, I. Cohen, and O. Shochet, Phys. Rev. Lett. **75**, 1226 (1995).

[38] S. T. Blackburn, *Maternal, Fetal and Neonatal Physiology: A Clinical Perspective* (Saunders-Elsevier, St Louis, Miss., 2007).

[39] R. E. Garfield and W. L. Maner, Sem. Cell Develop. Biol. **18** 289 (2007).

[40] J. A. Martin, B. E. Hamilton, P. D. Sutton, S. J. Ventura, F. Menacker, S. Kirmeyer and T. J. Mathews, *National Vital Statistics Reports* **57**(7), U.S. Dept. of Health & Human Services, Atlanta, 2009.

[41] M. F. MacDorman, W. M. Callaghan, T. J. Mathews, D. L. Hoyert and K. D. Kochanek, *Trends in preterm-related infant mortality by race and ethnicity: United States 1999-2004* (National Center for Health Statistics, Hyattsville, MD, 2007).

[42] A. Shmygol, A. M. Blanks, G. Bru-Mercier, J. E. Gullam and S. Thornton, Ann. N.Y. Acad. Sci. **1101**, 97 (2007).

[43] R. A. Duquette, A. Shmygol, C. Vaillant, A. Mobasheri, M. Pope, T. Burdyga and S. Wray, Biol. Reproduction **72**, 276 (2005).

[44] L. M. Popescu, S. M. Ciontea and D. Cretoiu, Ann. N.Y. Acad. Sci. **1101**, 139 (2007).

[45] S. M. Miller, R. E. Garfield and E. E. Daniel, Am. J. Physiol. **256**, C130 (1989).

[46] H. Miyoshi, M. B. Boyle, L. B. MacKay and R. E. Garfield, Biophys. J. **71**, 1324 (1996).

[47] V. Jacquemet, Phys. Rev. E **74**, 011908 (2006).

[48] A. K. Kryukov, V. S. Petrov, L. S. Averyanova, G. V. Osipov, W. Chen, O. Drugova and C. K. Chan, Chaos **18**, 037129 (2008).

[49] W. Chen, S. C. Cheng, E. Avalos, O. Drugova, G. Osipov, P. Y. Lai and C. K. Chan, EPL **86**, 18001 (2009).

[50] R. E. Garfield, G. Saade, C. Buhimschi, I. Buhimschi, L. Shi, S. Q. Shi and K. Chwalisz, Human Reproduction Update **4**, 673 (1998).

[51] W.-C. Tong, C. Y. Choi, S. Karche, A. V. Holden, H. Zhang and M. J. Taggart, PLoS One **6**, 18685 (2011).

[52] P. Kohl, A. G. Kamkin, I. S. Kiseleva and D. Noble, Exp. Physiol. **79**, 943 (1994).

[53] W. J. E. P. Lammers, H. Mirghani, B. Stephen, S. Dhanasekaran, A. Wahab, M. a. H. Al Sultan and F. Abazer, Am. J. Physiol. Regul. Integr. Comp. Physiol. **294**, R919 (2008).

[54] A. C. Guyton and J. E. Hall, *Textbook of Medical Physiology* (12th ed., Saunders Elsevier, Philadelphia, 2011).

[55] S. Mesiano, J. Soc. Gynec. Invest. **11**, 193 (2004).

[56] M.-L. Tsai, K. Cesen-Cummings, R. C. Webb and R. Loch-Caruso, Toxicol. Appl. Pharmacol. **152**, 18 (1998).

[57] G. Bub, A. Shrier and L. Glass, Phys. Rev. Lett. **88**, 058101 (2002).

[58] A. Pumir, A. Arutunyan, V. Krinsky and N. Sarvazyan, Biophys. J. **89**, 2332 (2005).

[59] M. Falcke and H. Engel, Phys. Rev. E **50**, 1353 (1994).

[60] S. Sinha, J. Saramäki and K. Kaski, Phys. Rev. E **76**, 015101 (2007).

[61] L. G. Morelli, K. Uriu, S. Ares and A. C. Oates, Science **336**, 187 (2012).

[62] S. Kondo and T. Miura, Science **329**, 1616 (2010).

[63] M. Inaba, H. Yamanaka and S. Kondo, Science **335**, 677 (2012).

[64] B. C. Goodwin, Symp. Soc. Exp. Biol. **18**, 301 (1964).

[65] A. Gierer and H. Meinhardt, Kybernetik **12**, 30 (1972).

[66] Z. Gong, N. J. Matzke, G. B. Ermentrout, D. Song, J. E. Vendetti, M. Slatkin and G. Oster, Proc. Natl. Acad. Sci. USA **109**, E234 (2012).

[67] T. C. Butler, M. Benayoun, E. Wallace, W. van Drongelen, N. Goldenfeld and J. Cowan, Proc. Natl. Acad. Sci. USA **109**, 606 (2012).

[68] P. Liang, Phys. Rev. Lett. **75**, 1863 (1995).

[69] I. R. Epstein, Science **315**, 775 (2007).

[70] C. H. Orchard, D. A. Eisner and D. G. Allen, Nature **304**, 735 (1983).

[71] A. Goldbeter, *Biochemical Oscillations and Cellular Rhythms* (Cambridge Univ. Press, Cambridge, 1997).

[72] G. Buzsáki and A. Draguhn, Science **304**, 1926 (2004).

[73] I. Z. Kiss, Y. Zhai and J. L. Hudson, Science **296**, 1676 (2002).

[74] R. Singh, J. Xu, N. Garnier, A. Pumir and S. Sinha, Phys. Rev. Lett. **108**, 068102 (2012).

[75] M. Toiya, V. K. Vanag and I. R. Epstein, Angew. Chem. **47**, 7753 (2008).

[76] J. Delgado, N. Li, M. Leda, H. O. González-Ochoa, S. Fraden and I. R. Epstein, Soft Matter **7**, 3155 (2011).

[77] K. Bar-Eli, Physica D **14**, 242 (1985).

[78] D. M. Abrams and S. H. Strogatz, Phys. Rev. Lett. **93**, 174102 (2004).

[79] R. Singh, S. Dasgupta and S. Sinha, EPL **95**, 10004 (2011).

[80] E. R. Berlekamp, J. H. Conway and R. K. Guy, *Winning Ways for your Mathematical Plays* (Academic, New York, 1982), Vol. 2.

[81] S. Wolfram, Rev. Mod. Phys. **55**, 601 (1983).

[82] S. Wolfram, Phys. Rev. Lett. **54**, 735 (1985).

[83] M. Cook, Complex Systems **15**, 1 (2004).

[84] E. M. Izhikevich, SIAM J. App. Math. **60**, 1789 (2000).

[85] V. K. Vanag and I. R. Epstein, Phys. Rev. E **84**, 066209 (2011).

[86] P. M. Chaikin and T. C. Lubensky, *Principles of Condensed Matter Physics* (Cambridge Univ. Press, Cambridge, 2000).

[87] M. Heinrich, T. Dahms, V. Flunkert, S. W. Teitsworth and E. Schöll, New J. Phys. **12**, 113030 (2010).

[88] G. Ertl, Science **254**, 1750 (1991).

[89] E. I. Volkov and V. A. Romanov, Phys. Scr. **51**, 19 (1995).

[90] T. Lee and M. Cross, Phys. Rev. Lett. **106**, 143001 (2012).

[91] J. A. Acebrón, L. L. Bonilla, C. J. P. Vicente, F. Ritort and R. Spigler, Rev. Mod. Phys. **77**, 137 (2005).

[92] A. K. Engel, P. Fries and W. Singer, Nature Rev. Neurosci. **2**, 704 (2001).

[93] M. I. Rabinovich, P. Varona, A. I. Selverston and H. D. I. Abarbanel, Rev. Mod. Phys. **78**, 1213 (2006).

[94] S. Olmi, A. Politi and A. Torcini, EPL **92**, 60007 (2010).

[95] M. L. Steyn-Ross, D. A. Steyn-Ross and J. W. Sleigh, Phys. Rev. X **3**, 021005 (2013).

[96] E. R. Kandel, J. H. Schwartz and T. M. Jessell, *Principles of Neural Science* (McGraw-Hill, New York, 4th edition, 2000).

[97] W. Singer, Ann. Rev. Physiol. **55**, 349 (1993).

[98] L. D. Lewis V. S. Weiner, E. A. Mukamel, J. A. Donoghue, E. N. Eskandar, J. R. Madsen, W. S. Anderson, L. R. Hochberg, S. S. Cash, E. N. Brown and P. L. Purdon, Proc. Natl. Acad. Sci. USA **109**, E3377 (2012).

[99] H. Markram, Nature Rev. Neurosci. **7**, 153 (2006).

[100] C. Zhou, L. Zemanová, G. Zamora, C. C. Hilgetag and J. Kurths, Phys. Rev. Lett. **97**, 238103 (2006).

[101] C. van Vreeswijk and H. Sompolinsky, Science **274**, 1724 (1996).

[102] G. Deco, V. K. Jirsa, P. A. Robinson, M. Breakspear and K. Friston, PLoS Comput. Biol. **4**, e1000092 (2008).

[103] J. W. Scannell, C. Blakemore and M. P. Young, J. Neurosci. **15**, 1463 (1995).

[104] P. Hagmann, L. Cammoun, X. Gigandet, R. Meuli, C. J. Honey, V. J. Wedeen, and O. Sporns, PLoS Biol. **6**, e159 (2008).

[105] D. S. Modha and R. Singh, Proc. Natl. Acad. Sci. USA **107**, 13485 (2010).

[106] G. Palm, Hippocampus **3**, 219 (1993).

[107] C. Johansson and A. Lansner, Neural Networks **20**, 48 (2007).

[108] G. M. Shepherd (Ed.), *The Synaptic Organization of the Brain* (Oxford University Press, New York, 4th edition, 2003).

[109] R. Morris, in *The Hippocampus Book* (Eds. P. Andersen, R. Morris, D. Amaral, T. Bliss and J. O'Keefe) (Oxford University Press, Oxford, 2007).

[110] E. A. Leicht and M. E. J. Newman, Phys. Rev. Lett. **100**, 118703 (2008).

[111] A. Schnitzler and J. Gross, Nature Rev. Neurosci. **6**, 285 (2005).

[112] P. J. Uhlhaas and W. Singer, Nature Rev. Neurosci. **11**, 100 (2010).

[113] B. H. Jansen and V. G. Rit, Biol. Cybern. **73**, 357 (1995).

[114] C. J. Honey, R. Kotter, M. Breakspear and O. Sporns, Proc. Natl. Acad. Sci. USA **104**, 10240 (2007).

[115] F. Marten, S. Rodrigues, O. Benjamin, M. P. Richardson and J. R. Terry, Phil. Trans. R. Soc. A **367**, 1145 (2009).

[116] H. R. Wilson and J. D. Cowan, Biophys. J. **12**, 1 (1972).

[117] A. Destexhe and T. J. Sejnowski, Biol. Cybern. **101**, 1 (2009).

[118] S. Kar, A. Routray and B. P. Nayak, Clin. Neurophysiol. **122** 966 (2011).

[119] C. J. Chu, M. A. Kramer, J. Pathmanathan, M. T.Bianchi, M. B. Westover, L. Wizon and S. S. Cash, J. Neurosci. **32** 2703 (2012).

[120] A. Haimovici, E. Tagliazucchi, P. Balenzuela and D. R. Chialvo, Phys. Rev. Lett. **110**, 178101 (2013).

[121] H. E. Stanley, Rev. Mod. Phys. **71**, S358 (1999).

[122] Y. Kuramoto and D. Battogtokh, Nonlinear Phenom. Complex Syst. **5**, 380 (2002).

[123] D. M. Abrams and S. H. Strogatz, Int. J. Bifurcation Chaos **16**, 21 (2006).

[124] G. C. Sethia, A. Sen and F. M. Atay, Phys. Rev. Lett, **100**, 144102 (2008).

[125] O. E. Omel'chenko, Y. L. Maistrenko and P. A. Tass, Phys. Rev. Lett. **100**, 044105 (2008).

[126] D. M. Abrams, R. Mirollo, S.H. Strogatz, and D.A. Wiley, Phys. Rev. Lett. **101**, 084103 (2008).

[127] C. R. Laing, Chaos **19**, 013113 (2009).

[128] R. Ma, J. Wang and Z. Liu, EPL **91**, 40006 (2010).

[129] C. R. Laing, Phys. Rev. E **81**, 066221 (2010).

[130] E. A. Martens, Phys. Rev. E **82**, 016216 (2010).

[131] E. A. Martens, Chaos **20**, 043122 (2010).

[132] L. J. de Jongh and A. R. Miedema, Adv. Phys. **23**, 1 (1974).

[133] J. M. Kincaid and E.G.D. Cohen, Phys. Rep. **22**, 57 (1975).

[134] E. Stryjewski and N. Giordano, Adv. Phys. **26**, 487 (1977).

[135] D. J. Amit, *Modeling Brain Function* (Cambridge Univ. Press, Cambridge, 1989).

[136] C. Castellano, S. Fortunato and V. Loreto, Rev. Mod. Phys. **81**, 591 (2009)

[137] E. A Martens, C. R. Laing and S. H. Strogatz, Phys. Rev. Lett. **104**, 044101 (2010).

[138] A. M. Hagerstrom, T. E. Murphy, R. Roy, P. Hövel, I. Omelchenko and E. Schöll, Nature Physics **8**, 658 (2012).

[139] M. R. Tinsley, S. Nkomo and K. Showalter, Nature Physics **8**, 662 (2012).

[140] E. A. Martens, S. Thutupalli, A. Fourriérec and O. Hallatscheka, Proc. Natl. Acad. Sci. USA **110**, 10563 (2013).

[141] M. E. J. Newman, *Networks: An Introduction* (Oxford Univ. Press, Oxford, 2010).

[142] A. Barrat, M. Barthélemy and A. Vespignani, *Dynamical Processes on Complex Networks* (Cambridge Univ. Press, Cambridge, 2008).

[143] S. Jain and S. Krishna, Proc. Natl. Acad. Sci. USA **98**, 543 (2001).

[144] T. Gross, C. J. D. D'Lima and B. Blasius, Phys. Rev. Lett. **96**, 208701 (2006).

[145] T. Gross and B. Blasius, J. Roy. Soc. Interface **5**, 259 (2008).

[146] B. D. MacArthur, R. J. Sánchez-García and A. Ma'ayan, Phys. Rev. Lett. **104**, 168701 (2010).

[147] R. Durrett, J. P. Gleeson , A. L. Lloyd, P. J. Mucha, F. Shi, D. Sivakoff, J. E. S. Socolar and C. Varghese, Proc. Natl. Acad. Sci. USA **109**, 3682 (2012).

[148] A. Goudarzi, C. Teuscher, N. Gulbahce and T. Rohlf, Phys. Rev. Lett. **108**, 128702 (2012).

[149] W. Liu, B. Schmittmann and R. K. P. Zia, EPL **100**, 66007 (2012).

[150] A. Barrat, M. Barthélemy, R. Pastor-Satorras and A. Vespignani, Proc. Natl. Acad. Sci. USA **101**, 3747 (2004).

[151] A. Barrat, M. Barthélemy and A. Vespignani, Phys. Rev. Lett. **92**, 228701 (2004).

[152] J.-P. Onnela, J. Saramäki, J. Hyvönen, G. Szabó, D. Lazer, K. Kaski, J. Kertész and A.-L. Barabási, Proc. Natl. Acad. Sci. USA **104**, 7332 (2007).

[153] V. A. Traag and J. Bruggeman, Phys. Rev. E **80**, 036115 (2009).

[154] K. H. Fischer and J. A. Hertz, *Spin Glasses* (Cambridge Univ. Press, Cambridge, 1991).

[155] M. Mezard, G. Parisi, M. A. Virasoro, *Spin Glass Theory and Beyond* (World Scientific, Singapore, 1987).

[156] F. Heider, J. Psychol. **21**, 107 (1946).

[157] D. Cartwright and F. Harary, Psychol. Rev. **63**, 277 (1956).

[158] T. Antal, P. L. Krapivsky and S. Redner, Phys. Rev. E **72**, 036121 (2005).

[159] S. A. Marvel, S. H. Strogatz and J. M. Kleinberg, Phys. Rev. Lett. **103** 198701 (2009).

[160] K. Kułakowski, P. Gawronski and P. Gronek, Int. J. Mod. Phys. C **16** 707 (2005).

[161] S. A. Marvel, J. Kleinberg, R. D. Kleinberg and S. H. Strogatz, Proc. Natl. Acad. Sci. USA **108**, 1771 (2011).

[162] T. H. Summers and I. Shames, EPL **103** 18001 (2013).

[163] M. D. Fox, A. Z. Snyder, J. L. Vincent, M. Corbetta, D. C. Van Essen and M. E. Raichle, Proc. Natl. Acad. Sci. USA **102**, 9673 (2005).

[164] D. O. Hebb, *The Organization of Behavior* (Wiley, New York, 1949).

[165] B. L. McNaughton, Phil. Trans. R. Soc. B **358**, 629 (2003).

[166] C. T. Fernando, A. M. L. Liekens, L. E. H. Bingle, C. Beck, T. Lenser, D. J. Stekel and J. E. Rowe, J. R. Soc. Interface **6**, 463 (2009).

[167] R. A. Watson, C. L. Buckley, R. Mills and A. Davies, in *Artificial Life XII*, edited by H. Fellermann *et al.* (MIT Press, Cambridge, 2010), p. 194.

[168] G. Facchetti, G. Iacono and C. Altafini, Proc. Natl. Acad. Sci. USA **108**, 20953 (2011).

[169] G. Facchetti, G. Iacono and C. Altafini, Phys. Rev. E **86**, 036116 (2012).

[170] R. K. Pan and S. Sinha, EPL **85**, 68006 (2009).

[171] R. S. Ostfeld, G. E. Glass and F. Keesing, Trends in ecology & evolution **20**, 328 (2005).

[172] B. T. Grenfell, O. N. Bjørnstad and J. Kappey, Nature **414**, 716 (2001).

[173] D. A. T. Cummings, R. A. Irizarry, N. E. Huang, T. P. Endy, A. Nisalak, K. Ungchusak and D. S. Burke, Nature **427**, 344 (2004).

[174] D. M. Johnson, O. N. Bjørnstad and A. M. Liebhold, Eco. Lett. **7**, 967 (2004).

[175] C. Viboud, O. N. Bjørnstad, D. L. Smith, L. Simonsen, M. a Miller and B. T. Grenfell, Science **312**, 447 (2006).

[176] P. Rohani, D. J. Earn and B. T. Grenfell, Science **286**, 968 (1999).

[177] I. B. Schwartz and L. B. Shaw, Physics **3**, (2010).

[178] B. Karrer and M. E. J. Newman, Phys. Rev. E **84**, 036106 (2011).